



UNIVERSITE CATHOLIQUE DE LOUVAIN  
Faculté des Sciences Appliquées  
Unité de Physico-Chimie et de Physique des Matériaux

# Static Secondary Ion Mass Spectrometry of Thin Organic Layers

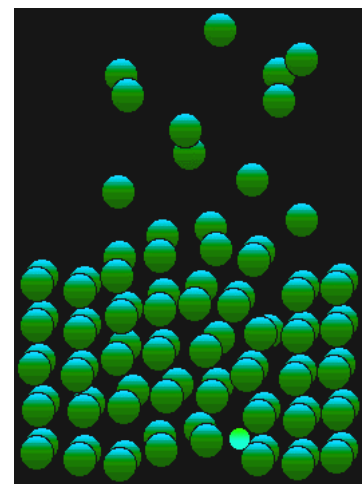
Dissertation présentée en vue de l'obtention du grade de  
*Docteur en Sciences Appliquées*  
par

Arnaud Delcorte

**Promoteur :** Prof. P. Bertrand

**Membres du jury :**

Prof. G. Decher (Institut Charles Sadron)  
Prof. E. De Hoffmann (UCL/CHIM)  
Prof. J.-P. Issi (UCL/MAPR)  
Prof. A. Laschewsky (UCL/CHIM)  
Prof. R. Legras (UCL/MAPR)  
Prof. J. C. Vickerman (UMIST)



Janvier 1999



*Celui qui n'a pas vu croître et mûrir pour lui le fruit de la vérité  
Ne marche pas d'un pied ferme sur la route.  
Quiconque inclina vers soi l'arbre de la science  
Sait qu'aujourd'hui est comme hier et demain comme le premier jour.*

*Omar KHAYYAM, Quatrains, XI<sup>e</sup>-XII<sup>e</sup> s.*

*Cette thèse est le fruit d'une collaboration entretenue avec des chercheurs - et tout d'abord des individus - issus d'horizons scientifiques et géographiques variés. Au terme du voyage, je crois pouvoir affirmer que la réunion de nos personnalités, uniques et complémentaires, a produit plus que la somme des parties constitutives, tant au niveau professionnel qu'humain. Si ce travail de recherche a généré des résultats nouveaux, souvent inattendus, c'est aussi parce qu'une des conditions primordiales de son développement était remplie, à savoir la Liberté. Liberté de penser, de choisir, d'expérimenter, de mettre en doute, de proposer des explications nouvelles.*

*Cette Liberté, Patrick me l'a offerte pendant quatre ans, et c'est le plus beau cadeau qu'il ait pu me faire. Je l'en remercie. Son ouverture d'esprit lors de nos fréquentes discussions nous a permis de mettre de côté les "vieilles habitudes" pour aller de l'avant.*

*Je dois avouer ici que les moments d'excitation les plus intenses me vinrent lors de l'étude des mécanismes de désorption d'ions moléculaires en SIMS. Merci encore à Patrick de m'avoir poussé à continuer dans cette voie. A toi aussi, Bila, venu de loin, dont les nombreuses mesures nous ont fait beaucoup cogiter, et finalement trouver. In this study, I'm greatly indebted to Bruno Schueler from Phi-Electronics for the development of the energy distribution measurements, and the fruitful fax-discussions we had along these years concerning the interpretation of the results. Fraser, I wish to thank you, too: it was a great lesson and a pleasure to work together. I'm also grateful to two pure physicists, Igor, from Tashkent, who gave me the idea to look at "negative energies", and to Joao, from Rio, who helped me to make the connection with the world of PDMS.*

*In the same context, I wish to thank Pr. John Vickerman for his enthusiasm concerning the fundamental aspect of this work and for his involvement and support in the exciting project we will start soon in Penn State University. I'm honoured by his presence in this thesis jury.*

*En février 1996, alors que je débutais des dépôts de polyélectrolytes sur le PET, le Pr. Gero Decher me dit quelque chose de ce genre: "we don't know exactly why, but it seems that these polyelectrolyte assemblies may be grown on any kind of substrate, you just have to try". Je tiens à le remercier pour cet encouragement et pour avoir bien voulu accepter d'évaluer le résultat de mes "essais". Son travail de*

*pionnier et son impressionnante bibliographie nous ont servi de référence tout au long de ce travail.*

*La genèse de ces nouvelles tentatives est intimement liée à la dynamique du programme LAMINAP. Dans cette mouvance, il y avait à l'origine André Laschewsky, Roger Legras et Patrick Bertrand, membres de mon comité d'encadrement et copromoteurs du projet, qui lui donnèrent vie et y insufflèrent leurs idées. Merci à eux. Merci également à la Communauté Française de Belgique sans qui rien n'aurait été possible. Puis vint le temps de la réalisation, et du travail de recherche au quotidien. Bravo à Alain pour la qualité de son investissement grâce auquel le navire a pu tenir le cap contre vents et marées. Je tiens aussi à remercier particulièrement Erik Wischerhoff, dont la facilité à aller vers les autres et la boulimie de travail nous ont beaucoup bénéficié. Il a été pendant trois ans un véritable ciment entre nos laboratoires. Merci également à Xavier, vieux comparse, et Bruno du "POLY", ainsi qu'à Bernd, Peter Hendlinger (au début) et Peter Fisher (à la fin). Dans le cadre de ce travail, des mesures complémentaires furent réalisées à Lausanne, dans le groupe du Pr. Hans-Jorg Matthieu. Qu'il en soit remercié. Toute ma reconnaissance va également à Franck, pour son accueil chaleureux et son amitié, ainsi qu'à Didier, dont la bonne humeur à franchi intacte les frontières qui séparent nos pays.*

*Outre mon comité d'encadrement et les Prs. Decher et Vickerman, déjà cités plus haut, deux autres personnalités composent mon jury de thèse. Il s'agit tout d'abord de son Président, Jean-Paul Issi, toujours disponible, attentif et d'excellent conseil. Je l'en remercie. Je suis également redevable au Pr. Edmond De Hoffmann grâce à qui le lien a pu être établi avec la spectrométrie de masse "traditionnelle". Merci à chacun pour la lecture attentive et les commentaires pertinents.*

*Je n'oublie pas ceux que j'ai eu le plaisir d' "encadrer" pour un travail de fin d'études ou un stage AGCD et qui m'ont fait découvrir un autre aspect du métier. Etudiants, licenciés ou docteurs, ils se reconnaîtront.*

*Du travail expérimental, il y a au moins une chose que les résultats ne montrent pas, à savoir le temps passé à surmonter les tracas de toutes sortes qui occupent le plus clair de nos journées. Pour leur aide précieuse lors des nombreux et inévitables problèmes techniques, électroniques et informatiques, je me dois de remercier Claude et Jean-Michel, particulièrement brillants dans les situations désespérées.*

*Et bien sûr il y a ceux dont j'ai partagé la vie de tous les jours pendant... pas mal d'années, à savoir l'équipe 'SURFACE' de Patrick. Passés, présents ou à venir, merci à Youssef, Xavier, Lu-Tao, Laurent, Véronique, Didier, Jean-Benoit, Paul-André, Stoyka et Laurence. Et tous les autres... qu'ils soient de "TRANSPORT", d' "AB INITIO" ou du staff administratif, grâce à qui mon passage au PCPM fut beaucoup plus qu'une thèse.*

*Enfin, mes pensées vont naturellement à ceux qui m'entourent et me (sup)portent en toutes circonstances : Annie et Max, mais aussi Gilles et Christine, Nicole, Gauthier et Jean-Marie.*

*Mon dernier mot sera pour vous qui m'attendiez à la maison; pour ton amour, Valérie, et pour le vôtre, Ophélie et Andréa, grâce à qui le verso de mes papiers aura vu naître plus d'un chef-d'oeuvre. MERCI.*

## Table of contents

Abstract	iii
List of papers	iv
List of abbreviations, acronyms and symbols	vi

### PART I. SURVEY

<b>I.1. General introduction: scope and outline of the thesis</b>	1
I.1.1. Scope of the thesis	1
I.1.2. Outline	3
<b>I.2. Literature Review</b>	5
<b>I.2.A. Fundamentals of ion emission</b>	5
I.2.A.1. Historical benchmarks, concepts and applications	5
I.2.A.2. Kinetic energy distribution of molecular secondary ions	7
I.2.A.3. Models of molecular secondary ion emission	9
I.2.A.3.1. Secondary ion emission	9
I.2.A.3.2. Charge exchange between the primary particle and the surface (i)	9
I.2.A.3.3. Energy deposition in the target (ii)	9
I.2.A.3.4. Target atoms motion (iii)	10
I.2.A.3.5. Transfer of momentum towards the surface and molecular secondary particle emission (iv-v)	10
I.2.A.3.6. Charge state of the secondary particles and charge exchange with the surface (vi)	17
I.2.A.3.7. Unimolecular dissociation of excited secondary ions (vii)	20
<b>I.2.B. Organic Multilayers</b>	21
I.2.B.1. Ultrathin organic coatings and supramolecular organisation	21
I.2.B.1.1. Molecular scale engineering: technology and applications	21
I.2.B.1.2. Methods for producing thin organic multilayers	23
I.2.B.2. Multilayer buildup by adsorption of alternate polyelectrolytes	28
I.2.B.2.1. Polyelectrolyte adsorption	28
I.2.B.2.2. Nature and Structural study of the multilayers	30
I.2.B.2.3. Properties of the multilayers	39
I.2.B.3. Application of static SIMS to the study of ultrathin organic films	42
I.2.B.3.1. Static SIMS and thin organic films	42
I.2.B.3.2. Langmuir-Blodgett mono- and multilayers	42
I.2.B.3.3. Self-assembled monolayers of thiols and disulfides	45
I.2.B.3.4. Self-assembled monolayers of silanes	47

<b>I.3. Aims of the thesis</b>	49
<b>I.4. Summary of the Results</b>	51
<b>I.4.A. Fundamentals of Static SIMS</b>	51
I.4.A.1. Introduction	51
I.4.A.2. Experimental setup	52
I.4.A.3. Samples	54
I.4.A.4. Emission of molecular fragment ions from thin organic films	56
I.4.A.5. Unimolecular dissociation of fragment ions in the vacuum	62
I.4.A.6. Emission of large parent ions from organic adsorbates	69
I.4.A.7. Towards a comprehensive picture of molecular ion emission	73
I.4.A.8. Conclusion	75
<b>I.4.B. Surface analysis of alternate polyelectrolyte multilayers</b>	77
I.4.B.1. Introduction	77
I.4.B.2. Characterisation techniques	78
I.4.B.3. Samples	78
I.4.B.4. Information depth in SIMS and XPS	80
I.4.B.5. Adsorption of multilayers on silicon	84
I.4.B.6. Adsorption of multilayers on polymers	91
I.4.B.7. Conclusion	101
<b>I.5. Concluding Remarks</b>	103
I.5.1. Conclusion	103
I.5.2. Outlook	105
References	106

## **PART II. ARTICLES**

<b>II.A. Fundamentals of ion emission in Static SIMS</b>	
II.A.1. Emission of molecular fragment ions from thin organic films	
II.A.2. Unimolecular dissociation of fragment ions in the vacuum	
II.A.3. Emission of parent ions from large organic adsorbates	
<b>II.B. Application of ToF-SIMS to the study of alternate polyelectrolyte multilayers</b>	
II.B.1. Adsorption of polyelectrolyte multilayers on silicon	
II.B.2. Adsorption of polyelectrolyte multilayers on polymers	

## **List of papers**

### **1. Publications included in this thesis:**

This thesis is based on the following papers, published in international journals and conference proceedings. They constitute the second part of the notes.

#### **Part II.A. Fundamentals of ion emission in Static SIMS**

A. Delcorte, P. Bertrand, *Kinetic energy distributions of secondary molecular ions from thin organic films under ion bombardment*, Nucl. Instr. Meth. B 115 (1996) 246

A. Delcorte, P. Bertrand, *Energy distributions of hydrocarbon secondary ions from thin organic films under keV ion bombardment : correlation between kinetic and formation energy of the ions sputtered from tricosenoic acid*, Nucl. Instr. Meth. B 117 (1996) 235

A. Delcorte, P. Bertrand, *Energy distributions of molecular secondary ions from polymer thin films under keV ion bombardment*, in SIMS X proceedings, Eds. A. Benninghoven, B. Hagenhoff and H. W. Werner, J. Wiley & sons publs., (Chichester, 1997) p 731

A. Delcorte, P. Bertrand, *Influence of chemical structure and beam degradation on the kinetic energy of molecular ions in keV sputtering of polymers*, Nucl. Instr. Meth. B 135 (1998) 430

A. Delcorte, B. G. Segda, P. Bertrand, *ToF-SIMS analyses of polystyrene and dibenzanthracene: Evidence of the fragmentation and metastable decay processes in the molecular secondary ion emission*, Surf. Sci. 381 (1997) 18; Surf. Sci. 389 (1997) 393

A. Delcorte, P. Bertrand, *Unimolecular dissociation of metastable secondary ions in SIMS of polymers*, SIMS XI proceedings, Eds. R Lareau and G. Gillen, J. Wiley & sons publs., (Chichester, 1998) p. 447

A. Delcorte, P. Bertrand, *Sputtering of parent-like ions from large organic adsorbates on metals under keV ion bombardment*, Surf. Sci. 412/413 (1998), 97.

#### **Part II.B. Application of ToF-SIMS to the study of alternate polyelectrolyte multilayers**

A. Delcorte, P. Bertrand, X. Arys, A. Jonas, *ToF-SIMS study of alternate polyelectrolyte thin films : Chemical surface characterization and molecular secondary ions sampling depth*, Surf. Sci. 366 (1996) 149

A. Delcorte, P. Bertrand, E. Wischerhoff et A. Laschewsky, *Characterization of alternate polyelectrolyte thin films by ToF-SIMS and XPS*, proceedings of the second international conference on polymer-solid interfaces (ICPSI 2), Eds. J.-J. Pireaux, J. Delhalle and P. Rudolf, Presses Universitaires de Namur (Namur, 1998) p. 65

A. Delcorte, P. Bertrand, E. Wischerhoff, A. Laschewsky, *ToF-SIMS and XPS study of thin multilayered coatings realized by successive adsorption and functionalization of charged polymer layers*, SIMS XI proceedings, Eds. R Lareau and G. Gillen, J. Wiley & sons publs. (Chichester, 1998) p. 533

A. Delcorte, P. Bertrand, E. Wischerhoff, A. Laschewsky, *Adsorption of Polyelectrolyte Multilayers on Polymer Surfaces*, Langmuir 13 (1997) 5125

## **2. Related publications which are not included in the text:**

A. Delcorte, L. T. Weng, P. Bertrand, *Secondary molecular ion emission from aliphatic polymers bombarded with low energy ions : effects of the molecular structure and the ion beam induced surface degradation*, Nucl. Instr. Meth. B 100 (1995) 203

A. Laschewsky, B. Mayer, E. Wischerhoff, X. Arys, A. Jonas, P. Bertrand, A. Delcorte, *A new route to thin polymeric, non-centrosymmetric coatings*, Thin Solid Films 284/285 (1996) 334

A. Laschewsky, E. Wischerhoff, S. Denzinger, H. Ringsdorf, P. Bertrand, A. Delcorte, *Molecular recognition by hydrogen bonding in polyelectrolyte multilayers*, Chem. European J. 3 (1997) 34

P. Hendlinger, A. Laschewsky, P. Bertrand, A. Delcorte, R. Legras, B. Nysten and D. Möbius, *Partially fluorinated maleimide copolymers for langmuir films of improved stability. Part 2. Spreading behaviour and multilayer formation*, Langmuir 13 (1997) 310

A. Laschewsky, E. Wischerhoff, P. Bertrand and A. Delcorte, *Polyelectrolyte multilayers containing photoreactive groups*, Macromol. Chem. Phys. 198 (1997) 3239

P. Bertrand, A. Delcorte, *Secondary molecular ion emission in static SIMS of organic materials*, SIMS XI proceedings, Eds. R Lareau and G. Gillen, J. Wiley & sons publs., (Chichester, 1998) p. 437

A. Delcorte, P. Bertrand, *Metastable decay of molecular fragment ions sputtered from hydrocarbon polymers under keV ion bombardment*, Int. J. Mass Spec. Ion Proc., submitted

A. Delcorte, P. Bertrand, F. Reich, *Influence of the primary ion beam parameters (nature, energy and angle) on the kinetic energy distribution of molecular fragments sputtered from PET by keV ions*, in preparation

## **List of abbreviations, acronyms and symbols**

AFM	Atomic Force Microscopy
atom %	Atomic fraction of the elements as determined by XPS (i.e. excluding hydrogen)
$\Delta E_f$	Difference of formation energy
$\Delta E_k$	Kinetic energy deficit
(dE/dx)	Stopping power
DBA	Dibenzanthracene
DNA	Desoxyribonucleic acid
$E_a$	Electron affinity
$E_b$	Binding energy
$E_{cm}$	Center-of-mass kinetic energy
$E_{int}$	Internal energy (vibration + rotation)
$E_k$	Kinetic energy
$E_{rel}$	Relative kinetic energy
$E(r)$	Energy deposited at a distance $r$ around the primary ion impact point
ESA	Electrostatic Analyser
ESCA	Electron Spectroscopy for Chemical Analysis (XPS)
FAB-MS	Fast Atom Bombardment Mass Spectrometry
FS	Freely Suspended films
FTIR	Fourier-Transform Infrared spectroscopy
FWHM	Full Width at Half Maximum
IL	Immersion Lens
$I_p$	Ionisation potential
ITO	Indium-Tin-Oxide
KED	Kinetic Energy Distribution
$\lambda_{SIMS}$	Mean emission depth of secondary ions
$\lambda_{XPS}$	Inelastic mean free path of photoelectrons
LB	Langmuir-Blodgett
LDMS	Laser Desorption Mass Spectrometry
LED	Light-Emitting Diode
m/z	Mass / charge number for secondary ions
M	Molecule
Me	Metal
(M-H) <sup>-</sup>	Deprotonated parent ion
(M+H) <sup>+</sup>	Protonated parent ion
$M_{PCM}^+$	Monomer ion of PCM
$M_{PSS}^-$	Monomer ion of PSS
NLO	Non-Linear Optics
$p^\pm$	Ionisation probability
PAH	Poly(allylamine hydrochloride)
PBD	Poly(butadiene)
PCM	Poly(choline methacrylate)
PDMS	Plasma Desorption Mass Spectrometry
PE	Poly(ethylene)
PEI	Poly(ethylene imine)

*Static Secondary Ion Mass Spectrometry of Thin Organic Layers*

PEIm	Poly(ether imide)
PET	Poly(ethylene terephthalate)
PIB	Poly(isobutylene)
PMA	Poly(methacrylic acid)
PMMA	Poly(methyl methacrylate)
PP	Poly(propylene)
PPO	Poly(2,6-dimethyl-p-phenylene oxide)
PPV	Poly(phenylene vinylene)
PS	Poly(styrene)
PSS	Poly(styrene sulfonate)
PTFE	Poly(tetrafluoroethylene)
PVDF	Poly(vinylidene fluoride)
PVS	Poly(vinyl sulfate)
QCM	Quartz-Crystal Microbalance
r	Dissociation rate of metastable ions
R	Reflectivity
$\sigma$	Secondary ion disappearance cross section
$\sigma_i$	Surface roughness
$\sigma_s$	Interfacial roughness
SA	Self-Assembly
SALI	Surface Analysis by Laser Ionisation
SAM	Self-Assembled Mono- or Multilayers
SHG	Second Harmonic Generation
SIMS	Secondary Ion Mass Spectrometry
SNMS	Secondary Neutral Mass Spectrometry
SPAn	Sulfonated poly(aniline)
SPR	Surface Plasmon Resonance spectroscopy
$\tau_{1/2}$	Half-life of metastable parent ions
TC	Triacontane
TL	Transfer Lens
ToF-SIMS	Time-of-Flight Secondary Ion Mass Spectrometry
TPN	Tetraphenylnaphthalene
TSA	Tricosenoic Acid
u	Atomic mass unit
UHV	Ultra High Vacuum
UV/vis	Ultra Violet / visible spectroscopy
$v_{\perp}$	Component of the velocity perpendicular to the surface
$v_B$	Bohr velocity
XPS	X-Ray Photoelectron Spectroscopy (ESCA)
XRD	X-Ray Diffraction
XRR	X-Ray Reflectivity
Y	Sputter yield
$Y^{\pm}$	Secondary ion yield
$Y_d$	Yield of daughter ions
$Y_{\text{metastable}}$	Yield of secondary ions produced in the vacuum
$Y_p$	Yield of parent ions
$Y_{\text{surface}}$	Yield of secondary ions produced at the surface
2D	Two-dimensional

**PART I**

*Survey*



# I.1.

---

## General introduction

---

### I.1.1. Scope of the thesis

---

Systems of reduced dimensionality are challenging for both chemists and physicists. In this multidisciplinary context, the elaboration of ultrathin organic or composite assemblies constituted of two-dimensional, piled up layers is of particular interest regarding applications in the microelectronics and biological fields, as well as coating technology. Their development requires to cross the borders between organic chemistry, applied physics and materials science.

For twenty years, the activity in this area has grown impressively and there exists a huge amount of publications addressing the realisation, structure and properties of organic mono- and multilayers prepared by the well-established Langmuir-Blodgett (LB) and self-assembly (SA) methods. Beside a fundamental interest, this development is motivated by high-tech applications as transducers, chemical and biosensors, bioelectronic devices, information storage components, resists, membranes, etc. In particular, applications at the interface with the biological field seem promising, since these supramolecular assemblies are able to copy two major features of the living world: self-organisation and molecular recognition.

In addition to LB and SA, a new method for producing organic supramolecular assemblies, based on the electrostatic interaction between oppositely charged amphiphile or polyelectrolyte layers, has been introduced recently. The obtained coatings exhibit a lower degree of orientation in the layer, but a greater stability, and the procedure appears easy to develop, much more versatile and less substrate-dependent than for the previous techniques. By this way, assemblies with more than hundred layers and with a low surface roughness may be built-up. On the other hand, there is very few limitation concerning the nature of the layers (amphiphiles, polymers, nanoparticles, mineral sheets, proteins, etc).

Up to now, alternate polyelectrolyte multilayers have been mainly built-up on model silicon and glass supports, and characterised by optical methods such as UV/vis absorption spectroscopy, X-ray reflectometry (XRR), ellipsometry or, alternatively, by surface plasmon resonance spectroscopy, quartz crystal microbalance and atomic force microscopy. These techniques bring detailed data concerning the thickness, roughness and structural

properties of the layers, but few information about their surface composition and chemistry. In addition, most of them are limited to model substrates, which must be either transparent, extremely flat or different from the coatings by optical or mechanical features.

In this thesis, we will develop time-of-flight secondary ion mass spectrometry (ToF-SIMS), in combination with X-ray photoelectron spectroscopy (XPS), for the surface analysis of thin organic films in general and of alternate polyelectrolyte multilayers in particular. In a first stage, the use of well-characterised, model samples built-up on charged silicon substrates will facilitate the interpretation of the ToF-SIMS and XPS data. After that, the same techniques will be applied to the study of polyelectrolyte multilayers adsorbed on different polymer substrates, which can not be directly characterised by the various other methods cited above. It will be shown that the multilayer growth may also occur on these uncharged substrates.

However, prior to achieve a relevant study of thin organic coatings by ToF-SIMS, several difficult practical and fundamental questions related the technique itself must be elucidated. For instance, what is the information depth of ToF-SIMS for such systems ? In a complex mass spectrum, how can we select the more appropriate secondary ions to develop reasonable interpretations ? Are there artefacts which may prevent a direct interpretation of the data (pronounced fragmentation, recombination, dissociation in the vacuum), and how can they be circumvented ? Which are the sputtering mechanisms leading to the emission of large organic ions ? What are the roles of the substrate on the sputtering and ionisation processes in the case of ultrathin films ? Are there important matrix effects connected to the substrate nature and chemical environment ? The wish to answer all the questions listed above is certainly ambitious, but a first look into these matters is required before to start the investigation of new materials by SIMS.

To address these issues, the first part of the results will be devoted to the elucidation of the emission processes for molecular ions sputtered from thin organic films bombarded by keV primary ions. Information will be obtained from the detailed analysis of the yield and kinetic energy distribution of the sputtered species, from high fluence ion beam bombardment studies and from the correlation between SIMS, XPS and XRR data. We will show that several sputtering processes take place, including direct emission of intact precursor-like fragments, extensive fractionation of the more excited ejecta, delayed dissociation in the vacuum, ejection of large parent-like ions, etc. The substrate effect and the secondary ion information depth will be investigated, too. Concerning the latter, we will show that large molecular ions are more surface specific than monoatomic ions, which have a larger emission depth. This fundamental approach of the SIMS experiment will constitute the basis for a more applied study of polyelectrolyte multilayers.

## **I.1.2. Outline**

---

The following notes will address two separate topics, referenced by letters A, for the fundamentals of ion emission in Static SIMS, and B, for the applied study of polyelectrolyte multilayers by SIMS and XPS.

The first part of the thesis will start with the literature review concerning the sputtering and ionisation processes in SIMS, the different kinds of organic mono- and multilayers, the alternate polyelectrolyte physisorption method and the advances of Static SIMS in the field of thin organic films (section I.2). Based on this review, the objectives of the thesis will be more precisely defined in section I.3. Finally, the main results of the thesis in the two above-mentioned directions will be reviewed (section I.4) and general conclusions will be drawn (section I.5).

The detailed results will be presented in the second part of the thesis, in the form of articles. For sake of clarity, indexes of the results and references to the articles will be inserted all along the overview of section I.4.



# I.2.

---

## Literature Review

---

### I.2.A. Fundamentals of Static SIMS

#### I.2.A.1. Historical benchmarks, concepts and applications

The bombardment of solid surfaces by keV and MeV primary particles leads to a complex sequence of interactions which may end up with the sputtering of fragment, parent and cluster ions or neutrals. As an important analytical consequence, the sputtering phenomenon has allowed the development of surface analysis techniques like ToF-SIMS, secondary neutral mass spectrometry (SNMS), fast atom bombardment mass spectrometry (FAB) or plasma desorption mass spectrometry (PDMS).

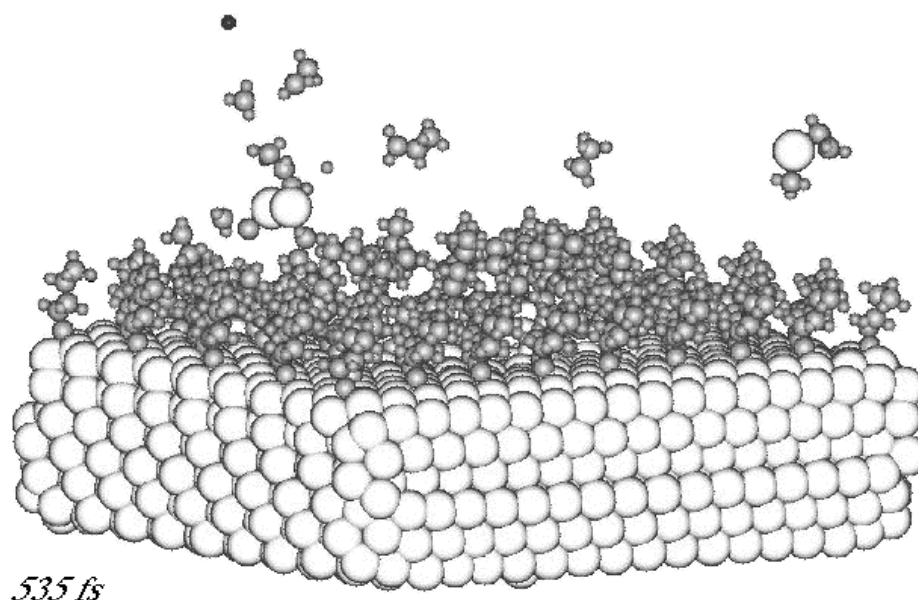


**Fig. 1.** Sputtering of a C<sub>5</sub>H<sub>9</sub> overlayer chemisorbed on platinum;  $t = 5 \times 10^{-13}$  s after the impact of the primary argon ion [1].

Strictly speaking, *sputtering* (or *desorption*) is the transfer of surface material from the condensed to the gas phase as a result of energetic particle bombardment (Fig. 1). Although the phenomenon was first observed by Grove [2] in gas discharges in the middle of the 19th century, the sputtering of a gold cathode by an ion beam was clearly demonstrated much later by Goldstein [3]. Later again, the particle-induced emission of charged particles was evidenced by Thomson, in his article entitled "Rays of positive electricity" [4]. Naturally, sputtering occurs for instance at the surface of celestial bodies and asteroids hit by the stellar wind or, on earth, by the decay of radioactive isotopes producing energetic particles [5]. For example, it has been shown by Voyager spacecrafts that sputtering of the iced moons of Jupiter and Saturn by energetic ions trapped in the planets magnetospheres was one source of the plasma torus found around these planets [6,7]. Sputtering by low energy oxygen atoms and N<sub>2</sub> molecules also leads to the fast erosion of protective spacecraft materials in the low earth orbit [8]. In the laboratory, sputtering is observed in plasma discharges and thermonuclear fusion technology. It is also used in microelectronics to design microcircuits or micromechanical devices (by etching) and to build thin inorganic coatings (by redeposition) [9]. Other applications of ion beam etching exist in the fields of optical and magnetic devices, biomedicine (implantology), etc.

To characterise the erosion in sputtering, one defines the *sputter yield*  $Y$  as the number of sputtered particles per impinging primary ion. By extension, the *secondary ion yield* is the number of sputtered ions per primary particle,  $Y \times P^\pm$ , i.e. the sputter yield times the ionisation probability  $P^\pm$ . Beside the total and specific yields, other important quantities for the understanding of the sputtering process are the *angle of emission* and the *kinetic energy* of the particles, and their respective distributions. The *internal energy* and *formation time* distributions of the ejecta are very informative too, but difficult to measure. On the other hand, the energy deposition in the solid by the primary particle is described in terms of *stopping powers*, *range* and *straggling*. The stopping power is the energy lost by length unit in the solid,  $(dE/dx)$ . As the energy loss is shared between collisions with nuclei and excitations of the electronic sub-systems, one refers more precisely to the *nuclear*  $(dE/dx)_n$  and *electronic*  $(dE/dx)_e$  stopping powers. The *range* and *straggling* relate to the depth and radius of the primary ion trajectories into the solid.

From the analytical viewpoint, two sputtering regimes are used for material characterisation by SIMS: *dynamic SIMS* uses high primary ion currents, up to some A/cm<sup>2</sup>, to erode the sample and gives an in-depth analysis of the material's chemical composition; in contrast, the aim of *static SIMS* is to get chemical information concerning the uppermost monolayers, with the lowest achievable degradation, and the primary current required does not exceed 10<sup>-9</sup> A/cm<sup>2</sup>. Historically, the first commercial instrument using the detection of sputtered ions to characterise solid surfaces was built by Herzog et al. in 1963 [10]. Static SIMS as a surface analysis technique was introduced by Benninghoven et al. in 1969 [11]. Later on, the ability of MeV and keV primary ion beams to desorb large organic molecules were demonstrated respectively by Torgerson et al. (1974) [12,13] and Benninghoven et al. (1976) [14]. Finally, the adjunction of a Time-of-flight spectrometer to a keV pulsed primary beam was achieved by Chait et al. [15].

In ToF-SIMS, the *mass* of the detected secondary ions is determined by its inertial properties, according to Newton's second law of mechanics,  $F = ma$ . In first approximation, the time-of-flight of a secondary ion of charge  $z$ , accelerated by a voltage  $V$ , in a spectrometer of length  $L$  is directly related to the ion mass  $m$  by the equation:

$$t = L \times [(m/z)/2eV]^{1/2} \quad (1)$$

With a high mass resolution ( $m/\Delta m \sim 10000$ ) resulting from appropriate primary beam bunching, fast detection electronics and efficient compensation of the secondary ion kinetic energy, the recent ToF-SIMS instrument generations allow to distinguish ions with the same nominal mass and to attribute precise chemical compositions to the molecular fragment masses appearing in the spectra. Various examples of the application of Static SIMS, ToF-SIMS and SIMS Imaging to the characterisation of organic materials and polymers can be found in the literature [16,17,18,19,20,21]. Concerning thin organic films, a detailed review will be given in section I.2.B.3.

### **I.2.A.2. Kinetic energy distribution of molecular secondary ions**

In the results part, the kinetic energy distribution (KED) of organic secondary ions will be used to get information about the sputtering process. Therefore, a short overview of the experimental results involving organic ions KED seems useful. First, it must be kept in mind that the KED of secondary ions may always reflect both sputtering and ionisation mechanisms. Excepting the case of preformed ions, the number of secondary ions is then expressed as a function of energy by the general equation:

$$Y^\pm(E) = Y(E) \times P^\pm(E) \quad (2)$$

where  $N(E)$  is the energy distribution of sputtered neutrals and  $P^\pm(E)$  is the ionisation probability. It will be shown in the results that the influence of  $P^\pm(E)$  is negligible for  $C_xH_y^\pm$  organic ions (section II.A.1.1). Nevertheless, the effect of the ionisation mechanism on the KED has been clearly evidenced for atomic ions (see for example refs. [22,23,24] and section II.A.1.4). Empirically, a negative exponential dependence on the inverse of the normal component of the velocity  $v_\perp$  has been most often reported [23,24,25,26,27]:

$$P^\pm(v_\perp) \div \exp(-v_0/v_\perp), v_0 = \text{constant} \quad (3)$$

For inorganic surfaces, the experiments demonstrate that the KED of atomic ions is very broad (FWHM  $\sim 10$ -20 eV) [28,29]. In general, the distributions reported for cluster ions are narrower, shifted to lower kinetic energies and with a faster high energy decrease [28,30]. The KED narrowing with increasing cluster complexity has also been observed [31,32,33,34] and modelled [35] for neutrals. Interestingly, this trend has been verified for carbon clusters sputtered from graphite, too [36].

Although few KED measurements have been reported in the case of organic secondary ions, some general trends can be deduced from the literature. For large parent, fragment and cluster ions sputtered from poly(ethylene glycol), glycerol and various biological compounds, Kelner et al. showed that the KED peaks at 1-2 eV, with a very fast intensity decay beyond the maximum [37,38]. Van der Peyl et al. confirmed the very narrow KED of glycerol molecular and cluster ions (0.3 - 0.7 eV) [39]. They found a high energy dependence in  $E^{-2}$ ,  $E^{-3}$  for the small fragments and in  $E^{-4.5}$ ,  $E^{-5}$  for the large fragments and parents [40,41]. For  $\text{NH}_3$  and  $\text{CH}_4$  sputtered from the corresponding condensed gases, the group of de Vries also found a steeper high energy slope than  $E^{-2}$  [42,43]. In the study of tetrabutylammonium bromide, Gillen detected secondary ions with a kinetic energy deficit, indicating the gas-phase decomposition of sputtered fragments and molecules [44]. These unimolecular dissociation reactions will be discussed in details in the results (section II.A.2).

No detailed studies, but singular reports exist for large hydrocarbon molecules and polymers. First, Briggs and Wootton measured the KEDs of hydrocarbon fragment ions sputtered from paraffin wax [45]. Although the energy resolution was poor, indicating either an experimental limitation or a charging effect, the broadening of the KEDs with decreasing ion size could be evidenced by these authors. For poly(ethylene terephthalate) (PET), Brown and Vickerman showed that the KED of the characteristic fragment  $\text{C}_6\text{H}_4\text{COO}^-$  was narrower than those of atomic ( $\text{C}^-$ ) and smaller fragment ions ( $\text{C}_2\text{H}^-$ ) [46]. Finally, similar effects were observed by Gilmore and Seah for poly(tetrafluoroethylene) (PTFE) [47].

The same year as our first paper on the subject (section II.A.1.1), Zubarev et al. presented integral KEDs of small  $\text{CH}_y^+$  fragments sputtered from a peptide bombarded by 25 keV  $\text{Ga}^+$  primary ions [48]. In these results, the mean kinetic energy of the secondary ions decreases drastically with increasing hydrogen atoms number  $y$ . It is interesting to note that the same effect was *not* observed by these authors for MeV primary beam excitation. Concerning MeV ion bombardment, the impressive work of Papaléo et al. has to be mentioned, too. From *radial* velocity distribution measurements, these authors also deduced a periodic variation of the  $\text{C}_x\text{H}_y^+$  and  $\text{C}_x\text{H}_y\text{F}^+$  fragments (radial) KE as a function of the hydrogen atoms number  $y$  for poly(vinylidene fluoride) (PVDF), poly(ethylene) (PE) and poly(styrene) (PS) targets [49,50]. The results were interpreted in terms of primary ion energy deposition at the surface and primary ion track structure. An attempt to model the spatial distribution of the energy around the primary impact point was made, too [51].

In summary, the kinetic energy distributions of polyatomic ions sputtered from organic and polymer targets under keV ion bombardment are narrow, centred around 1-2 eV, and with a sharp cut-off on the high energy side. Moreover, the literature suggests that there could be a correlation between the size and specificity of the secondary ions and the mean kinetic energy of the distributions. The gas-phase decomposition of sputtered particles has been highlighted, too. These features will be discussed hereafter from the viewpoints of the theoretical models (following section) and of the new results obtained in our group (sections II.A.1 - II.A.3).

### **I.2.A.3. Models of molecular secondary ion emission**

#### I.2.A.3.1. Secondary ion emission

The aim of this section is to give an overview of the models developed to explain the 'complex sequence of interactions' mentioned in the introduction. In theory, the particle-induced emission of secondary ions can be described by a chronological sequence of processes involving the primary particle and the target atoms:

- (i) Charge exchange between the incoming particle and the sample surface;
- (ii) Energy deposition in the target;
- (iii) Motion of the target atoms;
- (iv) Transfer of momentum towards the surface;
- (v) Bond-breaking and secondary particle emission;
- (vi) Charge exchange between the departing particle and the surface;
- (vii) Unimolecular dissociation of excited secondary ions.

In the following, a brief description of the different stages of the process will be given. More attention will be paid to the models proposed in the literature for the second part of the process, concerning the secondary ion ejection itself.

#### I.2.A.3.2. Charge exchange between the primary particle and the surface (i)

Primary particles approaching the surface may first neutralise by surface-particle electron transfer. Although this process might accelerate organic surfaces degradation by the creation of electronically excited states, its effect on the kinetic energy of keV and MeV primary ions, governing nuclear and electronic stopping, is insignificant. In this respect, it has been shown by Della Negra et al. that the influence of the primary ion charge state ( $\text{Ar}^+$  to  $\text{Ar}^{11+}$ ) on the secondary ion yield of valine was negligible [52].

#### I.2.A.3.3. Energy deposition in the target (ii)

The kind of energy deposition mechanism is governed by the kinetic energy (or velocity) of the primary particle.

When the primary particle velocity ( $v$ ) is higher than the Bohr velocity ( $v_B = 0.22 \text{ cm/ns} = \sim 25 \text{ keV/u}$ ), as in PDMS, the primary particle interacts mainly with the electrons of the target. An important part of the energy is deposited in a cylinder of  $\sim 5 \text{ \AA}$  radius (positively charged infratrack), whereas the remaining is transferred into a much larger cylinder (ultratrack) by energetic secondary electrons [53, 54].

When  $v < v_B$ , as in SIMS and FAB, energy is lost predominantly by nuclear stopping, i.e. by elastic collisions with the screened nuclei of the solid. In both cases, the medium surrounding the projectile path receives a very high energy density which causes extensive molecule fragmentation.

#### I.2.A.3.4. Target atoms motion (iii)

In keV projectile bombardment, the atoms of the target are directly set in motion by the collision with the primary particle (billiard balls). High energy secondary particles may be emitted by a direct recoil process (knock-on) [55], i.e. by a transfer of momentum from the primary ion. However, the emission of fragile molecular ions by such a process is unrealistic. Instead, energetic recoil atoms penetrating into the solid may displace other target atoms, leading to a succession of binary elastic collisions in the solid, also called *collision cascade* [55]. By this cascade process, the primary particle energy transferred to the target may gradually diffuse in the surface region. One distinguishes *linear cascades*, where the collision sequences do not spatially overlap, from *thermal spike* regime, where a large overlapping of the cascades occurs. In the spike regime, the excited volume behaves like a dense gas at high temperature [56].

The linear collision cascade model, developed by Thompson [57] and Sigmund [55,58] and based on elastic binary collisions, is the most widely accepted theory describing energy transfer and secondary particle emission in Static SIMS. Indeed, in this technique, very low primary ion currents are used to prevent cascades overlapping. The particularity of Sigmund's model is to treat the successive collision processes in the framework of Boltzmann's transport theory. Owing to Boltzmann's equation, he could determine the statistical function  $f(r,v,t)$  giving the average state of particles with time. With this statistical formalism, the initial conditions for the subsequent collisions at time  $t$  are determined solely by the function  $f(r,v,t)$ , and not by the detailed configuration of particles (assumption of molecular chaos). The input data are the collision cross-sections (Thomas-Fermi-type at high energy and Born-Mayer-type at low energy) and the binding energies in the solid. As it is the case in Thompson's treatment too, the solution of Boltzmann's integral equation shows that the energy dependence of the recoil atom distribution in the solid scales as  $E^{-2}$ .

In the case of MeV primary ions, the motion of the target atoms is caused indirectly by the relaxation of the electronically deposited energy [53]. The conversion of electronic excitation into nuclear motion can be achieved by several mechanisms: relaxation of repulsive electronic states (Coulomb explosion); coupling to vibrational excitation leading to molecular expansion and motion; self-trapping of excitons and coupling to phonons, etc. For high excitation densities, the deposited energy flows rapidly in the ultratrack, because the energy gradient in the infratrack is very high.

#### I.2.A.3.5. Transfer of momentum towards the surface and molecular secondary particle emission (iv-v)

##### *a) KeV primary ions*

In the thermal spike model, the energised region, where all the target atoms are set in motion, can be described by a local temperature  $T$ . The energy diffusion by heat conduction leads to the cooling down of the impact region and to the secondary particle

emission by single molecule evaporation or by bulk desorption. In such a case, the relation between the yield and the stopping power is non-linear. The kinetic energy distribution of secondary ions is expected to follow a Maxwell-Boltzmann distribution. Examples in which the thermal contribution is significant have been given by Hofer [59] and by Betz et al. [60].

In the collision cascade model, the ejection of low-energy ( $< 10$  eV), secondary particles is caused by collision sequences intercepting the sample surface. Amongst the success of Sigmund's theory, one may notice the correct prediction of yields and energy of the sputtered atoms as a function of target and primary particle features (nature, energy and even angle). For example, the KED of atoms sputtered by this process show a maximum at the half of the binding energy  $E_b$ , a linear increase below the maximum and a  $E^{-2}$  dependence beyond the maximum, which is experimentally verified. Again, it is worth mentioning that the same high energy dependence had been first derived by Thompson when calculating the flux of atoms refracted by a planar surface barrier, as a result of binary collisions in the solid [57].

However, some authors have argued that the restriction of the collision cascade model to binary collisions might be too simple, especially in the later stages of the process [61]. Moreover, the atomic picture becomes erroneous at the end of the cascade, when strong intramolecular bonds play a dominant role. Therefore, the application of the collision cascade theory to the emission of large molecular species is not straightforward.

The steeper energy dependence of sputtered molecules and clusters as compared to atoms has led to alternative collisional models of emission. Very soon, the two ideas of direct (non-reactive) emission [62] and recombination [63] after ejection have been proposed to explain the clustering process for inorganic targets. One of the first attempts to quantitatively describe the kinetic energy distributions of sputtered clusters has been formalised by Können et al. [64]. These authors consider a system of  $k$  particles receiving  $k$  uncorrelated momenta from the same collision cascade. To model the molecular character of the ejectum, they use a simple condition for the cluster association and stability: if the relative energy of the particles exceeds the dissociation energy, the molecule is unstable. This criterion has been commonly used in the subsequent treatments of molecule sputtering, too. For example, the model of Können describes accurately the steep decrease of the yield of  $W_3^+$  clusters at high energy, but it presents a marked discrepancy with the data at low energy.

More qualitatively, Rabalais et al. [65,66] used a similar recombination concept and described the clustering mechanism as an adiabatic expansion into the vacuum. They introduced the notion of 'selvedge', as a diffuse boundary between the solid and the vacuum in which rearrangement can occur. These concepts were applied to the sputtering of alkali halide, frozen water, benzene and cyclohexane clusters. In addition to recombination, they recognised the existence of non-reactive ejection and cluster fragmentation in the gas-phase [67].

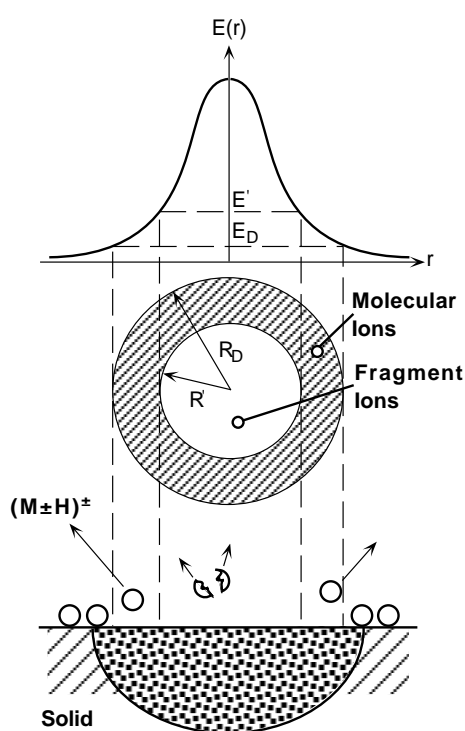


**Fig. 2.** Precursor model for parent-like ion emission. The energy distribution  $E(r)$  represents the average kinetic energy transmitted by a collision cascade to a surface molecule.  $E(r)$  does not describe one single impact process, but averages a large number of events. (adapted from Ref. [68]).

For large molecules, the concepts of violent ejection, leading to fragmentation, as opposed to the emission of intact molecules by softer mechanisms have been rationalised by Benninghoven in the precursor model [68], in which these processes are correlated to the distribution of the cascades energy at the surface. According to the shape of this distribution, extensively fragmented ions are produced near the primary impact point whereas intact molecular ions are formed farther away (Fig. 2). In the same optics, the steep energy dependence also observed for molecular ions which can not originate from recombination processes, was qualitatively explained by Haring et al. by fragmentation [42,69]. Their argument, i.e. *the fragmentation probability increases with increasing molecule kinetic energy, leading to a depletion of the high energy tail of the distributions of molecular species*, involves implicitly a direct correlation between the internal and kinetic energies of the sputtered particles.

Instead, Michl et al. proposed a two-steps mechanism leading first to the prompt knocking out of little energetic fragments, followed by the late, low-energy emission of larger pieces of material due to the induced 'dislocation' of the excited surface region [70]. The emission of this second batch of ions might be reinterpreted as the late evolution of the cascades towards a collision spike. The same group also emphasised that the important damages created along the primary ion track are responsible for the creation of highly reactive species. These are expected to undergo fast reactions with the surrounding molecules, before, during or even after cluster ejection, resulting in the formation of uncharacteristic, complex fragments. Nevertheless, the ideas of Rabalais, Benninghoven, Haring and Michl at that time lacked of quantitative background and, hence, they were hard to verify or to discard.

Later on, Snowdown used Monte-Carlo calculation to simulate angular resolved kinetic energy distributions for selected electronic states of diatomic molecules sputtered by single and double collision [71]. The model enlightens the partitioning of the recoil energy into the internal (vibration and rotation) and the translational energy modes of the molecule, as well as the high-energy cut-off of the kinetic energy distributions due to dissociation of the molecule. Rotational and vibrational excitation of the sputtered molecule are treated extensively in Ref. [72]. With this treatment, Snowdown modelled the experimentally observed characteristics for the energy spectra and evidenced the independence of the spectra on polar ejection angle.

In the case of polyatomic molecules, Haring et al. kept the idea of Können concerning the uncorrelated momenta transferred to each atomic component and they assumed the isotropic  $E^{-2}$  distribution of energies predicted by the collision cascade model for the recoil atoms interacting with the molecule [73]. In this model, the molecule is considered as a structureless, heavy atom if it satisfies the stability criterion. The energy distributions after refraction through the planar surface potential are obtained by numerical integration. As main results, the steep asymptotic behaviour of the experimental kinetic energy distributions is respected ( $E^{0.5-2.5k}$  for  $k$  components molecule) and the energy spectrum of  $Kr_2$  is well described. In addition, Haring gave a correction to the model of Können et al., predicting a  $E^{1-3k}$  energy dependence for clusters with  $k$  atoms. In the same period, Urbassek proposed an analytical model of diatomic molecule emission based on uncorrelated double collision and found a  $E^{-5}$  energy dependence, too [74]. Concerning the sputtering of large clusters, Urbassek also argued that a collective mechanism might operate, leading to the emission of the excited clusters from well-defined, high energy density regions, in the later stages of the cascades [75].

Alternatively, Hoogerbrugge et al. considered the molecule (or cluster) as a system of two bound sub-units receiving uncorrelated momenta [76]. For this system, they calculated analytically the internal and kinetic energy distributions, and found a high energy decrease of the yield scaling as  $E^{-4.5}$ . Experimental molecular ion distributions for NaCl sample dissolved in a glycerol matrix were found to support such a multiple collision process [40].

To explain the emission of large molecules or ions, the relaxation of the deposited energy into the vibration modes of the surface molecules has been invoked, too. For keV primary ions, the vibrational model of King et al. has been quite successfully applied to fit the energy distribution of neutral  $SF_6$  molecules sputtered from a frozen  $SF_6$  target [77,78]. Based on polymer degradation and tandem SIMS studies, Leggett et al. proposed a qualitative model involving similar arguments to explain large molecular ion emission from polymers [79]. According to their description, the macro-radicals created by the primary ion impact can be emitted after transformation of the cascade atom kinetic energy into vibrational energy of bonds at the surface.

For real systems, the development and applicability of analytical models is compromised, because of the rapidly increasing complexity of the equations. Even in the mentioned cases, the physical meaning of the equations and simplifying hypotheses is not always clear, and numerical methods are needed to solve the integrals. In the two last

decades, the fast development of molecular dynamics simulation has brought a new point of view and a detailed information about the collisional emission processes.

For organic adsorbates onto metals, Garrison et al. achieved a very important work. In their early publications [80,81], they found that the ejection of intact benzene adsorbates could be induced by single or multiple collision with substrate nickel atoms. To explain the single collision induced sputtering, they invoked the larger size of the nickel atoms, leading to simultaneous interaction with several carbon atoms of the molecule. The formation of organometallic NiC<sub>6</sub>H<sub>6</sub> clusters was attributed to recombination after ejection. Also, a correlation between fragmentation and kinetic energy was evidenced. For example, the experimental and calculated distributions of C<sub>2</sub>H<sub>2</sub> are broader than those of the original molecule C<sub>6</sub>H<sub>6</sub>, as a result of a more violent emission event leading to fragmentation. The effects of geometry and bonding state were found to be crucial for the emission of the intact molecule [80,82], as observed experimentally by Vickerman for little molecular adsorbates [83]. Recently, Garrison's group found a correlation between the size of the adsorbate and the fraction of sputtered intact molecules for saturated hydrocarbons adsorbed on metal [84]. The lateral motion of the organic ejecta was also highlighted, as well as the subsequent collision-induced fragmentation and chemical reactions often involving hydrogen abstraction [85,86,87].

In the arena of molecular dynamics simulation, the careful study of metal cluster emission by Betz and Husinsky [35] must be mentioned too. For Cu(111) bombarded by 5 keV Ar, they observe the formation of a protrusion at the crystal surface. The detailed analysis of the sputtering events shows that clusters are emitted from the rim of the protrusion, supporting the idea that a highly correlated momentum transfer is the key of large clusters emission, as proposed by Urbassek (*vide supra*). The observed increasing emission time with increasing cluster size also confirms Urbassek's predictions. Last but not least, the calculated energy distributions are in good agreement with the experimental data.

In most of the reviewed models, the effects of the electronic stopping power have been neglected, which could be a too severe approximation in the case of insulating organic and polymer targets [79]. For these compounds, the energy transmitted to the electronic system of the atoms creates excited states, which may be relaxed by fragmentation, or by coupling with the vibration modes of the solid. The consequences are increased degradation and sputter rates. For example, the high susceptibility of PTFE to electronic interactions leads to degradation by preferential sputtering of fluorine [88].

In summary, it appears from the models and observations that the linear collision cascade theory remains well-adapted to describe the first stages of the primary particle-solid interaction, when the energy of the recoil atoms is rather high. However, in the last stages of the cascade, when the energy of the recoil atoms is much lower ( $\leq 10$  eV), the influence of correlated or uncorrelated multiple collisions, chemical and vibrational effects, might become predominant. Because the kinetic and binding energies become similar, the role of chemistry increases, leading to the soft emission of large molecular fragments reflecting the structure of the analyte (Fig. 3). In the following, we will see that the models developed for

MeV particle-solid interactions bring additional concepts which might be transposed to keV ion bombardment.

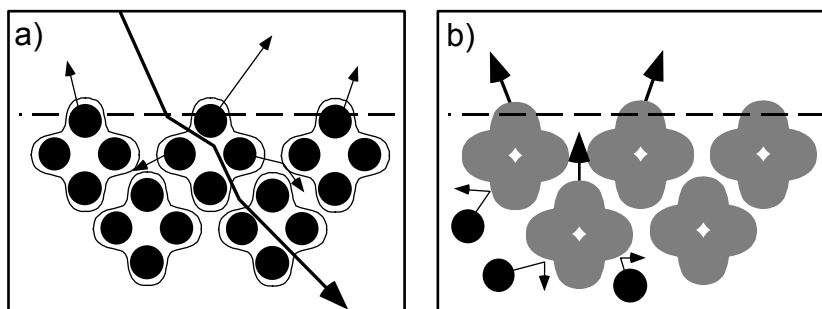


**Fig. 3.** Collision cascade in an organic solid. a) the cascade has an atomic character in the first stages of the particle-solid interaction. b) In the last stages, the cascade becomes 'molecular', because the recoil atoms kinetic energies become similar to the intermolecular bond strengths. Entire molecules are ejected by the combined action of several cascade atoms. Adapted from Ref. [53].

#### *b) MeV primary ions*

In addition to thermal models, two kinds of processes are invoked to explain the desorption of large molecules from organic surfaces in the case of MeV ion bombardment. In the hit theory, the molecule can be desorbed if a sufficient number of secondary electrons interact with it. The condition for desorption is that the interaction with secondary electrons leads to external bond-breaking, keeping the internal bonds intact. This theory accounts for the  $(dE/dx)_e$  dependence of the molecular ion yield at large stopping power, but it fails to explain the  $(dE/dx)_e^3$  dependence of the neutral yield measured for amino acids. Amongst its drawbacks, this model can not explain the great similarity of the mass spectra obtained with MeV and keV ion induced desorption, as the number of secondary electrons is very low in the latter [53]. Following Johnson, this model applies best in the case of low excitation densities (fast primary protons and electrons) [7].

The second category of theories, adapted to higher excitation densities, includes the macroscopic 'shock-wave' and 'pressure-pulse' models, which use continuum mechanics arguments. In the first one, the high energy density deposited within the vicinity of the ion track (spike) leads to the propagation of a supersonic mechanical disturbance through the medium, resulting in the mechanical ablation of material at the surface [53]. As shown by thermodynamical arguments, thermal energy is left in the sample after the release of the compression energy, which can also result in the vaporisation of material from the excited region (thermal desorption). The 'shock-wave' model explains the evolution of the ion yield as a function of stopping-power, angle of incidence and charge state for various biomolecular targets and predicts an energy dependence of the secondary particle yield

scaling as  $E^{-2}$  [89]. Nevertheless, this model needs additional assumptions to account for the cubic stopping power dependence of the measured neutral yields (vide supra). Interestingly, the probability of an energy spike formation, related to nuclear energy loss, has been calculated by Bitenski for keV ion bombardment too [90]. The spike probability is found to increase with the mass of the target, due to higher energy loss. This applies nicely to the case of very thin organic films deposited on a heavy substrate, and might partially explain the molecular yield enhancement observed for such samples.

In the pressure pulse model [91], the kinetic energy directly or indirectly transferred along the primary ion path propagates by diffusion, due to the initial kinetic energy gradient, and the momentum acquired by the molecules is proportional to the time integral of this energy density gradient. Desorption occurs when the energy corresponding to this momentum exceeds the surface binding energy. Consistently with the experiment by Hedin et al. [92], the stopping power dependence of the neutral yield  $Y \sim (dE/dx)e^3$  is predicted by the pressure-pulse model. As mentioned by Wong and Röllgen [93], the pressure pulse model may also account for the ejection of intact molecules in FAB of liquid matrices (spraying process). Although promising, the application of this model to keV ion bombardment needs further developments [94]. It is important to notice that in both 'shock-wave' and 'pressure-pulse' models, the intact ejection of large molecules is ensured by the highly correlated momentum transfer directed towards the surface.

To summarise this section, Table 1 recalls the different models proposed for keV and MeV ion induced particle ejection.

**Table 1.** Sputtering models.

<i>keV primary ions</i>	<ul style="list-style-type: none"> <li>• Collision spike model [55,56]</li> <li>• Linear collision cascade model                             <ul style="list-style-type: none"> <li>• single collision [55,57,58]</li> <li>• multiple uncorrelated collision</li> <li>• direct emission [71,73,74,76]</li> <li>• recombination [64,65,66,67]</li> <li>• multiple correlated collision [75]</li> <li>• fragmentation [42,68,69]</li> <li>• MD simulation [35,80,81,82,84,85,86,87]</li> </ul> </li> <li>• Vibrational model [77,78,79]</li> <li>• Electronic effects [56,79]</li> </ul>
<i>MeV primary ions</i>	<ul style="list-style-type: none"> <li>• Thermal model [53]</li> <li>• 'Electronic' model [7,53]</li> <li>• Shock-wave model [7,89,90]</li> <li>• Pressure-pulse model [7,91,93]</li> </ul>

#### I.2.A.3.6. Charge state of the secondary particles and charge exchange with the surface (vi)

General overviews concerning the different ionisation mechanisms can be found in the literature [56,95,96]. These models are based on different premises, often restricted to selected classes of materials or experimental conditions, and aiming to describe the behaviour of atomic secondary ions. For cluster and molecular ions, the situation is even more complex, as stability effects interfere with pure ionisation effects. The brief review hereafter will be structured as an answer to several questions: (i) Regarding the chronology of the sputtering event, when (and how) does ionisation happen? (ii) After ejection, how can the secondary particle charge state be modified? (iii) What about molecular ions?

##### *a) Ionisation before, during or after ejection*

A first important issue, which remains debated, is to know whether the particle ionisation may occur before, during or after ejection. As will be shown, the answer to this question varies according to the considered material and, in some cases, to the chosen theoretical model.

For elemental targets and medium bombardment energies, Joyes considers that binary collisions in the target might cause a core hole in the sputtered atom, resulting in the subsequent ionisation by Auger deexcitation after ejection (described in [97]). For transition metals, Slodzian also proposes that the atoms escape as neutral species, in an excited autoionising state  $M^*$ . After surface crossing, they can experience deexcitation, following the reaction  $M^* \rightarrow M^+ + e^-$  [98] (vide infra). On the contrary, the same author assumes that the ion state is the ground state for ionic solids. Depending on the distance at which the neutral and ion potential energy curves cross, this state may remain energetically favourable or may not, determining the final state of the particle. This bond-breaking model has been further developed for partially ionic materials, like metal oxides [99].

In contrast, to explain the ion yield enhancement for metal oxide surfaces, Thomas suggests that a large fraction of ejecta leave the surface as neutral molecules (molecular model) [100]. Then, ionisation occurs upon dissociation at some distance of the surface, by similar level-crossing processes as in the bond-breaking model. This model has been extended by Plog and Gerhard, who assume that very few particles can leave their position inside the solid in the ionic state (direct emission), due to the high efficiency of the neutralisation processes directly above the surface (vide infra) [101]. Instead, they give indications based on model calculations that atomic and molecular ionic fragments are due to the dissociation of larger neutral molecules leaving the surface (nascent ion molecule, Fig. 4).

In the SIMS community, the Local Thermal Equilibrium (LTE) model has been widely diffused [102], partly because it fits the experimental data for many different material standards including steel, alloys, multicomponent oxides, etc. Under the assumption of a local thermal equilibrium plasma at the sputtering site, two dissociative reactions are written to explain the production of positive and negative ions, respectively:



Then, the degree of ionisation is calculated using the Saha-Eggert ionisation equation. It is expressed by a negative exponential function of the ionisation potential  $I_p$  for positive ions and of the electron affinity  $E_a$  for negative ions. Despite the success of this model, its physical basis remains uncertain. In particular, there are evidences against the existence of an equilibrium plasma around the primary impact point. Nevertheless, the subsequent developments of the bond-breaking model have integrated the exponential dependence on  $I_p$  and  $E_a$  [103].

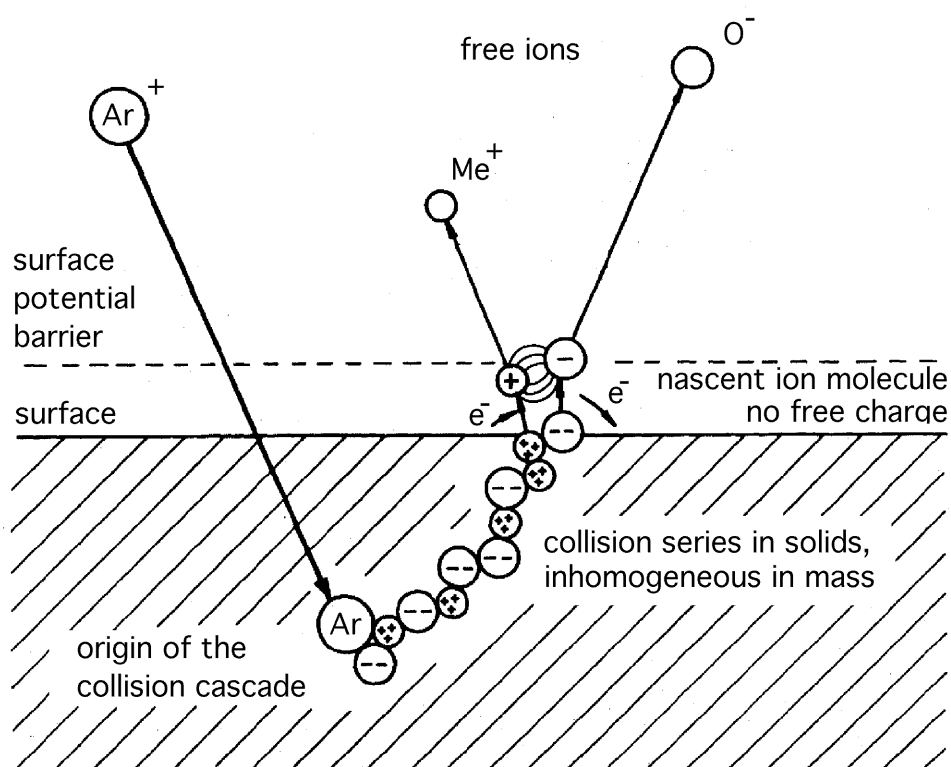


**Fig. 4.** The nascent ion molecule model for metal oxides [101]. As a result of the collision cascade, a neutral molecule leaves the surface and dissociates at some distance, producing a metal cation and an oxygen anion.

#### b) Charge exchange above the surface

The central question of the conservation of the particle charge state after ejection, underlying several of the above-mentioned models, is of particular interest for analytical applications, too. The fast charge exchange processes ( $10^{-13}$  -  $10^{-14}$  s) occurring after desorption have been discussed at length by Rabalais and co-workers (band structure model [67]), and the concepts involved apply to metals as well as insulators. Two types of charge exchange processes are considered, resonance tunnelling and Auger transitions, depending

on the adequation between the energy levels of the particle and those of the solid. In general, both surface-to-particle and particle-to-surface electron transfer may exist. However, the probability of Auger particle-to-surface transitions, in which an electron of the particle is transferred in the solid valence band, promoting a second electron, should be negligible for non-metals, as the valence band of the solid is generally full. For rare gas atomic particles, the survival probability, i.e. the probability to conserve the initial charge state as a function of the distance from the surface, depends strongly on the particle velocity. For typical sputtered particles ( $< 10$  eV) at infinite distance, the calculated survival probability does not exceed 0.1, indicating the importance of the charge exchange processes when a possible transition exists.

*c) Polyatomic secondary ions*

The case of metal clusters has been investigated by Wucher et al., who observe a relative increase of positive charge states versus neutrals with increasing cluster size [104]. The authors explain this behaviour by the corresponding decrease of  $I_p$ . An alternative interpretation is based on the cooling down of the neutral clusters by the emission of an electron. Indeed, this process would also favour large cluster ions since the internal energy excess is more important.

For organic molecules, Cooks et al. argue that preformed ions can escape the surface without fragmentation nor charge exchange, producing intense peaks in the mass spectra [56]. Ion/molecule reactions, ionisation by secondary electrons in the selvedge and later dissociation would account for the other species observed in the mass spectra. The concept of preformed ions is also the basis of Benninghoven's precursor model [68], which explains successfully the variation of the molecular  $(M\pm H)^\pm$  yields for aminoacids adsorbed on metal surfaces [105]. Indeed, the detected species reflect the binding state of the molecules at the surface. Alternatively, ionisation of neutral ejecta by secondary electron capture has been proposed by Spool and Kasai, and it has been applied to the case of fluorinated polyethers [106].

On the other hand, Leggett suggests that the comparison of SIMS with surface analysis by laser ionisation (SALI) might provide some clues concerning the ionisation of molecular ions [107], arguing that the SIMS and SALI spectra [108] should be similar if ionisation occurs after desorption in SIMS. Conversely, the emission of preformed ions in SIMS would lead to different mass spectra from the two techniques. However, it seems that this interpretation is biased by the strong dependence of the ionisation probability on the chemical structure of the ejectum in SIMS, which is different for single-photon post-ionisation in SALI. In fact, the comparison of the SIMS and SALI particle yields would rather provide an estimation of the ionisation probability of molecular fragments, which is partly governed by the relative stability of the ionic state. In the case of PS [108], the predominance of even-mass particles in SALI and not in SIMS probably reflects the relatively high ionisation probability and ion stability of odd-mass hydrocarbons, due to their stable electronic structure as even-electron ions.

#### I.2.A.3.7. Unimolecular dissociation of excited secondary ions (vii)

After ejection, molecular secondary ions often have an internal energy excess, due to the nature of the emission process. If the energy excess is sufficient, these ions may dissociate within the timescale of the SIMS analysis. Such metastable decay reactions are well described by the unimolecular reactions theory [109], which predicts that the number of metastable parents follows a negative exponential law as a function of time. The constant appearing in the exponential law is defined as the rate of dissociation ( $r$ ), and the half-life of the parents is proportional to the inverse of the rate ( $\tau_{1/2} = \ln(2)/r$ ). For a given reaction, the rate of dissociation is correlated to the internal energy in a non-linear fashion [110]. The practical analysis of metastable decay reactions becomes more complicated if the internal energy distribution is broad.

In the field of ion-induced particle desorption, metastable decay processes have been investigated by several authors for organic [44,48,111,112,113,114,115] and inorganic samples [116,117,118,119], using keV and MeV primary ions. In these works, the nature and importance of the metastable decay processes and, in several cases, the decay rates and lifetimes of the parent ions have been studied.

In the results part, I will show that several ideas presented in paragraphs I.2.A.3.5 and I.2.A.3.7 may be developed to account for the kinetic energies of molecular fragment (section II.A.1) and parent ions (section II.A.3) sputtered from organic and polymer thin films and to explain the energy deficits due to unimolecular dissociation observed in the secondary ion energy spectra (section II.A.2).

## **I.2.B. Organic Multilayers**

---

### **I.2.B.1. Ultrathin organic coatings and supramolecular organisation**

#### I.2.B.1.1. Molecular scale engineering: technology and applications

During the last decades, the techniques of engineering at the molecular scale have acquired an ever growing importance. Gradually, the materials sciences have introduced organic and polymeric materials as new candidates for high-tech applications, leading to a new world of organic or composite assemblies beside metals and inorganics. In this context, three powerful methods for producing ultrathin organic multilayers by a wet process have emerged [120,121]: the Langmuir-Blodgett technique [122], the self-assembly by chemisorption [123] and, recently, the alternate polyelectrolyte physisorption [124,125]. These will be described in section I.2.B.1.2.

In parallel, alternative techniques for organic and polymeric coatings elaboration have been developed too. In the case of polymers, ten nm to  $\mu\text{m}$  thick ordered and disordered coatings are obtained by epitaxial polymerisation from vapour deposition [126] and by plasma-enhanced vapour deposition (plasma polymers) [127,128], respectively. Very thin coatings and submonolayers can be prepared by the evaporation of organic molecules onto substrates in vacuum chambers, too [120,129,130]. Spin-coating from solution leads to micron and submicron film thicknesses with many polymers. At the other extreme, polymerisation at the interface between a monomer solution and a crystalline solid produces ultrathin films (nm thick) of highly oriented polymers [131,132]. These alternative methods will not be discussed here.

In general, the three techniques quoted in the first paragraph have not passed the door of industry yet, but there exists an important potential in various areas: in the biomedical field, first, because these new objects can mimic the living world [133,134]. Indeed, organic multilayers can be made of the same materials as cells, e. g. Langmuir-Blodgett (LB) layers of fatty acids, phospholipids and even proteins (streptavidin) [120]. The similarity between "living" and artificial supramolecular assemblies is illustrated in Fig. 5. Among the applications, organic mono- and multilayers may serve as biomaterials, biosensors [135,136,137], bioreactors [138], or bioelectronic components [139] and may constitute very specific devices for molecular recognition in general [140,141,142]. In this respect, polypeptides [143], DNA [144,145], proteins and enzymes [146,147,148,149,150, 151,152], blood constituents [153] and even viruses [154] have been immobilised in polyelectrolyte multilayers. Biospecific recognition of streptavidin by biotin has been achieved with polyelectrolyte multilayers too, by grafting biotin to a poly-L-lysine-based polycation [155]. On the other hand, patterned self-assembled monolayers (SAMs) have been shown to constrain cell attachment and growth [156].

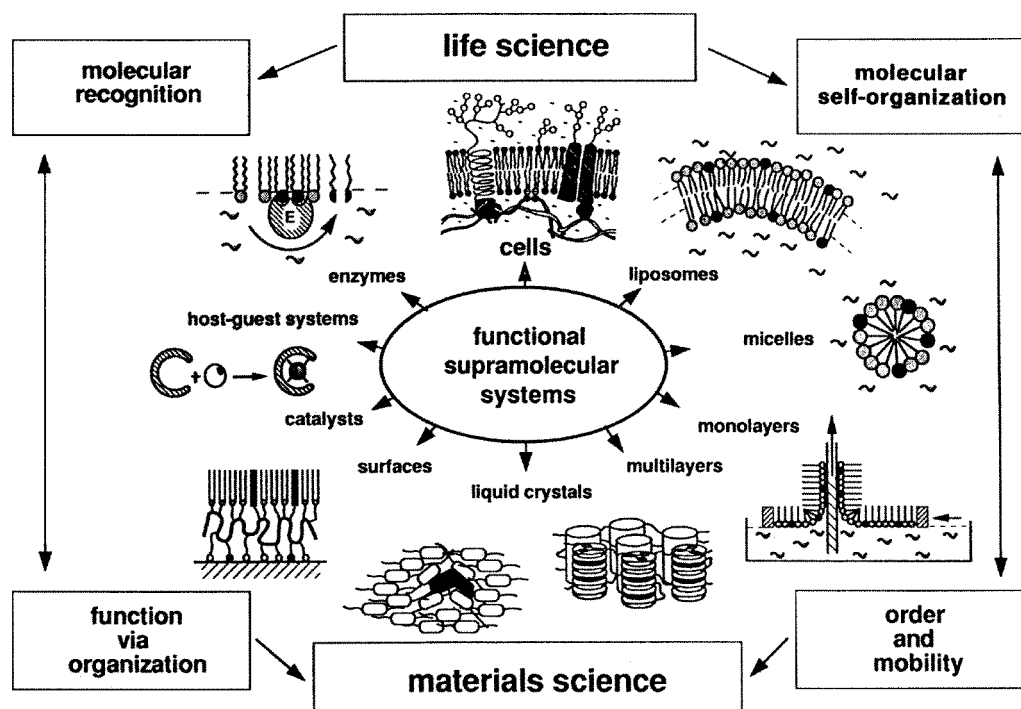


**Fig. 5.** Supramolecular organisation. The similarity between living and artificial assemblies [133].

In the microelectronics area, SAMs are used for patterning by photochemical methods, by microcontact printing and by micromachining with modified AFM tips [157]. Polymerisable fatty-acids LB films find an application as photo- and electron beam resists too [120]. Concerning polyelectrolyte multilayers, conjugated polymers have been deposited in alternance with polyanions to form two-dimensional conducting layers [158,159], reaching up to  $300 \text{ Scm}^{-1}$  conductivities [160]. The same group has also created light emitting diodes (LEDs) based on multilayered structures containing poly(p-phenylene vinylene) (PPV) in which the properties of PPV, e.g. the emission wavelength, are tuned by the choice of the polyanion [161,162]. The application of physisorbed multilayers to LEDs is certainly promising [163,164,165,166].

Particular optical properties are obtained by the incorporation of dyes in multilayers [143,167,168] and the use of special chromophore-bearing polyions, allowing for non-centrosymmetric ordering, leads to significant second harmonic generation [169,170,171,172]. In the same domain, non-centrosymmetric LB multilayers with significant second harmonic generation can be achieved by alternating layers of different compounds (ABAB...) [120]. Photoresponsive and non-linear optic-active assemblies are made with SAMs, too [173,174,175]. On the other hand, rigid-rod LB films of polyglutamates and phtalocyanines show promising properties suggesting applications as optical memory and transistor-based pH sensor, respectively [122]. Among others, SAMs are also used in electrocatalytic applications [176]. In a different area, LB optical gas sensors [177] as well

as gas separation membranes [178] and chemical sensors [179] using polyelectrolyte multilayers have been elaborated.

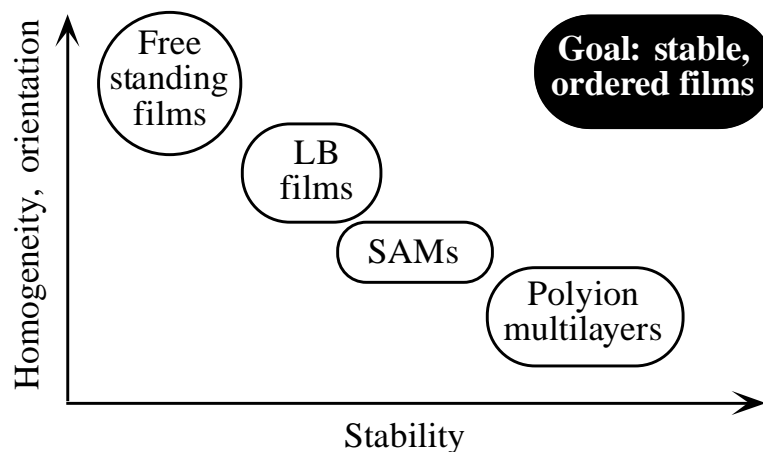


**Fig. 6.** Comparison between different types of organised films. Adapted from [180,181].

Although organic multilayers appear very versatile and suggest a variety of potential applications, their development is often hampered by several factors: the complexity of the methods, the need of specialised equipments and characterisation tools, the limited number of appropriate substrate-multilayer pairs. Moreover, the limited structural quality and/or stability of the assemblies constitute severe obstacles in most of the applications. For example, the lack of resistance against heat, radiation and chemical reagents, and the propensity to rearrangement, are common drawbacks of highly organised films. To illustrate this, Fig. 6 gives a classification of the methods with respect to organisation and stability [181]. Very well ordered freely suspended (FS) films of liquid crystals are the less stable. The degree of order decreases, but the stability increases, when going to transferred FS and LB films, SAMs and polyion complexes. Of course, the goal of industry is to bring these two aspects together in a single material.

In the following, the other characteristics, advantages and drawbacks of the Langmuir-Blodgett, self-assembly and alternate polyelectrolyte physisorption techniques will be described and compared.

#### I.2.B.1.2. Methods for producing organised multilayers.

The *Langmuir-Blodgett* technique holds its name from the scientists Irving Langmuir, who studied the behaviour of amphiphilic compounds at the air/water interface, and Katharine Blodgett, who first discussed the properties of multilayers of these

compounds built-up on a solid substrate [182]. In this technique, amphiphilic molecules are spread at the air/water interface of the trough, and they are compressed to form a solid-like interphase in which the molecules are aligned by the interaction with the nearest neighbours. Then, the film is transferred onto a solid surface by dipping a hydrophobic or hydrophilic substrate through the air/water interface (Fig. 7). Multilayers are obtained by repeating the last step of the procedure.

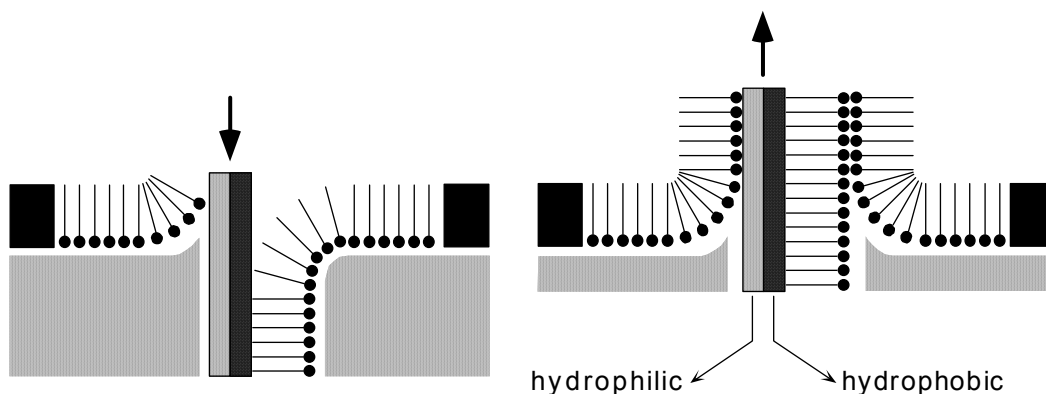


**Fig. 7.** Langmuir-Blodgett technique. Transfer of the compressed film onto the substrate.

The transferred films are ordered, with a uniform thickness, but often polycrystalline because the compression stage on the water subphase leads to the formation of numerous islands of two-dimensional crystals. Beside a limited thermal and mechanical stability and a poor resistance to solvents, the layer quality may also suffer from pinholes or defects which worsen when the layer number increases. In addition, the coexistence of different crystalline phases at the air/water interface as a function of the surface pressure demonstrates that these 'simple' systems may well be highly complex in reality [122]. Recently, the development of sophisticated characterisation techniques like AFM imaging allowed to revisit the various lattice structures of fatty acids LB films [183].

To solve the problems of instability and chemical resistance, films of polymerisable molecules (e.g.: diacetylene) have been designed. However, the polymerisation of the monomers, for instance by UV or electron irradiation, has been found to induce stress in the layers, which may even lead to cracks [120,184]. Alternatively, polymer films have been directly formed on the water subphase and transferred onto substrates. In this case, the self-organisation can be driven either by the amphiphilic side groups or by the polymer backbones (rigid rods) [121]. To further improve thermal and mechanical stability, limited for instance by the presence of long alkyl chains, particular polymers have also been designed, in which pyrolytically sensitive groups were missing [185,186]. Although the desired resistance is greatly improved by this means, the problem of grainy structure remains. On the other hand, the self-alignment of rigid rod polymers in the dipping direction results in anisotropic layers, where the rigid backbones are 'embedded in a continuous matrix of liquid-like side chain segments' [122]. For example, rigid rod LB films are based on phtalocyanines, polypeptides, cellulose or polysilanes.

Siloxane multilayers based on the *self-assembly* technique have been first elaborated by Netzer and Sagiv in 1983 [187]. They prepared a surfactant with a trichlorosilyl head group, an hydrocarbon body and terminated by a an ethylenic double bond. A layer of this compound was epitaxially chemisorbed on the hydroxyl-terminated glass substrate after hydrolysis of the chlorinated head and it was cross-linked. In the second step, the double bond was activated to graft hydroxyl end groups, restoring the surface for a new chemisorption step. Alternatively, alkyl chains with a triethoxysilyl head were used instead of chlorosilanes. Other variants of the technique have been developed but, due to the fast degradation of the layer quality, the thicker assemblies did not exceed some tens of layers. Nevertheless, silanol-based SAMs continue to be studied currently [188].

There are two inherent limitations to the method of Netzer and Sagiv, which may be valid for chemical self-assembled multilayers in general: (i) the epitaxial growth is observed for few surfaces (glass, silicon oxide, aluminium oxide, mica, zinc selenide, germanium oxide and gold [123]), restricting the application of the method; (ii) the optimum multilayer build-up requires a 100 % reaction yield in the second step of the process. Otherwise, defects appear and grow with the layer number, which finally prevent any deposition. To solve the second problem, Sagiv and co-workers have recently proposed a new kind of silane multilayer based on interlayer hydrogen bonding and allowing for the intercalation of a controlled number of silane bilayers in the initial assembly [189]. Multilayers have also been built up using a first layer of phosphate-ended silanol chemisorbed on silicon oxide, followed by successive layers of bis-phosphonic acid which were cross-linked by the reaction with  $ZrOCl_2$  [190]. Also using the zirconium-phosphonate interaction, Katz et al. built up NLO-active multilayers with more than thirty layers of a phosphonic acid-terminated dye [191].

In the same period as Netzer's finding, Nuzzo and Allara reported on the chemisorption of close-packed monolayers of disulphides on gold [192]. Later on, layers of alkanethiols on gold were obtained and extensively characterised, showing well organised, defect-free structures for the longest alkyl chain molecules [193]. To overcome the relative fragility and increase the cohesion of sulphide-anchored layers, strategies have been recently developed involving, for instance, polymerisable thiols [194] or polymers containing sulphide residues [195]. The interest in thiol-based SAMs has not decreased these last years, as witnessed by the number of related publications addressing fundamental questions concerning, for instance, adsorption kinetics [196], lattice structure [197,198] or bonding types [199,200]. Extensive characterisation of thiols and disulphides by SIMS has been performed, too (see section I.2.B.3.3). One of the reasons of these efforts is probably the diversity of functionalised sulphide layers [201], making them perfect model systems in the fields of molecular recognition and biosensors, but also good candidates for optical and electronic applications [202]. However, the elaboration of multilayers based on sulphur compounds is more demanding. Although they are also capable of forming ordered monolayers, the same is true for fatty acids adsorbed on aluminium oxide surfaces [203].

The successive physisorption of alternate layers on a charged substrate, based on electrostatic interactions, has been pioneered by Iler in his article 'Multilayers of Colloidal Particles' [204]. In the early 1990s, Decher et al. extended this concept to ionic amphiphiles [205] and polymers [206,207], giving rise to the *alternate polyelectrolyte physisorption* method. The principle of this step-by-step deposition technique is very simple (Fig. 8): first, a charged substrate is dipped into an oppositely charged polyelectrolyte solution, which results in the adsorption of a thin polyelectrolyte layer owing to electrostatic interactions. If overcompensation of the substrate charges occurs, the adsorption of this layer leads to a reversal of the surface charge polarity, and a second polyelectrolyte layer with the opposed charge sign can be adsorbed. Again, the successful charge overcompensation at this second adsorption step restores the initial surface polarity, and the two-steps adsorption cycle can be repeated. The crucial point of charge reversal will be discussed in section I.2.B.2.1.

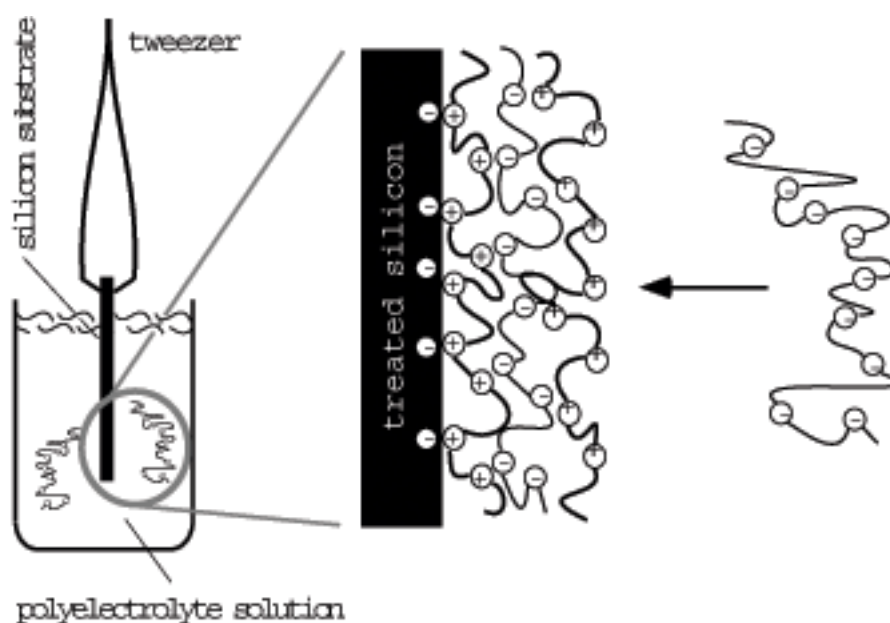


**Fig.8.** Step-by-step method for alternate polyelectrolyte physisorption.

With this method, very thin polymer layers ( $\sim 1$  nm) and complex supramolecular assemblies (more than 100 layers) may be designed [207]. In comparison with the traditional LB and SA systems, the use of polymers reduces the degree of order in the layers. Nevertheless, stratified layered structures with a limited roughness are easily obtained [208], and means to improve the lateral order in the layers are proposed. As suggested in the introduction, the method is very versatile and composite multilayers may be built by replacing one or both of the polyelectrolytes by different organic or inorganic materials. In contrast with the LB and SA techniques, no special equipment or complex procedure are required, and the substrate shape is not a limiting factor, which is beneficial for potential applications. Some fundamental aspects of the alternate (poly)electrolyte physisorption will be reviewed in the following.

To summarise this section, Table 2 compares the properties, advantages and drawbacks of the different methods, which can be seen as competitors for various applications, but also as complementary to some extent. This becomes apparent, for instance, when returning to Fig. 6: indeed, the performances of the techniques balance between very high order, but poor stability, and good stability, but lower order, so that they involve slightly different application areas.

**Table 2.** Properties of the multilayer elaboration methods (adapted from [121,209]).

Langmuir-Blodgett (LB)	Self-Assembly (SA)	Polyelectrolyte Physisorption
<p>Interaction:</p> <ul style="list-style-type: none"> <li>- hydrophobic, Van der Waals (weak, low specificity)</li> </ul> <p>Materials:</p> <ul style="list-style-type: none"> <li>- subphase insoluble</li> <li>- can be compressed in 2D film (amphiphiles, lipids)</li> <li>- hydrophobic or hydrophilic substrates</li> </ul> <p>Organisation:</p> <ul style="list-style-type: none"> <li>- high level of intra- and interlayer ordering</li> <li>- pinholes and imperfections, persist with thicker films</li> </ul> <p>Stability:</p> <ul style="list-style-type: none"> <li>- limited mechanical, thermal and chemical stability</li> </ul> <p>Coating thickness:</p> <ul style="list-style-type: none"> <li>- nm to <math>\mu\text{m}</math></li> </ul> <p>Others:</p> <ul style="list-style-type: none"> <li>- low molecule and substrate limitation</li> <li>- size and shape limitations</li> <li>- special equipment</li> <li>- 2 steps physical process</li> </ul>	<p>Interaction:</p> <ul style="list-style-type: none"> <li>- covalent bonds (strong, high specificity)</li> </ul> <p>Materials:</p> <ul style="list-style-type: none"> <li>- specific molecules (sulphides, silanes) and supports</li> </ul> <p>Organisation:</p> <ul style="list-style-type: none"> <li>- high level of intra- and interlayer ordering (silanes)</li> <li>- defects, degrade with thicker films (silanes)</li> </ul> <p>Stability:</p> <ul style="list-style-type: none"> <li>- good mechanical, thermal and chemical stability</li> </ul> <p>Coating thickness:</p> <ul style="list-style-type: none"> <li>- nm to tens of nms</li> </ul> <p>Others:</p> <ul style="list-style-type: none"> <li>- important molecule and substrate limitation (epitaxy)</li> <li>- limited layer number</li> <li>- 2 steps chemical process</li> </ul>	<p>Interaction:</p> <ul style="list-style-type: none"> <li>- electrostatic (medium strength, medium specificity)</li> </ul> <p>Materials:</p> <ul style="list-style-type: none"> <li>- charged adsorbates and substrates* (amphiphiles, polyelectrolytes, biomolecules, colloids...)</li> </ul> <p>Organisation:</p> <ul style="list-style-type: none"> <li>- stratified layers</li> <li>- poor lateral organisation</li> <li>- defects, anneal with thicker films</li> </ul> <p>Stability:</p> <ul style="list-style-type: none"> <li>- good thermal, mechanical and chemical stability</li> </ul> <p>Coating thickness</p> <ul style="list-style-type: none"> <li>- nm to <math>\mu\text{m}</math></li> </ul> <p>Others:</p> <ul style="list-style-type: none"> <li>- low molecule and substrate limitation</li> <li>- every size and shape</li> <li>- simple equipment</li> <li>- 2 compounds</li> </ul>

\*not always required.

### **I.2.B.2. Multilayer buildup by adsorption of alternate polyelectrolytes**

The elaboration of organic multilayers by alternate adsorption of oppositely charged polyelectrolytes is a very new technique and yet impressive efforts have been developed to investigate its properties and applications. This is reflected by the rapidly increasing number of publications in the field. In this section, the basic concepts of polyelectrolyte adsorption and the abundant literature concerning physisorbed multilayers will be reviewed.

#### I.2.B.2.1. Polyelectrolyte adsorption

The *polyelectrolytes* are macromolecular compounds bearing a large number of ionisable groups when dissolved in a polar solvent. To respect the condition of electroneutrality, these macromolecules are accompanied by a cloud of low molar mass *counterions*. The distinction is made between *strong polyelectrolytes*, fully charged in solution, and *weak polyelectrolytes*, partially dissolved in pure solvent, and for which the degree of dissociation can be conveniently tuned by addition of a strong acid (HCl) or base (NaOH). In general, the polyelectrolytes (polyions) adopt an extended configuration in solution as a result of the mutual Coulomb repulsion between charged segments. The addition of neutral salt in the solution restores symmetric polymer coils, because the electrostatic repulsions are then shielded by the salt.

The *adsorption* of a polymer on a solid substrate, i.e. the transfer of a macromolecular chain to the surface from solution, is the result of the competition between low-mass (solvent) and high-mass molecules (solute) adsorption. In comparison with a small molecule, the entropy loss per molecule upon adsorption is greater for a macromolecule, but it is compensated by the important energy decrease due to the multiple attachment of the macrochain. In practice, the replacement of several solvent molecules by a polymer chain leads to a decrease in free energy, related to the entropy gain associated with the return of a large number of solvent molecules to the solution.

For polyelectrolytes, two situations must be distinguished. The adsorption of a polyion onto an oppositely charged surface is strongly favoured, because it permits the counterions of the polymer *and* of the substrate to return to the solution, which leads to an important entropy increase. To maximise this gain, a quantitative charge compensation is expected (ion-exchange theory), but we will see that it does not occur in most cases. On the other hand, the role of the electrostatic interactions is twofold: as already mentioned, the attraction between polyion and surface opposite charges favours adsorption, but, in contrast, the repulsion between polyelectrolyte charges hinders it. Both of these effects favour a flat conformation on the surface. With the increase of the ionic strength, these two influences vanish gradually, resulting in more 'loopy' conformations, and, at high salt concentration, the non-electrostatic affinities may become predominant [210].

In contrast, the adsorption of a polyion onto an uncharged surface is far less evident. In this case, the polyion is removed from the solution with its counterions, to respect the condition of electroneutrality, and there is no entropy gain anymore. Unless large

interaction energies with the substrate are involved, the adsorption is poor. When salt is added to the solution, the shielding of the electrostatic potential often leads to a more efficient adsorption.

In a recent study concerning polyelectrolyte adsorption on oxide surfaces (SiO<sub>2</sub> and TiO<sub>2</sub>), Hoogeveen et al. concluded that the adsorbed amount is a function of all the present interactions, electrostatic and non-electrostatic [211]. The important parameters governing adsorption are then the linear charge density of the polyelectrolyte, the surface charge density, the ionic strength of the solution (electrostatic), and the particular chemistry of the polymer and the surface, which may favour hydrogen bonding, hydrophobic or van der Waals interactions, etc. (non-electrostatic). A subtle change in one of these parameters may modify the conditions of adsorption. In addition to these interactions, the intrinsic polyelectrolyte flexibility or stiffness, steric features and propensity to organisation also related to the chemical structure will influence the molecule conformation in solution and at the surface [212]. Therefore, the case of polyelectrolytes is particularly complex, although the general trends of their behaviour can be deduced from models based on the electrostatic interactions.

The limited *reversibility* (adsorption hysteresis) is another characteristic of the polyelectrolyte adsorption. Following Hoogeveen et al., the desorption of polyions is kinetically hindered by the slowness of the adsorbed layer reformation, which is required in the exchange process [213]. This feature is explained by the strong electrostatic interactions. Consequently, the reversibility is favoured at high ionic strength. Due to this partial reversibility, in a polydisperse polymer solution, the replacement of the short chains (first arrived because of their high diffusion coefficient) by longer chains, although thermodynamically favoured, may not occur. On the other hand, the adsorption hysteresis, preventing the dissolution of adsorbed layers, is an important prerequisite to the elaboration of multilayers.

For the multilayer build-up, a pronounced *charge overcompensation* is crucial, too. Although not predicted by the theoretical models, it is experimentally verified in most cases. For poly(styrene sulfonate) (PSS) adsorbed on a primer ammonium monolayer, Berndt et al. have demonstrated that recharging occurs when the amount of polyelectrolyte in solution exceeds that of the amphiphile in the layer ( $> 5 \times 10^{-6}$  M) [214]. On the other hand, this overcompensation should be somehow related to the matching (or absence of matching) of the average distance between the charges on the surface and on the chain [215], which is required to maximise the number of ion pairs. In this respect, the theoretical treatments based on a mean surface potential might not be appropriate [216]. Concerning ion pairing, the experiments of Hoogeveen support a model in which the adsorption of long chains, as opposed to small molecules, leads to heterogeneous layers, with local charge overcompensation and unpaired surface sites. In this picture, the adsorption of a polyelectrolyte layer leaves free space at the surface, which can be subsequently occupied by neutral molecules.

Finally, from the macroscopic viewpoint, Lowack et al. describe the polyion adsorption as a 'kinetically hindered equilibrium' [215], in which the electrostatic repulsion due to charge over-compensation limits the adsorbed amount. Then, the increase of the adsorbed amount with increasing ionic strength would correspond to the parallel reduction of the activation energy. This characteristic behaviour of polyelectrolytes would explain the partial reversibility of the adsorption, too. The same authors suggest that the picture might be even more complicated for multilayers because negative and positive charges should coexist on the surface, due to the range of the electrostatic interactions and to the conformation of the adsorbed layers.

#### I.2.B.2.2. Nature and structural study of the multilayers

This section is devoted to the 'state of the art' in the field of step-by-step polyion physisorption. After some basic principles concerning the structural characterisation methods for ultrathin organic films, I will present the main studies dealing with the feasibility and characterisation of (poly)electrolyte multilayers.

##### *a) Structural characterisation techniques*

Most of the structural studies of (poly)electrolyte multilayers have been conducted using *X-Ray Reflectometry (XRR)*. In this technique, the sample surface is exposed to a low-angle X-Ray beam, and the intensity of the specular reflection is measured as a function of the incident angle (Fig. 9a) [217]. In the reflectogram, the reflectivity (R), i. e. the ratio of reflected to incident intensity, is usually presented as a function of the component of the wave vector perpendicular to the sample surface ( $k_{z0}$ ). Below the critical angle, total reflection occurs and  $R=1$ . Beyond this angle, the shape of the reflectogram is influenced by the film thickness, roughness and internal structure. In the ideal case of a flat organic layer deposited on a flat substrate, Kiessig fringes appear in the reflectogram, because of the interference between the beams reflected at the air/layer and layer/substrate interfaces (Fig. 9b). These interferences are constructive for certain values of the wave vector, and destructive for others. The thickness of the organic layer is proportional to the inverse of the fringes width. With increasing film roughness, the Kiessig fringes vanish gradually. In the case of a stratified multilayer, additional features emerge from the contrast of the different layers electron densities: the Bragg peaks, whose positions in the reflectogram indicate the characteristic length of the vertical repeat unit in the assembly. The Bragg peaks provide then a quantitative information concerning the internal structure of the assemblies. If the refractive index contrast is not sufficient to induce Bragg peaks, one may alternatively use neutron reflectometry, based on analogue principles, but for which Bragg peaks result from a contrast of neutron scattering length. For example, alternate protonated and deuterated polymer layers will produce Bragg peaks with neutrons, and not with X-rays. To refine the XRR information and obtain electron density profiles, the reflectivity curves may be fitted with a complex iterative algorithm applying the optics laws to a model multilayer with refractive index, thicknesses and roughnesses as parameters.

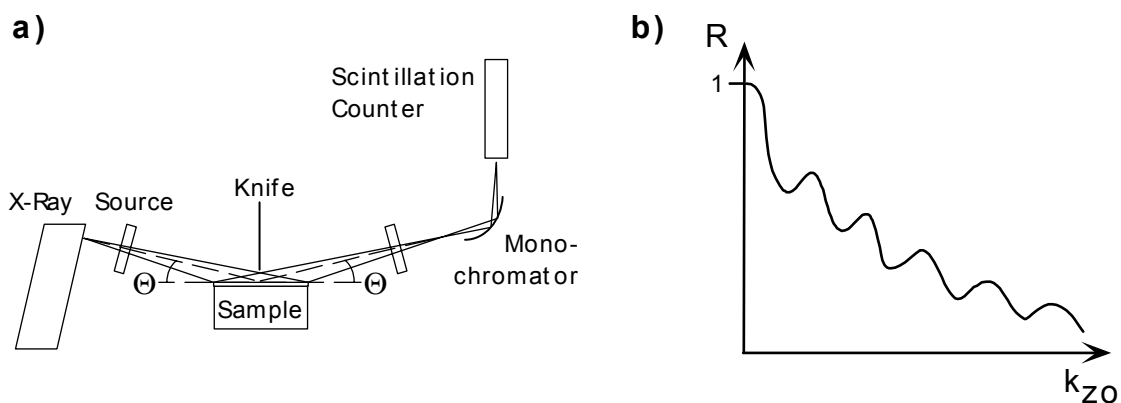


**Fig. 9.** X-Ray Reflectivity. a) experimental set-up; b) typical reflectogram with Kiessig fringes.

On the other hand, techniques like X-ray diffraction (XRD), ellipsometry, surface plasmon resonance spectroscopy (SPR), quartz-crystal microbalance (QCM), atomic force microscopy (AFM), profilometry, UV-vis and IR absorption spectroscopies, X-ray photoelectron spectroscopy (XPS), cyclic voltammetry, surface force apparatus, etc. have been used for the structural investigation of the multilayers, too. In the results part, I will concentrate on the development of ToF-SIMS and XPS for polyelectrolyte layer characterisation.

*b) The poly(allylamine hydrochloride)/poly(styrene sulfonate) system*

The more extensively studied polyelectrolyte multilayers are based on poly(allylamine hydrochloride) (PAH) as polycation and PSS or poly(vinyl sulfate) (PVS) as polyanions. In the older studies, the first polyanion layer was deposited on aminopropylsilanized glass, quartz or silicon. The PSS/PAH multilayers were first adsorbed from acidic solutions, with the PSS solution containing a  $\text{MnCl}_2$  salt [207]. The reflectivity of these PSS/PAH multilayers shows well defined Kiessig fringes, but no Bragg peaks. The linear increase of the total film thickness with the cycle number allows to deduce a bilayer thickness close to 23 Å, indicating the two-dimensional character of the deposition.

The effect of the added salt on the layer thickness has been clearly demonstrated later by Lvov and Decher [218,219]. For a NaCl concentration of 0, 1, 1.5 and 2 mol/L in the PSS solution, they found a bilayer thickness of 10.9, 17.7, 19.4 and 22.6 Å, respectively. With 0.5 mol/L  $\text{MnCl}_2$  in PSS and 2 mol/L NaBr in PAH, Tronin et al. even measured a bilayer thickness of 51 Å [220]. These results can be explained by the behaviour of polyelectrolytes in solution, in presence of salts: as the repulsion of the polyelectrolyte charges is screened by the salt, the polyelectrolyte adopts a more loopy conformation, which leads to a thicker adsorbed layer (Fig. 10). Without salt, the electrostatic repulsion of the polymer charges induces a quasi-linear conformation, and a subsequent adsorption of very thin layers.

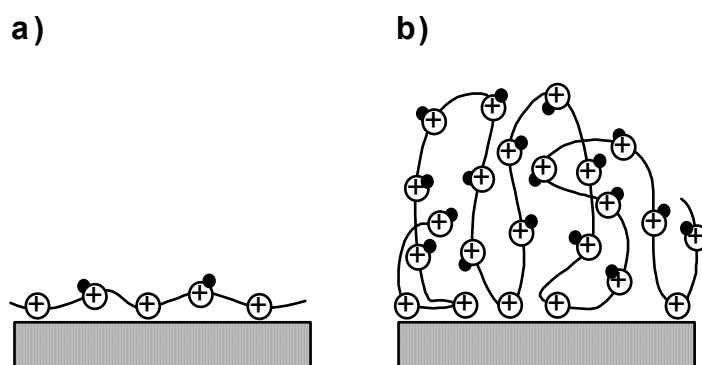


**Fig.10.** Effect of the salt on the layer conformation. a) without salt; b) with salt.

For the PVS/PAH system [219], fitting the reflectivity curves gave a bilayer thickness of 13.5 Å and a film roughness close to 5 Å for films with more than 30 layers. It was also deduced that the thickness of one PAH (PVS) layer was close to 7 Å. Again, the very small roughness was in good agreement with a well defined, stratified multilayer model. The lack of Bragg peaks was explained either by an uniform electron density profile due to layer interface roughness and layer interpenetration, or by the inherent lack of contrast due to the very close electron density of the two polyelectrolytes. Increasing the salt concentration above 0.2 mol/L NaCl led to very rough films. In a more complete study [181], UV measurements showed that the absorption of the PVS/PAH films is non-linear below then molecular layers, which was explained by the deposition of thinner layers in the first stage of the multilayer build-up.

The first objective proof of the existence of a stratified, though not layered structure came from the study of Schmitt et al., who inserted a perdeuterated PSS layer every six layer in PSS/PAH samples adsorbed with solutions of high ionic strength [208]. Indeed, deuteration is known to modify the neutron scattering length drastically. They first performed XRR measurements and found mean PAH and PSS layer thicknesses of 20 Å and 35 Å, respectively. In contrast to XRR, the neutron reflectivity curve showed intense Bragg peaks, corresponding to a repeat unit of 159 Å, which is very close to the expected value ( $3 \times 55 \text{ Å} = 165 \text{ Å}$ ). The calculated surface roughness was 13-15 Å and the model indicated a lower thickness for the firstly deposited layers (experiment.: ~10 Å for a single PSS layer). The rather large internal interfaces roughness (19 Å) was attributed to chain interdigitation. In addition, the results suggest that each polyelectrolyte unit is associated to ~0.5-0.8 counterion and, more surprisingly, that the PSS layers contain 27 wt % of water. Bragg peaks were also observed in the neutron reflectivity for assemblies with the perdeuterated PSS layer every four layers [221], but not for those with every perdeuterated PSS layers, probably because the interdigitation is too important in this system.

Further experiments showed that Bragg peaks could be obtained in the XRR measurements either by preparing  $(ABCB)_n$  structures with A, B, C being PSS, PAH and a polymer containing azo dyes, respectively, or by cyclic drying after a given number of PSS/PAH layer pairs [222]. In the first case, the effect was interpreted by the increased

electron density contrast, and in the second, by the rearrangement of the dried surface layer leading to a sharper interface with the following layers. The absence of optical contrast in the PSS/PAH multilayers was confirmed in a more recent study [223]. The authors determined an isotropic refractive index equal to 1.625 for these assemblies and they interpreted this observation by the extensive interpenetration of the layers. Decher confirmed the strong interdigitation of the layers in the PSS/PAH system and proposed a model structure in which the concentration of ionic groups adopts a gaussian distribution for each layer, resulting in a constant concentration of these groups for a sum of alternate layers [224]. A 1:1 stoichiometric ratio of anionic and cationic groups was also inferred from this structure and from the absence of counterions in the layers.

In order to develop a versatile surface charging procedure, Lvov et al. investigated different types of plasma treatments [225]. The best result was obtained with methane-plasma-deposited layers, followed by a short oxygen plasma discharge. PSS/PAH films deposited on such thick primer layers (several hundred of Å) exhibit well-defined Kiessig fringes. In a recent series of papers, Caruso et al. deposited PSS/PAH multilayers on gold surfaces treated with mercaptopropionic acid [226]. They showed that four polyelectrolyte layers are needed to reach the equilibrium thickness. Surprisingly, the use of salt in the PSS solution led to very thick bilayers ( $100 \pm 8$  Å), in comparison with previous reports.

### *c) Applications of the PAH/PSS model system and extension to biological assemblies*

PSS/PAH multilayers were also used as templates for the deposition of alternate biotinylated poly-L-lysine and streptavidin by biospecific recognition [155]. Uniform protein layers with an average thickness of 52 Å were obtained by this method. The same kind of process was used to sandwich virus layers between (PSS/PAH)<sub>6</sub> multilayers [154]. From the XRR data, the authors concluded that the virus penetrates partially into the multilayer, and that the important roughness of the virus layers is reduced by the following (PSS/PAH) multilayer deposition, restoring a flat surface. Alternate protein/polyion films were built up on substrates with a different surface treatment, too [147,148]: negatively charged quartz, glass and silicon wafers were successfully covered with a poly(ethylene imine) (PEI) layer, and further multilayer deposition was performed. The same procedure has been used in our group (see the results part). In a further step, Cooper et al. suppressed the classical polyelectrolytes, alternating cationic polypeptide layers (poly-L-lysine) with different anionic dyes [143]. The ellipsometric thickness of a bilayer was close to 20 Å.

The insertion of biological compounds in the multilayers, supported by the potential applications cited in the introduction, has been investigated by several groups since the initial findings of Decher and Lvov. The regular multilayer growth of these systems was confirmed by XRR [145,151], quartz crystal microbalance (QCM) [138,150] or surface plasmon resonance (SPR) measurements [152]. The elaboration of a complex 'biological' multilayer alternating glucoamylase and glucose oxidase with PEI/PSS layers and its use as a reactor for enzymatic reactions transforming starch in glucose has been elegantly demonstrated by Onda et al. [138].

*d) Conducting and electroactive polyelectrolyte multilayers.*

As mentioned in the introduction, the group of Rubner built-up conducting films with conjugated polyelectrolytes, reaching rather high conductivities [158,159,160]. To elaborate light emitting devices, Onoda et al. deposited multilayers of a sulfonated polyaniline and a positively charged precursor of poly(p-phenylene vinylene) (PPV) [227]. The PPV precursor was afterwards converted into PPV by a thermal treatment (200°C; 12H). The same procedure was used by Fou et al. to elaborate LEDs based on the poly(methacrylic acid) (PMA)/PPV and PSS/PPV pairs [161]. The assemblies were deposited on an indium-tin-oxide (ITO) electrode and coated with aluminium lines on top. Profilometry measurements indicated a mean thickness of 16 Å for PMA/PPV and of 8 Å for PSS/PPV. The multilayers based on the first pair behaved as pure diodes, with a linear increase of the photoluminescence with increasing layer number and a reasonable luminance level, as do spin-coated PPV films. In contrast, the multilayers based on the second pair exhibited near symmetric current-voltage curves, a non-linear increase of the photoluminescence with increasing thickness and a much lower luminance level, but they supported significantly higher current densities. These different performances were explained by the p-doping effect induced by the sulphonic acid groups of PSS. A marked influence of the conversion temperature on the device properties was evidenced, too.

To improve the LED device, Onitsuka et al. elaborated a complex multilayer of the kind ITO/(PSS/PPV)<sub>5</sub>/(PMA/PPV)<sub>15</sub>/Al, which showed a one order of magnitude higher luminance than the initial PMA/PPV-based device [162]. They also observed that the device efficiency was better with an insulating PMA layer on top. The same group built up multilayers incorporating various dyes and electro- and photoluminescent ruthenium complexes [165,228], or using a number of electroactive polymers [229]. On the other hand, Araki et al. demonstrated the feasibility of photoluminescent films exclusively based on oppositely charged porphyrin layers [230]. Unfortunately, few structural data exist concerning all these systems, which were mainly characterised by UV and IR absorption spectroscopies.

*e) Other polyelectrolyte, amphiphile/polyelectrolyte and organic/inorganic assemblies*

It is important to note that other polyelectrolyte pairs may exhibit different organisational behaviours than the PSS/PAH system. For instance, Kellogg et al. used neutron reflectometry to study assemblies based on the sulfonated polyaniline (SPAN)/PAH pair [231]. The use of deuterated SPAN/PAH blocks at regular intervals in the multilayers allowed them to find some interesting structural features of this system. Indeed, they found a bilayer thickness of 15 Å, along with a surface roughness  $\sigma_s$  of ~50 Å, and a roughness of the internal interfaces  $\sigma_i$  ranging from 22 Å to 38 Å with increasing film thickness. These large  $\sigma$  values were explained by real roughness of the interfaces, rather than by diffuse interfaces (interdigitation) as was the case with the PSS/PAH pair. The authors interpreted the results by the inherent stiffness and by the propensity to aggregation of the SPAN.

In a detailed study, Arys et al. showed that Bragg peaks could be observed in the XRR spectrum of a particular polyelectrolyte system, alternating PVS with an ionene-type polycation bearing a pendant chromophore [232]. Surprisingly, the multilayer thickness was shown to increase non-linearly with the layer number, although a fixed vertical repeat unit of 25 Å was preserved (as shown by the Bragg peaks). The fitting of the reflectivity data also indicated the presence of a loose layer at the air interface. These observations suggest a pronounced reorganisation of the film during the successive deposition steps. The authors describe the phenomenon as a 'surface-constrained supramolecular complexation'. In agreement with the marked supramolecular organisation, a small surface roughness was deduced from XRR ( $\sigma_s = 8\text{-}10$  Å [233]). The same kind of reconstruction was proposed by Kleinfeld and Ferguson [234] (vide infra). Arys et al. also demonstrated the strong dependence of the layer structure on the linear charge density parameter for ionenes differing by the alkyl spacer length [232].

In a different approach, Mao et al. [235] engineered alternate multilayers of photopolymerisable bipolar amphiphiles (cation) and poly(sulfonic acid) (anion) on naturally negatively charged mica surfaces. They reported a linear relationship between UV absorption and layer number up to 25 cycles. They found by surface force measurements (in water) that the amphiphile polymerisation reduces the surface potential, which was interpreted by a promotion of counterion binding. AFM revealed that the amphiphile layer was more ordered after the polymerisation step, with a hexagonal lattice structure. The area per molecule ranged from 32.9 Å<sup>2</sup> before to 32.0 Å<sup>2</sup> after polymerisation. The authors concluded that the polymerisation step produces more compact and strengthened amphiphile layers. Their following study focused on the effects of amphiphile chain length and counterion nature on the layer structure [236]. They observed that the amphiphiles lay flat on the substrate below a critical length of hydrophobic segments. For amphiphiles with a sufficient length, the photopolymerised layer thickness determined by AFM was ~65 % of the computed molecule length [237], indicating either a tilt or a distortion of the molecules in the layer. The appreciable roughness of the multilayer (30 Å) was maintained with increasing layer number, but it could be reduced by adding salt to the polyelectrolyte solution. The resistance of the polymeric layers to chloroform demonstrated the chemical stability improvement accompanying the photopolymerisation step.

On the other hand, Saremi et al. alternated PAH layers with photopolymerisable, negatively charged amphiphiles bearing a diacetylenic group [238]. In this case, AFM showed inhomogeneous layers constituted of a multitude of small domains in which the roughness was equivalent to the overall thickness of the assemblies. The same group reported on the multilayer formation of chromophoric amphiphiles with different polycations (PAH, poly-l-lysine, etc), followed by UV-vis absorption spectroscopy [167].

Gao et al. used bipolar amphiphiles to build up various types of multilayers. They developed multilayers with polymers bearing negatively charged azobenzene pendant groups [239], porphyrin and phthalocyanine [240], PbI<sub>2</sub> nanoclusters [241] and enzymes [149] as anions. The linear growth of the multilayers was inferred from UV absorbance for the first three systems, but no mention is made of such measurements for the enzyme-containing multilayers. In addition, the decrease of the enzyme activity with time suggested

that the enzymes were not stably immobilised between the amphiphile layers. For the first system, UV absorption, attenuated total reflection FTIR and X-Ray Diffraction studies allowed the authors to propose an ideally ordered multilayer structure in which the azobenzene groups align perpendicularly to the polymer main chain. They pointed to a preferential orientation of the disc-like molecules in the second case too. Finally, a stratified multilayer structure could be obtained with PbI<sub>2</sub> particles, as shown by the comparison between the period deduced from XRD and the characteristic amphiphile and nanoparticle sizes.

The formation of organic/inorganic hybrid thin films has excited much interest in recent years. Alternatively, Kotov et al. built up multilayers based on polycations and CdS, PbS and TiO<sub>2</sub> negatively charged nanoparticles [242]. The initial polycation layer was successfully deposited on various substrates (quartz, glass, gold, platinum and even Teflon). UV absorption and AFM measurements suggested the regular build-up of monoparticle layers. Later on, Gao et al. developed alternate multilayers by coupling CdS nanoparticles with an ionene-type polymer as cation, too [243]. Sun et al. repeated the same kind of experiment, alternating TiO<sub>2</sub>/PbS and PSS layers [244]. Anionic silica particles were also alternated with polycations to form multilayers [245], and the linear adsorption was confirmed by the regular frequency shift of a quartz crystal microbalance (QCM). Recently, Ichinose et al. characterised the growth of PAH/Mo<sub>8</sub>O<sub>26</sub> multilayers by QCM and XPS [246]. Interestingly, they found that the oxide thickness did not saturate, but increased with absorption time at a rate of 5.7 Å/min, due to the precipitation and subsequent loss of charges of the octamolybdate. Roughnesses of the order of 10 nm were determined by SEM.

In the field of organic/inorganic composite multilayers, Keller et al. [247,248] and Kleinfeld and Ferguson [234] reported respectively on the alternation of mineral, exfoliated sheets of  $\alpha$ -ZrP and hectorite with polycations. In both cases, a linear increase of the ellipsometric thickness demonstrated the regular multilayer build-up. Recently, Cochin et al. showed by UV absorption that multilayers could be obtained using delaminated hydrotalcite, as polycation, or montmorillonite, as polyanion, and liquid-crystalline polyelectrolytes as counterions [249]. In the field of 'exotic' assemblies, it must be mentioned that multilayers could be grown with fullerenes sandwiched between PEI layers [181] and with alternate dendritic macromolecules of various generations, bearing respectively amine and carboxylic groups [250,251]. In the latter, AFM and XRR studies point to the highly compressed state of the dendrimers in the layers with a (small diameter : large diameter) ratio in the range 1:3 to 1:6.

With some sense of humour, Lvov and Decher have summarised their investigations in 1994 by a 'virtual multilayer', showing the diversity of the available systems [181]. This virtual assembly has been extended in Fig. 11 to include the new systems created in the last four years. Some of these systems are presented by Decher et al. in a recent review concerning multicomposite films [252].

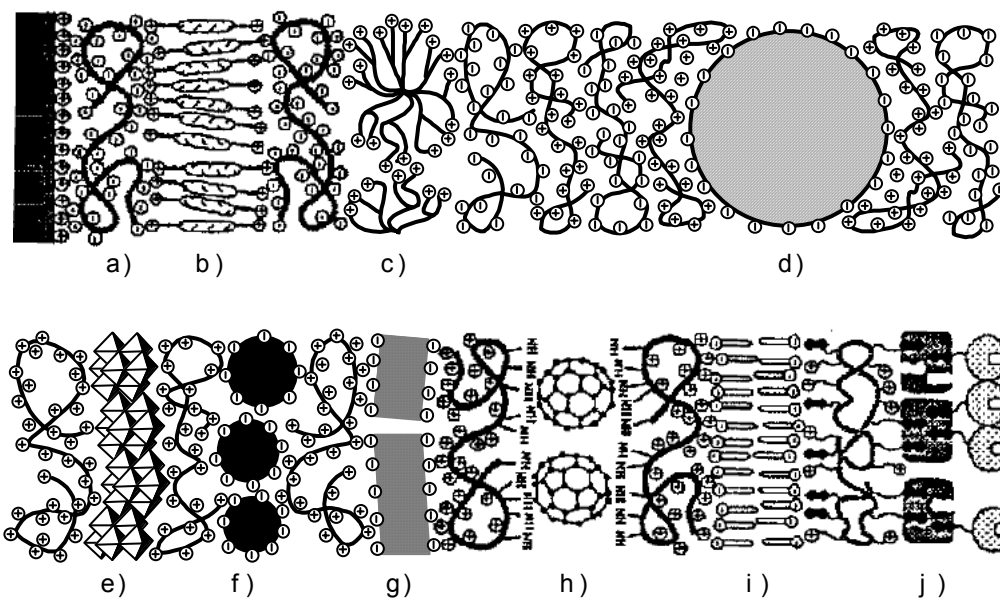


**Fig.11.** 'Virtual assembly' showing the different kinds of composite multilayers which have been prepared by step-by-step physisorption. a) polyelectrolytes; b) boladications; c) dendrimers; d) viruses; e) molybdenum oxide crystals; f) inorganic nanoparticles; g) inorganic sheets; h) fullerenes; i) lipid bilayers; j) biotinylated poly(L-lysine) and streptavidin. Adapted from Ref. [181].

*f) From model inorganic towards organic and polymeric substrates*

Most of the contributions cited above led to the development and application of new polyelectrolyte and hybrid systems, but few of them aimed to extend the diversity of the available substrates. One of the reasons may be that the structural characterisation techniques (XRR, ellipsometry, SPR, QCM, UV absorption spectroscopy) require particular substrates with model properties (very low roughness, transparency, metal coating, etc).

In this field, the group of McCarthy has made important advances. They showed for instance that PSS/PAH multilayers can be deposited on aluminium foils [253]. The aluminium oxide surface was functionalised with aminopropyltriethoxysilane in order to introduce positive charges on the surface. The multilayer build-up and coating stratification were assessed by XPS and the adhesive strength of the coating was confirmed by peel tests (cohesive failure in the tape).

In their subsequent works, they have developed surface treatments in order to introduce charges at the surface of standard polymers. I will show in the results that a different strategy has been elaborated in our group at the same period. To deposit multilayers on PTFE, they incorporated ammonium ions onto the substrate by plasma polymerisation of allylamine [254,255]. The thickness of the plasma-deposited layer was 120 Å. The subsequent adsorption of PSS and PAH layers was monitored by XPS and the periodic variation of the sulphur and nitrogen fractions showed the stratification of the coating beyond 10 polyelectrolyte layers. In another study [256], the same group built up

multilayer assemblies on poly(4-methyl-1-pentene), after chemical oxidation of the sample surface in a sulphuric acid solution containing chromium oxide. The creation of carboxylic acid functionality at the surface was confirmed by the pH dependence of the water contact angle, which indicated the presence of ionic CO<sub>2</sub><sup>-</sup> groups at high pH. For the multilayers, the stoichiometry found by XPS was 3 PAH for 2 PSS repeat units. In addition, the authors concluded to the presence of strongly bound water in the assemblies. They also determined a bilayer thickness of 21 Å for a PSS/PAH pair on silicon, which is larger than the value found by the group of Decher. Finally, the coated poly(4-methyl-1-pentene) films exhibit much better gas barrier properties than the pristine polymer.

To build-up multilayers on PET, Chen and McCarthy [257] used three types of substrates: unmodified PET, hydrolysed PET (PET-CO<sub>2</sub>H) and PAH-functionalised PET (PET-NH<sub>3</sub><sup>+</sup>). The latter could be obtained by amidation of the PET at high pH, as verified by XPS. The authors notice a slower adsorption on the uncharged PET, and a smaller layer thickness in comparison with the charged substrates. The effect of additional salt on the layer thickness (vide supra) occurs with neutral PET substrates, too. Unfortunately, the long discussion concerning the layer thickness is biased by the use of wrong values in the equation expressing the photoelectron attenuation. Indeed, atomic fractions are taken instead of absolute intensities, leading to the determination of aberrant layer thicknesses (2 Å per layer without salt). Nevertheless, XPS indicates layer stratification and shows the dependence of the layer pair stoichiometry on the concentration of salt in the solutions. Concerning the mechanical properties of the coated films, peel tests demonstrate that the cohesive failure occurs in the PET. Recently, alternate montmorillonite-polyelectrolyte assemblies have been deposited on untreated PET by Kotov et al. [258]. Remarkably, after the first layer deposition, AFM images show a dispersion of polyelectrolyte 'islands' (40 nm thick) surrounded by polyelectrolyte 'strands'. They also show that a polyelectrolyte network covers the whole sample. The extensive adsorption is attributed to hydrophobic interactions between the polyelectrolyte and the PET substrate. From the practical viewpoint, montmorillonite-polyelectrolyte multilayers are flexible, crack resistant and decrease the permeation rate of O<sub>2</sub>, but not the flux of water molecules, through the PET film.

Other groups have reported on the alternate physisorption on treated poly(ethylene), poly(urethane) and cellulose acetate [153] and carboxylic acid terminated SAMs [259]. The use of SAMs as template for subsequent polyelectrolyte adsorption offers interesting applications in the field of patterning. For example, microstructure creation with polyelectrolyte multilayers has been demonstrated by Hammond and Whitesides who use micro-contact printing to pattern self-assembled thiols with a carboxylic acid end, introducing negative charges along well-defined tracks on the surface [260]. The remaining part of the surface is 'blocked' with alcohol-terminated thiols. Ellipsometry and AFM measurements are consistent with a selective multilayer build up along the charged tracks. To develop gas separation membranes, Stroeve et al. have deposited PSS/PAH layers on untreated PP, but they give few indications concerning the film characterisation [178]. Recently, our group has reported on the deposition of polyelectrolyte multilayers on hydrophobic PP, too [261]. To compatibilise the substrate for the subsequent

polyelectrolyte layer adsorption, a copolymer based on choline methacrylate and bearing long alkyl residues, or a vinylpyridine-based copolymer with photoreactive groups are used as primer layer. The superposition of a fast and a slow adsorption process has been inferred from the UV absorption study of the deposition kinetics. For these systems, the linear increase of the absorbance with increasing layer number proves the regular multilayer build-up. Our approach of the multilayer deposition on polymers will be presented in details in the results part.

*g) New routes to organic multilayers*

In 1996, Laschewsky et al. introduced a hybrid method to create non-centrosymmetric coatings using polyelectrolyte physisorption [262]. In this method, a polycation with an benzene pendant group is physisorbed on the substrate, and the benzene residue is activated by the reaction with a salt of negatively charged diazonium, reversing the net surface charge and allowing for further polycation deposition. UV-vis spectroscopy and surface analysis techniques showed the regular build-up of multilayers by this way, and a thickness of 13 Å per layer was determined by XRR [262]. In addition, the marked second harmonic generation (SHG) showed that the arrangement of the chromophores was non-centrosymmetric. It must be recalled that SHG was also observed for samples made by alternate physisorption [263], indicating that the non-centrosymmetric alignment can be obtained by this method too.

Several authors have shown that the electrostatic interaction between oppositely charged polyelectrolytes is not the prerequisite for multilayer build-up. Stockton et al. demonstrated the successful growth of assemblies based on polyaniline and various non-ionic polymers containing amide, hydroxyl and ether groups [264]. The regular build-up was monitored by IR absorption and FTIR indicated the presence of hydrogen bonds, which were probably responsible for the multilayer cohesion. The thicknesses measured by profilometry were in the range 30-130 Å per bilayer following the choice of the polymer. Multilayers of poly(vinyl pyridine) and poly(acrylic acid) were developed by Wang et al. [265]. The nature of the interaction, i.e. hydrogen bonding, was again evidenced by IR spectroscopy. Following the AFM data, eighteen layers films exhibit a small roughness (6.4 Å). Recently, Shimazaki et al. deposited alternate polymers bearing respectively electron-donor and acceptor pendant groups [266]. Surface plasmon resonance demonstrated the regular increase of the film thickness, by mean steps of 35 Å per layer. The layer thickness reached its equilibrium value beyond 10 layers.

These extensions of the method of Decher and co-workers constitute a further step towards versatile surface modification by alternate polymer physisorption.

### I.2.B.2.3. Properties of the multilayers

In the following paragraphs, several properties of the alternate polyelectrolyte assemblies will be briefly reviewed. Although some of the properties investigated hereafter may appear as general features of polyelectrolyte multilayers, the reader must be aware that

the number of studies focusing on these issues is limited. Consequently, the generalisation of the observed behaviours to the ensemble of polyelectrolyte multilayer systems remains speculative.

*a) Thermal behaviour*

The thermal resistance of PSS/PAH has been firstly tested by Hong et al. with a 40 layers coating [146]. The film was annealed for 3 h at 190°C and subsequently cooled down. As indicated by the nice Kiessig fringes in the reflectivity profile, the thermal treatment preserved the smoothness of the coating, but the film thickness was reduced by 2 %. Complementary FTIR measurements indicated that the decrease in film thickness was connected to the loss of water. Similarly, a 42 layers PVS/PAH film showed a 6 % decrease in thickness as a result of step by step heating from 60 to 120 °C [219]. Subsequent heating up to 150 °C could be achieved without further shrinkage of the multilayer. Interestingly, the cooled down sample did not recover its initial thickness immediately, but only after two weeks. Again, the authors explained this hysteresis by the loss of water under heating and its slow re-entry from the air after cooling down. In a recent work, Sukhorukov et al. demonstrated that the reduction of the PSS/PAH films thickness upon heating (up to 100°C) was pronounced for films stored in an atmosphere with 100 % relative humidity, while it was negligible for films stored with 0 % humidity [267].

*b) Swelling in aqueous solution and humid atmosphere*

The formation of a superlattice by periodic drying of the multilayer in a stream of nitrogen has been mentioned in the preceding section [222]. In this case, the exposure of the dried PSS/PAH films to water resulted in the disappearance of the Bragg peaks in the reflectivity profile after 2 days. In addition, the authors noticed that the thicknesses of the films prepared in pure water and in an aqueous solution containing salts increased respectively by 11 % and 18 % after 10 days in water. Subsequent drying did not change the thickness anymore. In another study, the immersion of classical PVS/PAH and PSS/PAH films in solutions containing 0.1 mol/L NaCl [268] led to a significant increase of the film thickness within two hours. In that case, the initial thickness of the film could be recovered by drying. In contrast with pure water, swelling/drying cycles with a solution of different ionic strength results in the smoothing of the PVS/PAH coatings. Also, the authors found that the relative extent of swelling and shrinking is inversely proportional to the number of internal interfaces of the multilayer. On the other hand, Sukhorukov et al. showed that films prepared with or without salts exhibit the same proportional swelling as a function of relative humidity when stored at 28°C in humid atmosphere [267].

*c) Molecule transport properties*

The transport of water in the multilayers has been addressed in paragraph b). In a more quantitative study, Klitzing and Möwhald [269] prepared PSS/PAH multilayers with the first PAH layer labelled with a pH sensitive fluorescent dye. They showed that the pH change of the outside medium can be sensed by the buried dyes, thus proving the permeability of the films to protons. From the experiments with different multilayer

thicknesses, they were able to deduce the proton concentration profile in the film (exponential decrease from the film surface). In addition, they observed a marked variation of the dye fluorescence, and a change of the concentration profile, as a function of the nature of the surface layer (PSS or PAH). In subsequent studies, the same group demonstrated, with a similar procedure, the permeability of the PSS/PAH films to large molecules which act as quenchers of the fluorescent dyes (rhodamine; 2,2,6,6-tetramethyl-4-piperidinol-1-oxide; 6-carboxy-fluorescein) [270,271]. The penetration of 3,6-bis(dimethylamino)-acridine hydrochloride (acridine orange) into PAH/DNA films was reported by Sukhorukov et al., too [145]. The very slow increase of the absorbance led the authors to suggest that the PAH layers could act as diffusion barriers against this molecule. Indications concerning the diffusion of a diazonium salt of 4-nitroaniline through polyelectrolyte multilayers have been reported by Charlier et al., too [272].

*d) Resistance to solvents*

To our knowledge, very few studies report on the solvent resistance of polyelectrolyte multilayers. Lvov et al. claimed that PSS/PAH multilayers grown on silicon were very stable in different solvents [219]. Mao et al. demonstrated the resistance of photopolymerised bipolar amphiphile layers to chloroform [237]. As mentioned before, our group used polyelectrolytes containing hydrophobic parts to build-up multilayers on polypropylene [261]. Multilayers built up with the copolymer based on poly(choline methacrylate) (vide supra) exhibit cracks after 10 min in chloroform. The use of a photocrosslinkable copolymer based on poly(4-vinylpyridine) as first polycation layer prevents macroscopic defects, but UV absorption measurements indicate a gradual dissolution of the film as a function of the time spent in chloroform. Finally, when the photoreactive polycation is deposited as primer and top layers in the assembly and subsequently crosslinked, dissolution does not occur anymore.

*e) Mechanical properties*

The peel tests conducted by the group of McCarthy for PSS/PAH multilayers deposited on aluminium [253], and PET substrates [257] have been mentioned in the preceding section. These studies confirm the strong interaction between the adsorbed layers and the substrate. In our group, preliminary scotch tape tests with assemblies grown on PP show that the decohesion may occur either at the PP/multilayer interface (primer layer of choline methacrylate-based copolymer, vide supra), or at the multilayer/tape interface (primer layer of vinylpyridine-based copolymer, vide supra), following the appropriate choice of the primer polycation layer [261].

*f) Specific properties*

As quoted all along this review, very specific properties of the multilayer assemblies have been obtained by the use of particular polyelectrolytes, amphiphiles, biological molecules or inorganic particles as components of the coating. Therefore, the versatility of the alternate physisorption method has led to multilayers with various structural, electrical,

optical and biological properties, available for a number of applications [252]. The reader is invited to return to sections I.2.B.1.1. and I.2.B.2.2. for details about these applications.

### **I.2.B.3. Application of static SIMS to the study of ultrathin organic films**

#### I.2.B.3.1. Static SIMS and thin organic films

Twenty five years ago, static SIMS was applied to the study of a thin organic film, quite incidentally, by the group of Münster [273]. This film was a surface contamination, identified by Benninghoven et al. as an hydrocarbon layer on the basis of the characteristic  $C_xH_y^\pm$  ion pattern. Later on, the same group discovered the emission of large parent ions from amino acids deposited on metals from aqueous solutions, debuting a long history of organic overlayer analysis by static SIMS [14]. They continued the extensive study of amino acids with submono-, mono- and multilayers prepared under UHV by a molecular beam technique [105,274,275], which led to the development of the precursor model for secondary ion emission [68].

Since the original finding of the Münster group, an impressive number of studies devoted to organic films has been achieved, including bulk, cast and spin-coated homo- and copolymers, plasma-polymerised samples, amino acids, peptides and proteins, contaminants and additives, etc (see references [19,30,276,277] for reviews and [278] for mass spectra). In this review, I will focus on the analysis of thin organic mono- and multilayers prepared by the main methods described in section I.2.B.1.2. As all the reports on polyelectrolyte multilayers investigation by static SIMS came from our group, they will be presented extensively in the results part.

#### I.2.B.3.2. Langmuir-Blodgett mono- and multilayers.

Although the vacuum stability of LB films, required for the SIMS analysis, is not evident and depends on the considered system [279], in general, the reports presented in this section suggest or clearly claim that the investigated LB films are stable during the time of analysis.

The static SIMS analysis of LB films has been pioneered by the group of Gardella in 1985 [280]. They transferred LB monolayers of various fatty acids onto silver substrates and observed a number of parent-like and fragment ions, as well as underlying silver. Remarkably, silver cationised molecules were not detected for saturated fatty acids, suggesting that the silver cationisation occurs via the double bond of unsaturated molecules. The role of the substrate preparation on the adsorption of the first monolayer (with or without deprotonation) and on the observed parent-like ions was highlighted, too. In addition, they noticed that the silver emission could not be blocked, even with 15 stearic acid layers (375 Å) [281]. Based on similar experiments with fatty acid salt layers, it was suggested that this could be related to the limited integrity of the stearic acid layers (defects) [281,282]. Indeed, the substrate signal was shielded more efficiently with the fatty acid

salts, which are known to form more compact layers. The same works evidenced the influence of different substrates (silver, gold and germanium), too.

Later on, Gardella and co-workers used LB layers of fatty acids [283] and of dopamine and indolic derivatives [284] to develop a quantitative approach, correlating the dose-integrated intensity of the molecular ion to the amount of material on the surface. The sampling depths of atomic and molecular secondary ions were revisited in a subsequent paper, with multilayers of stearic, arachidic and behenic acids [285]. Although attenuated, the  $\text{Ag}^+$  and  $(\text{M-H})^-$  signals related to the silver substrate and to the buried behenic acid layer remained significant with 4 additional arachidic acid layers on top, suggesting a sampling depth of 150 Å or more. In contrast, the sampling depth of  $(\text{M-H})^+$  was found to be limited to 3 monolayers ( $< 100$  Å). Again, these very large values were most probably due to defects in the layers. On the other hand, the results showed that the deprotonated  $(\text{M-H})^-$  ions are mostly produced at the interface with the silver substrate, whereas the protonated  $(\text{M+H})^+$  ion formation is due to proton transfer from an adjacent acid molecule head, in the 'bulk' of the film.

Extending the quantification method cited above, the same group also studied the crosslinking kinetics of diacetylene LB films [286]. They found that the rate of conversion was best fitted with a biexponential function and derived a curve of the conversion percentage as a function of the UV exposure time. In the study of octadecylamine monolayers, they observed that the packing density and the emission of  $(\text{M+H})^+$  ions were correlated to the pH of the subphase: with increasing pH, the packing density increases and the  $(\text{M+H})^+$  signal decreases due to the deprotonation of the amine in contact with the subphase [287]. The decrease of the  $(\text{M+H})^+$  signal was interpreted as a clear indication of preformed ions in the layer, and the threshold  $(\text{M+H})^+$  signal at high pH was assigned to ions formed by a recombination process. To study the effects of pre-existing acid-base proton transfer in the multilayers, Li et al. alternated docosanoic acid (A) and 1-docosylamine (B) layers [288]. The proton transfer was first assessed by Reflection-absorption FTIR spectroscopy, then investigated by ToF-SIMS. As expected in the case of pre-existing proton transfer, the signal of  $(\text{B+H})^+$  was two times greater for trilayers with B on top of two A layers than for homogeneous B trilayers. Even trilayers with A on top of two B layers exhibited a higher  $(\text{B+H})^+$  signal. Unfortunately, these results could not be confirmed by the study of the  $(\text{A-H})^-$  ion, which behaved contrary to the expectations.

In 1988, Bolbach et al. published a combined SIMS and PDMS study of Cd stearate LB films transferred on gold, silver and aluminium [289]. Intense  $(\text{M-H})^-$  peaks were observed with both techniques, but the substrate ions  $\text{Au}^-$  and  $\text{Au}^+$  were detected in SIMS only.  $(\text{M-H})^-$  was found to be metastable. For Au substrates, this ion intensity increased with the layer number in PDMS but the opposite trend was observed in SIMS. It will be shown in the results part that such a decrease of the molecular ion SIMS intensity is observed for tricosanoic acid LB films, too. Remarkably, Bolbach explains this decrease by the high stopping power of the metal substrate as compared to the bulk organic film, and not by the 'preformed ion' hypothesis, as was the case for Gardella and Benninghoven. In SIMS, the substrate signal intensity decreases regularly with increasing layer number and vanishes after 8-10 layers (200-250 Å). To explain this very large value, channelling along the hydrocarbon chains and damages due to the primary beam are invoked. Interestingly,

the authors identify the two relevant processes governing the SIMS information depth: (i) the decrease of the substrate ion yield due to the energy loss of the primary ion in the organic coating. Roughly, the yield must fall to zero when the coating thickness exceeds the range of the primary ion (or the extent of the collision cascades); (ii) the attenuation of the secondary particles in the coating. The absence of metal ions in PDMS and the increase of the molecular ion intensity with increasing layer number are explained by the electronic character of the primary beam excitation.

In a subsequent study, Galera et al. determine the disappearance cross section  $\sigma$  of the  $(M-H)^-$  ions from LB monolayers of acids and amines ( $I = I^0 \exp(-\sigma Jt)$ ;  $I$  being the SIMS intensity and  $J$  the primary ion flux) [290].  $\sigma$  corresponds to the area damaged by the primary ion impact. The authors show that  $\sigma$  is influenced by the incident primary beam angle and energy, characteristic  $\sigma$  values being of the order of  $3000 \text{ \AA}^2$ . In addition, they report a linear relationship between  $\sigma$  and the energy dissipated by the primary ions *in the organic layer*, which is against the proposed hypothesis of the predominant substrate effect and of the collision cascade induced emission. They propose an explanation of the ejection of parent ions based on the formation of a vibrationally excited region. Concerning the observed linear relationship, one could argue that a correlation between the sputtering yield and the energy dissipated would be more convincing, as the disappearance cross section tells more about damages than about secondary ion emission itself. The same group performed the SIMS analysis of mixed layers of arachidic acid and barium arachidate, showing the decrease of the  $(M-H)^-$  and  $(M+H)^+$  intensities with increasing salt concentration [291]. This was explained by the parallel disappearance of H-bonded dimers in the bilayers. Galéra et al. also studied the fragmentation of the parent ions sputtered from LB films [292]. They evidenced the decrease of the fragmentation with increasing primary  $\text{Cs}^+$  ion energy for gold but not for silver substrates and proposed an interpretation based on the difference of binding energy for the two substrates. Later on, this group performed more applied studies concerning phosphine gas sensors based on LB multilayers, demonstrating the ability of static SIMS to elucidate the detection mechanism of the sensor by the identification of reaction products in the layers [293,294].

Langmuir-Blodgett multilayers have been extensively investigated by the group of Benninghoven, too. In an important series of papers, LB films constituted of stearic acid and of amphiphilic poly(methacrylate) are compared by Hagenhoff et al. [295,296,297, reviewed in 298]. The weak initial intensity of  $(M+H)^+$  and the very slow decrease of the  $\text{Ag}^+$  intensity with increasing layer number are confirmed for stearic acid, but the more interesting results come from the polymeric system: with five polymethacrylate layers, the substrate ions are completely masked (sampling depth of  $60 \text{ \AA}$ ), which shows that the substrate coverage with polymeric layers is much more efficient than with small molecules. In addition, the characterisation of LB films with a buried layer containing a fluorescent dye or a glycolipid allow Hagenhoff et al. to conclude to the diffusion of the buried compound in the multilayer. On the other hand, their results show the good stability of the poly(methacrylate) multilayers in atmosphere (nine months storage), and in boiling water (15 min). In the same period, Linton et al. observed, with mixed phospholipid layers, that the evolution of the fingerprint ion intensities as a function of the concentration of the components was non-linear, addressing by this way the difficult issue of binary mixture

quantification in SIMS [299]. Recently, Leufgen et al. used the chemical sensitivity of SIMS to image coexisting phases in binary phospholipid layers [300,301]. For the same system, complementary results were presented by Rulle et al. in a more technical approach of SIMS imaging [302]. The presence of several  $\mu\text{m}$  wide defects was demonstrated by the magnified images of the mixed phospholipid layers.

In Ref. [295], the discussion outlines the difference that should be made between *sampling depth* - the depth out of which secondary ions are detected [in practice] - and *information depth* - the [theoretical] thickness out of which secondary ions can be emitted due to the sputtering process [in the case of ideal samples]. It seems that this distinction can be disputed at least for the polymeric layers investigated in the results section, where possible sampling depth differences may not be due to true *defects* or pinholes as it is the case for small molecules, but to the *intrinsic structure* of the polymer layers. In contrast with the definition of Hagenhoff in which different samples exhibit different sampling depths (due to defects) but a single theoretical information depth (never observed), the polymeric samples can be 'ideal', with equivalent sampling and information depths for one sample structure, but with the information depth changing as a function of the layer structure. In that case, the distinction seems vain.

Other authors reported on the SIMS study of LB layers. Seki et al. compared Electron Stimulated Desorption Mass Spectrometry and SIMS for the analysis of barium stearate films [303]. Kudo and co-workers investigated cadmium arachidate mono- [304,305] and multilayers [306,307] in short reports. They studied the effects of the substrate nature, of the primary beam energy and angle and of the multilayer buildup on the secondary ion intensities. Interestingly, they could connect the observed fragment structures to the bond strength in the molecules. They also showed the relative decay of the substrate ion intensity when the primary beam-surface angle is reduced. Finally, Elman et al. demonstrated that the poly(dimethylsiloxane) oligomer distribution was narrower and shifted to higher masses for LB layers in comparison with spin-coated films, which was explained by the dissolution of the low molecular weight species in the aqueous subphase [308].

#### I.2.B.3.3. Self-assembled monolayers of thiols and disulphides.

The literature reporting on the SIMS characterisation of chemically self-assembled thiol monolayers has emerged in the nineties, i.e. approximately ten years after the discovery of Nuzzo and Allara. Although some information about the molecular secondary ions sputtered from alkanethiols had already been obtained from Laser Desorption Mass Spectrometry measurements (observation of thiolate and sulfonate negative ions) [309], the first SIMS study of alkanethiol monolayers on gold has been conducted by Tarlov and Newman in 1992 [310]. Among others, these authors detected thiolate ions  $(\text{M-H})^-$ , but also  $\text{Au}(\text{M-H})_2^-$ ,  $\text{Au}_2(\text{M-H})^-$  and various  $\text{Au}_x\text{S}_y^-$  cluster ions. In contrast with freshly analysed layers, the mass spectra of samples which had been stored for one month in air exhibited intense alkylsulphonate peaks due to oxidation; interestingly, these oxidised species could be replaced by thiols after one hour reimmersion in the thiol/ethanol solution.

On the other hand, the substrate signal was shown to depend strongly on the primary beam energy. In the same period, Frisbie et al. obtained molecular ion images of thiols adsorbed on patterned gold surfaces and observed gold-cationised thiolate secondary ions [311]. More complex patterned SA layers were successfully imaged by the same group later [312,313,314]. As a first step towards biosensor and microelectronics applications, Tarlov and co-workers investigated thiol patterning by another method, too: they patterned the surface of the monolayer by UV irradiation, oxidising the exposed thiols, and they replaced the newly created sulphonates by reimmersion of the layer into a different thiol solution [315,316]. The same authors demonstrated the feasibility of ion and electron beam patterning for thiols on silver [317] and, recently, reproduced the experiment with alkanethiol-derivatised homo-oligonucleotide layers [318]. In the latter work, cytosine oligonucleotides were replaced by thymine oligonucleotides in the patterned areas, and the specific binding of adenine in the thymine regions could be achieved. All along their work, the success of the various surface modifications was assessed by imaging the characteristic negative ions of the different compounds (thiolates, etc). It is interesting to mention that the observations of Tarlov and Frisbie support a mechanism in which the chemisorption of thiols involves proton elimination.

In a fundamental SIMS study, Leggett et al. analysed both frozen and self-assembled 3-mercaptopropanoic acid layers, showing indeed that different binding states give rise to different fragmentation patterns: for the frozen compound, the spectra show characteristic fragments retaining the sulphur as charged site, while for the self-assembled layer, fragments like  $(M-S)^+$  and gold-cationised thiolates are detected [319,320]. The same group revisited the thiol photooxydation process recently [321]. On the other hand, Hagenhoff et al. compared different adsorption procedures for sulphides and disulphides in ethanol solutions [322]: (i) deposition of one  $\mu\text{l}$  solution on a gold surface, (ii) immersion of the substrate for four hours in the solution with subsequent ethanol rinsing (SA preparation). While the mass spectra of the disulphide samples obtained using the first preparation procedure show intense parent ion and gold-cationised molecule peaks, those of the disulphides adsorbed by the SA method just exhibit fragments corresponding to the scission of the S-S bond, and their gold-cationised homologues. The authors concluded to the dissociative adsorption of disulphides in the SA preparation procedure. For biotinylated thiols, they also evidenced some correlation between chosen SIMS intensity ratios and the layer thickness, as determined by SPR, and they demonstrated the sensitivity of ToF-SIMS to the recognition of biotin by streptavidin [323]. Recently, thiols and alkyl xanthate on gold and copper were investigated by Simon et al., who noticed the presence of the heavy  $M_2Au_3^-$  in the spectrum of amyl xanthate ( $CH_3(CH_2)_4OCS_2^- Na^+$ ) on gold and of a remarkable  $Cu_xS_y^-$  cluster pattern (up to mass  $m/z = 4000$ ) for the same compound adsorbed on copper [324]. Luo et al. conducted a very extensive study of fluorinated SAMs modified by hyperthermal molecular projectiles [325]. Using SIMS, they evidenced three types of behaviour following the nature of the projectile: (i) soft landing, leading to the trapping of intact projectiles in the layer; (ii) dissociative soft landing, in which the dissociation products of the projectile are trapped in the layer and (ii) reactive soft landing, resulting in the reaction of the projectile with the surface species. This technique opens a new way for molecular scale surface modification.

Mixed monolayers of alkyl sulphides (and dialkyl disulphides) have been first investigated with SIMS by Offord et al., in a detailed multitechnique study [326]. They conclude that the adsorption is thermodynamically driven for sulphides (longer chains preferred) and kinetically driven for disulphides (no preference). Again, alkylsulfonate anions, identified as air oxidation products, are observed with a high intensity. In parallel, they demonstrate the usefulness of ToF-SIMS to determine the chemical structure and composition of mixed layers of alkanethiols [327]. Mixed layers of alkanethiols (12 and 18 carbon atoms) have been studied by Canry and Vickerman, with gold and silver as substrates, too [328]. The difference in fragmentation related to the different substrates are explained on the basis of acid-base interactions. In this formalism, the interaction of the soft base (thiolate) is expected to be stronger with the softer acid ( $\text{Au}^+$ ), which is in agreement with the intense thiolate anion peaks observed with silver and not with gold substrates. For mixed layers on gold, these authors confirm the combined action of thermodynamics, favouring long chains which are better stabilised by van der Waals forces, and kinetics, favouring shorter chains which diffuse faster to the surface during the adsorption. In addition, their results support the co-existence of two microscopic phases in the monolayer [329].

In recent reports, several authors have also used ToF-SIMS to analyse complex polymers anchored on gold surfaces by means of disulphide residues, including poly(peptides) [330] and perfluoropolyether-grafted poly(siloxanes) [331,332]. For the latter, the presence of gold atomic and cluster ions in the spectra showed that a monolayer thickness of 30-40 Å (as determined by ellipsometry and XPS) was not sufficient to screen the substrate signals.

Finally, it is worth mentioning some short fundamental papers which use alkanethiols on gold to propose new insights into the ion induced desorption mechanisms. In an elegant way, Rading et al. correlate the measured desorption energies and damage cross-sections of various thiols to model the shape of the lateral energy distribution around the primary ion impact point [333]. On the other hand, Riederer et al. have shown experimentally that the  $(\text{M-S})^+$  fragment ions are sputtered with a very low kinetic energy [334,335]. In contrast, molecular dynamics simulations performed by Liu et al. indicate that intact gold alkanethiolates and dialkanethiolates can be sputtered on the basis of purely elastic collisions [336], which seems difficult to reconcile with such a low kinetic energy.

#### I.2.B.3.4. Self-assembled monolayers of silanes.

Ordered silane multilayers made with the method of Netzer and Sagiv have not been characterised by SIMS. Nevertheless, several reports exist concerning, for instance, organofunctional trimethoxy-, triethoxy- and trichloro- silanes, which are used as protective coatings or as coupling agents to promote adhesion between glass or metal oxide surfaces and polymers. The aim of this paragraph is not to give an exhaustive review of the available studies, which is outside the scope of this thesis, but rather to pinpoint a few examples of the contribution of SIMS to this field.

$\gamma$ -aminopropyltriethoxysilane layers adsorbed on steel have been characterised by Van Ooij and Sabata [337]. They report evidences that a part of the silanes are covalently bonded to the surface, but also that another part of the molecules are adsorbed with the amino groups at the steel-coating interface. They insist on the importance of the substrate preparation treatment. In the characterisation of the same compound on glass, Wang et al. demonstrate the presence of a crosslinked poly(aminosiloxane) network [338]. Instead, Hagenhoff et al. have studied methyltrimethoxy-, -triethoxy- and -trichlorosilane layers on various substrates [339]. The secondary ion patterns indicate that the surface is constituted by completely hydrolysed siloxanes and, more precisely, by silsesquioxane derivatives (cage-like structures). The same group has analysed the desorption behaviour of various silane molecules as a function of the temperature, showing that chlorosilanes are covalently bonded to the hydrophilic silicon substrate, that ethoxysilanes and hydroxysilanes are bonded by covalent and hydrogen bonds and that butylsiloxanes are only physisorbed [340]. Poly(siloxanes) may be grafted onto oxide surfaces, too. For example, chemisorbed poly(methylhydrogensiloxane) monolayers on silicon oxide have been studied by Reihls et al. who fitted the observed SIMS intensities by a statistical model based on the fragmentation in the non bonded segments of the macrochains [341]. In the field of patterning, van der Wel et al. have demonstrated the success of the local chemical modification of a light sensitive organosilane by UV irradiation and, alternatively, of the removal of selected aminosilane areas by oxidation with UV ozone through a mask [342].

To end this review, Table 3 summarises the information that can be deduced from the SIMS characterisation of thin organic films.

**Table 3.** Contribution of Static SIMS to the characterisation of thin organic films

<b>LB films</b>	<ul style="list-style-type: none"> <li>• Integrity of the layers (defects, pinholes) by the substrate ions [281,295] by SIMS imaging [302]</li> <li>• Homogeneity of the layers (phases) by SIMS imaging [300,301]</li> <li>• Identification of bonding states [288] of chemical reaction products [293,294] of diffusion in the layers [295,296]</li> <li>• Quantification of mixed layers [283,299] of chemical reactions [286] of pH effects [287]</li> </ul>
<b>SA films</b>	
Thiols	• Sensitivity to the bonding states [310,319,320,322]
Disulphides	<ul style="list-style-type: none"> <li>• Identification of thiol oxidation [310,321]</li> <li>• Verification of surface patterns by molecular SIMS imaging [311-318]</li> <li>• Quantification of mixed layers [326,327,328,329]</li> </ul>
Silanes	<ul style="list-style-type: none"> <li>• Sensitivity to the bonding states [337,340]</li> <li>• Identification of the surface chemical structure (crosslinking) [338,339]</li> <li>• Verification of surface patterns by SIMS imaging [342]</li> </ul>

# I.3.

---

## Aims of the Thesis

In the first part of the literature review, it has been shown that the secondary ion emission processes, governing the nature and amount of detected species in Static SIMS, may be rather complex. This complexity arises partly from the combination of the sputtering and ionisation mechanisms, but, in the case of molecular ions, we must recognise that these processes are poorly understood even separately. Although many theories coexist, the experimental data are insufficient to validate one model with a high degree of certainty. Moreover, it seems that the unique initial interaction of a primary ion with the atoms of the solid may give rise to a multiplicity of emission mechanisms. Therefore, the information provided by Static SIMS, although very wealthy, remains often qualitative and partly unused. The lack of quantitative results and comprehensive data treatments demonstrates the need of a deeper understanding of molecular ion sputtering.

On the other hand, the application of Static SIMS to the study of thin organic films (LB, SA, etc) brings a new insight into the properties of these layers. Among them, SIMS is able to assess the layer chemical structure, quality and homogeneity, the molecule bonding states, the success of surface chemical reactions, the modification of the preparation or environmental conditions, the diffusion of buried molecules, etc. Thus, in combination with complementary techniques, SIMS has proved to be valuable for the investigation of such systems.

The apparent contradiction between the limited understanding of the basic sputtering processes and the unique analytical capabilities of the method may be easily alleviated: although absolute values for the ion intensities may not be predicted by the theory even in the case of 'simple' organic or homopolymer layers, the ion identification procedure, the comparison with standard samples and, recently, the use of statistical methods for the data treatment allow one to derive a qualitative - and sometimes quantitative - information from the forest of peaks constituting the mass spectrum.

In the context described above, the objectives of this work will be two-fold: first, in a fundamental approach, we will take advantage of the different kinds of available organic layers for the development of the SIMS technique. In this respect, very thin layers of organic molecules and polymers cast on silicon and silver, or deposited as bilayers by the LB technique will be investigated as model systems. Even the use of certain polyelectrolyte

assemblies built-up on silicon will be justified in this context provided that they have been extensively studied by other methods like UV/vis, XRR, XPS or AFM.

In this context, the KED measurement will constitute a powerful tool to improve our knowledge of the molecular ion sputtering processes. The KEDs of atomic, fragment and parent ions will be measured and interpreted, leading to a tentative description of the different stages of the secondary ion emission. Together with the KEDs, the ion yields and ion beam degradation effects will provide interesting details concerning the involved mechanisms. In a different approach, the information depth of atomic and molecular secondary ions will be determined by the analysis of multilayer samples with well-known thicknesses.

Second, we will apply the analytical capabilities of ToF-SIMS and XPS to the investigation of thin organic multilayers obtained via the successive physisorption of alternate polyelectrolytes. In this part of the work, the objective is to apply Static SIMS to the study of multilayers built-up on polymer supports. Indeed, for technical reasons, these systems are difficult to investigate by means of other characterisation techniques like XRR and AFM. Instead, the combined use of ToF-SIMS and XPS will bring us a detailed information about the multilayer growth process. To achieve this goal, preliminary studies of multilayers built-up on model silicon supports will be required.

In summary, we will derive benefit from the application of ToF-SIMS analysis to thin organic films to improve our understanding of both the SIMS experiment and the polyelectrolyte multilayer adsorption.

# I.4.

---

## Summary of the Results

---

### I.4.A. Fundamentals of Static SIMS

---

#### I.4.A.1. Introduction

The mechanisms of secondary ion emission from organic materials bombarded by keV ions are not very well known yet. In particular, the emission of molecular ions from organic and polymer surfaces is difficult to understand on the basis of the existing theoretical models (see section I.2.A.3).

To gain a deeper understanding of the ion sputtering from organic surfaces, the analysis of the kinetic energy distributions (KED) of molecular secondary ions sputtered from organic compounds and polymers has been initiated during this thesis. Indeed, beside the secondary ion yields, the sputtered particle KEDs provide important information concerning the mechanism of emission itself [60].

First, the interpretation of the KED of molecular fragment ions ejected from triacontane (tricosenoic acid) layers will give indications about the fragmentation occurring in the surface region, and will highlight the predominant effect of the chemical structure of the bombarded species. To explain the experimental results, we will develop a phenomenological model based on the emission of precursor-like secondary ions, followed by their internal energy dependent fragmentation.

Second, the daughter ions resulting from unimolecular dissociation of their metastable parents in the linear part of the spectrometer, appearing in the secondary ion KEDs, will be analysed and identified. The analytical consequences of metastable decay will be discussed. Finally, the KED of parent-like ions sputtered from large adsorbates on metals will be presented. They support a view of the sputtering of these large molecular cations based on multiple collision processes and possible subsequent dissociation in the vacuum.

The information deduced from the interpretation of the KEDs will be tentatively summarised in a unified description of the molecular ion emission process. All the results presented in this part of the thesis refer to the articles of sections II.A.1-3.

### I.4.A.2. Experimental setup

The secondary ion mass analyses and the KED measurements have been performed in a Charles Evans & assoc. Time-of-Flight SIMS (TRIFT 1) (Fig. 12) [343]. The characteristics of this analyser are described in the following paragraphs. Complementary measurements have been performed on a similar apparatus at EPF Lausanne (Switzerland), using a Cs<sup>+</sup> 11 kV primary ion column.

#### a) Primary ion beam

The primary ion column is a FEI 83-2 LI liquid metal ion gun providing a (5 kHz) pulsed Ga<sup>+</sup> beam (400-800 pA DC, 20 ns pulse width bunched down to less than 4 ns). In this work, it has been operated at 15 kV, corresponding to a primary ion impact energy of 12 keV in the positive acquisition mode and 18 keV in the negative acquisition mode.

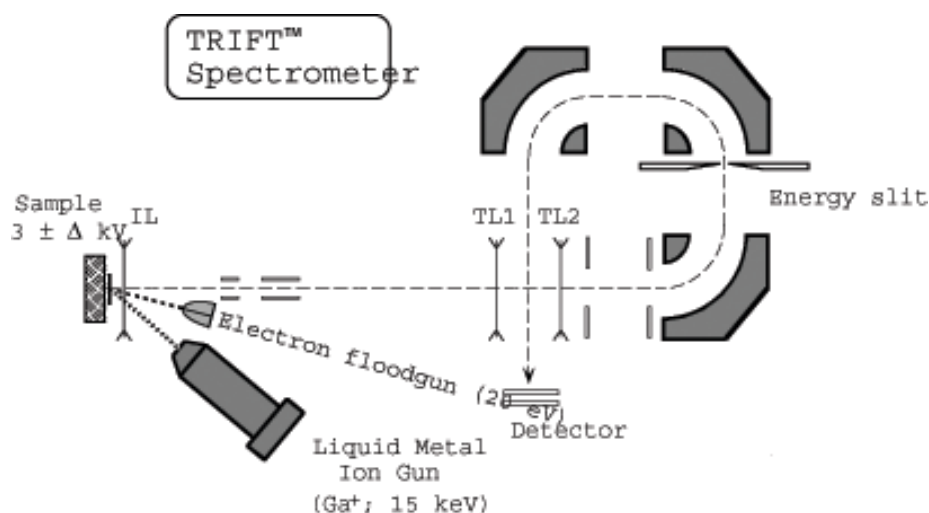


**Fig. 12.** ToF-SIMS experimental setup (gallium beam column, electron floodgun and TRIFT™ spectrometer).

The angle between the gallium column and the sample normal (spectrometer axis) is 35°, which corresponds to an impact angle of ~40° at 12 keV in the positive acquisition mode. The beam deflection is ensured by an electrostatic octupole located after the lens assembly. To avoid organic sample degradation [344,345], the focused primary beam (0.2 μm diameter) is rastered onto a 0.017 mm<sup>2</sup> area (130 μm × 130 μm), allowing to keep the ion fluence in the range 0.5 - 1 × 10<sup>12</sup> ions/cm<sup>2</sup> for one spectrum acquisition.

#### b) Analysis chamber and sample holder

The analysis chamber is kept under ultra high vacuum (10<sup>-9</sup> torrs) during the analysis. The sample is mechanically mounted on a vertical sample holder allowing x and y movements. It is maintained at a high positive (negative) voltage in the positive (negative) acquisition mode (usually: ± 3 kV), which explains the different beam energies in the two acquisition modes (vide supra).

*c) Time-of-flight mass spectrometer*

After emission, the secondary ions are extracted in the acceleration section of the spectrometer (~2 mm in the current configuration), which is located between the sample surface (3 kV) and the extraction plate (grounded). The extraction plate constitutes the aperture of the 'immersion lens' (IL), focusing the secondary ions in the field-free drift region. The secondary ion image is then magnified by the combined action of the immersion and transfer (TL) lenses and transmitted to the position sensitive detector (resistive anode encoder) by a set of three electrostatic analysers (ESAs). Briefly, the role of these ESAs is to compensate the effects of the initial energy distribution by elongating (shortening) the fast (slow) ions trajectory. The energy passband of the analyser is about 240 eV [346]. The detection system is based on a time-to-digital converter, with a deadtime of ~5 ns. As the detector efficiency decreases drastically for slow (high mass) ions, the secondary ions can be post-accelerated (0-10 kV) in front of the detector. By appropriate transformation (Eq. 1, section I.2.A.1) and calibration procedures, the secondary ions time-of-flight is converted into mass.

*d) Charge compensation*

In the case of insulator samples, the charge compensation is ensured by an electron floodgun (Fig. 12) providing a pulsed, low-energy electron beam (24 eV). The number of ion pulses per electron pulse can be tuned from 10 to 3. Usually, the charge neutralisation is not needed for thin organic layers, except if they are deposited on a thicker polymer film (see section II.B.2).

*e) Imaging SIMS*

To control the lateral homogeneity of the sample surface, secondary ion mappings (imaging SIMS) may be recorded on  $256 \times 256$  pixels by scanning the 15 keV beam over the chosen sample areas. The mass ranges of interest are defined by cursors in the mass spectrum, allowing for the separate imaging of several preselected secondary ions.

*f) Ion beam degradation measurement*

For the surface degradation studies, continuous bombardments on a larger area (e.g.  $0.036 \text{ mm}^2$ ) with the same  $\text{Ga}^+$  source are alternated with routine ToF-SIMS analysis periods, in order to reach a maximum fluence of  $10^{16}$  ions/cm<sup>2</sup>.

*g) KED measurement*

In the routine analysis conditions, a maximum energy dispersion occurs in the centre of the second ESA. For the KED measurement, the IL and TL voltages are increased in order to bring this energy dispersion maximum back to the energy filter, located in front of the second ESA (Fig. 13). The secondary ions are then energy selected by the slit of the energy filter (100  $\mu\text{m}$  corresponding to a passband of 1.5 eV). To obtain of a complete

energy spectrum, secondary ion mass spectra are collected for different *sample* voltages ( $3000 + \Delta V$ ), a  $\Delta V$  increase of the sample potential corresponding to a  $\Delta eV$  decrease in the KED. An alternative way to measure the KED is to keep the sample voltage at the fixed nominal value (3 kV) and to shift the energy slit perpendicularly to the beam in order to accept different regions of the KED. The spatial distribution is then converted into an energy distribution owing to an empirical equation derived from the simulation of the ion trajectories [347].

During the KED measurement,  $\sim 20$  spectra are recorded on the same sample area with different energy windows in order to keep the total ion fluence below  $10^{13}$  ions/cm<sup>2</sup>. The zero of energy scale is estimated from the intersection between the tangent to the increasing part of the KED of the atomic substrate ions ( $Si^+$ ,  $Ag^+$ ) and the energy axis. The corrected value of the sample voltage, giving the initial kinetic energy of the secondary ions, will be called 'apparent kinetic energy' in the results.

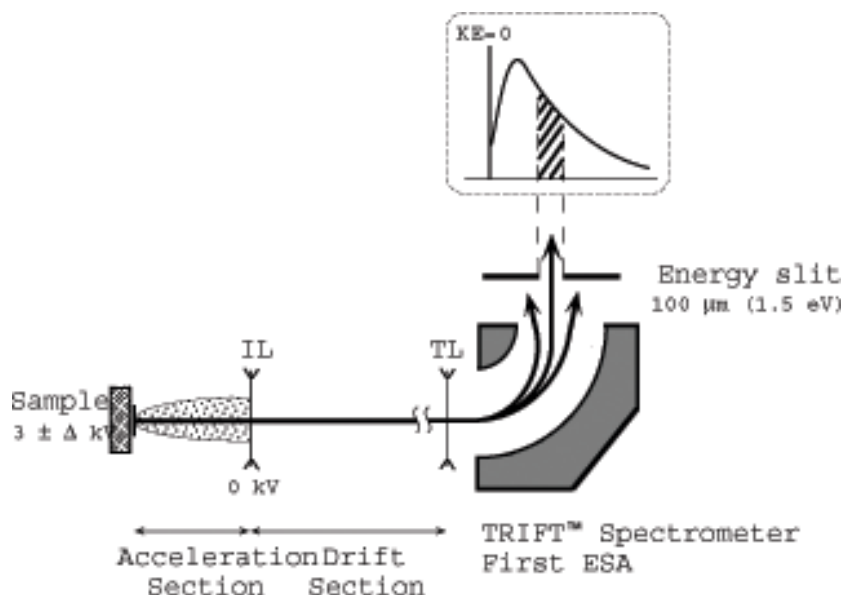


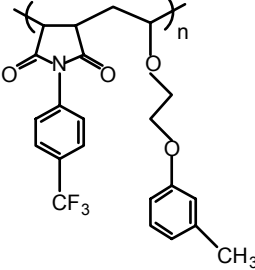
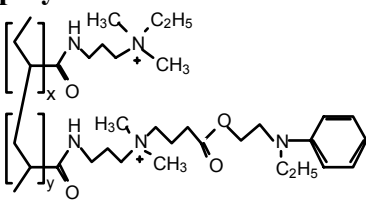
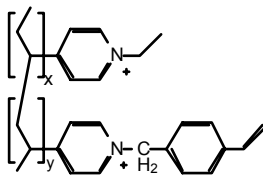
**Fig.13.** Detail of the first part of the spectrometer (acceleration section, drift section, first ESA and energy slit) showing the energy selection principle.

### I.4.A.3. Samples

The samples used for the fundamental ToF-SIMS study of thin organic films are described in Table 4. The substrate secondary ions could be detected in all of these samples, indicating the limited thickness of the adsorbed layers. With such thicknesses, a good electric contact between the sample substrate and the top surface is ensured, which is crucial for the KED measurement.

Summary of the Results

**Table 4.** Samples used for fundamental SIMS studies

Name and Formula	Molecular Weight	Origin	Preparation	Section
<b>TSA</b> , tricosenoic acid C <sub>23</sub> H <sub>44</sub> O <sub>2</sub>	352	Pr. J.-P. Issi, Dr. L. Langer, UCL	LB bilayers	II.A.1.
<b>TC</b> , triacontane C <sub>30</sub> H <sub>62</sub>	422	Aldrich	cast films	I.4.A.4, II.A.3
<b>DBA</b> , dibenzanthracene C <sub>22</sub> H <sub>14</sub>	278	Aldrich	cast films	II.A.2 II.A.3
<b>TPN</b> , tetraphenylnaphtalene C <sub>10</sub> H <sub>4</sub> (C <sub>6</sub> H <sub>5</sub> ) <sub>4</sub>	432	Aldrich	cast films	II.A.3
<b>PIB</b> , poly(isobutylene) [-CH <sub>2</sub> -C(CH <sub>3</sub> ) <sub>2</sub> -] <sub>n</sub>	> 1000000	Aldrich	cast films spin-cast films	I.4.A.4 I.4.A.5 II.A.1
<b>PBD</b> , poly(butadiene) [-CH <sub>2</sub> -CH=CH-CH <sub>2</sub> -] <sub>n</sub>	> 1000000	Aldrich	cast films spin-cast films	I.4.A.5
<b>PS</b> , Poly(styrene) [-CH <sub>2</sub> -CH(C <sub>6</sub> H <sub>5</sub> )-] <sub>n</sub>	700 (M <sub>n</sub> ) 1100 (M <sub>n</sub> ) 60000 (M <sub>n</sub> )	Scientific Polymer Products, Inc Pr. R. Jérôme, ULg Pr. R. Jérôme, ULg	cast films spin-cast films	I.4.A.5 I.4.A.6 II.A.1 II.A.2 II.A.3
<b>PET</b> , Poly(ethylene terephthalate) [-CO <sub>2</sub> -C <sub>6</sub> H <sub>4</sub> -CO <sub>2</sub> -C <sub>2</sub> H <sub>4</sub> -] <sub>n</sub>	High	Pr. R. Legras, UCL	spin-cast films	II.A.1
<b>MV copolymer</b> 	-	Pr. A. Laschewsky, Dr. P. Hendlinger, UCL	LB bilayers	II.A.1
<b>polycation P1</b> 	-	Pr. A. Laschewsky, Dr. E. Wischerhoff, UCL	Polyelectrolyt emultilayers	II.A.2
<b>polycation P2</b> 	-	Pr. A. Laschewsky, Dr. E. Wischerhoff, UCL	Polyelectrolyt emultilayers	II.A.2

#### I.4.A.4. Emission of molecular fragment ions from thin organic films

In this study of fragment ions emission, thin layers of tricosenoic acid transferred on gold by the LB technique and of triacontane cast on silicon and silver have been chosen as model molecule systems, in which the sputtering can occur after one single bond-breaking. The extensive study of ion sputtering from tricosenoic acid on gold will be described in section II.A.1. To introduce these detailed results, we will present here the case of triacontane cast on another heavy substrate, silver. The similar effects observed for the two systems, TSA/Au and TC/Ag, support the general character of the results.

The partial positive ion mass spectrum of TC adsorbed on Ag is displayed in Fig. 14. The complete spectrum is available in section II.A.3, Fig. 1. Peaks corresponding to the dehydrogenated molecule and dimer appear around  $m/z = 420$  and  $840$ , respectively. Intermediate hydrocarbon series, separated by 14 mass units indicate that the fragmentation of the molecule at each C-C bond is allowed. In the low mass region, hydrocarbon clusters of the form  $C_xH_{2x\pm 1}$  are predominant (for hexatriacontane, see Ref. [348]). In the following, a particular attention will be paid to these molecular fragments.

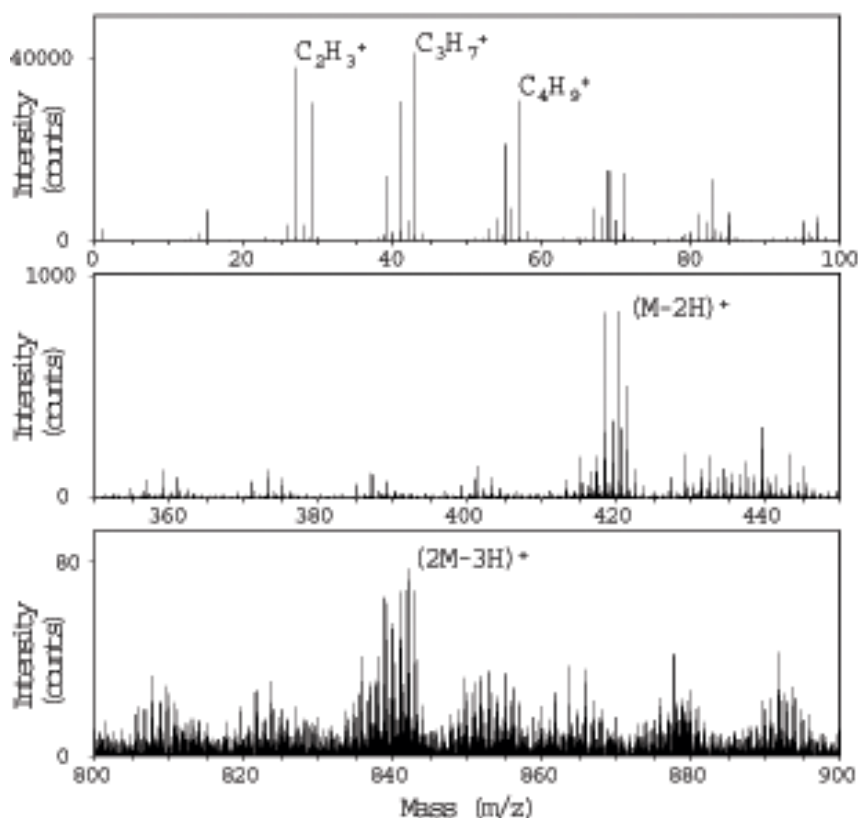
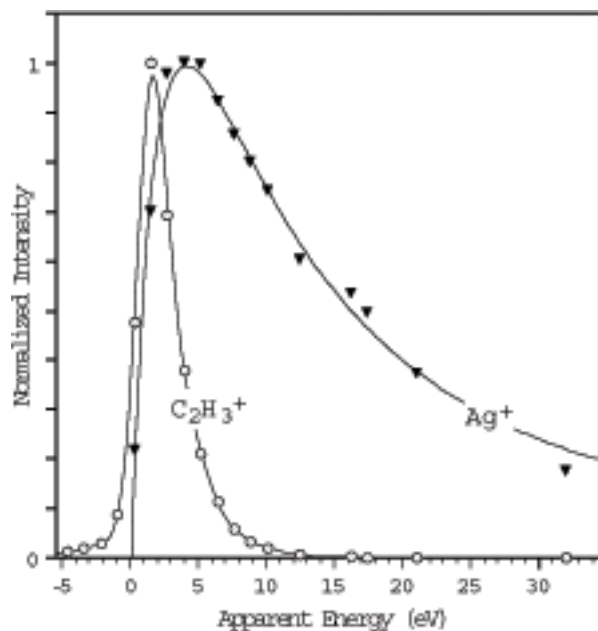
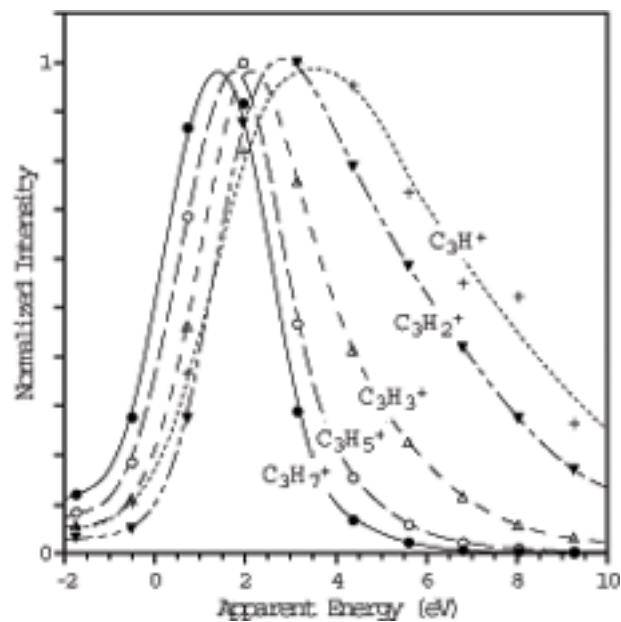


Fig. 14. Partial positive mass spectrum of triacontane cast on silver



**Fig. 15.** KEDs of  $\text{Ag}^+$  and  $\text{C}_2\text{H}_3^+$  sputtered from TC adsorbed on silver.



**Fig. 16.** KEDs of the  $\text{C}_3\text{H}_y^+$  ions sputtered from TC.

For the KED measurements, samples with a low TC coverage, i.e. with a significant Ag peak in the spectrum, were chosen to investigate the cationisation process (section II.A.3) and to avoid any charging effect. To illustrate the behaviour of atomic ions, Fig. 15 compares the KEDs of  $\text{Ag}^+$  and  $\text{C}_2\text{H}_3^+$  sputtered from a TC/Ag sample.

The KED of  $\text{Ag}^+$  is broad (FWHM  $\cong 10$  eV), with a fast increase at low energy, a maximum around 4 eV and an important high energy tail. The full line corresponds to the fit by a Sigmund-Thompson equation [ $Y(E) \div E / (E+E_b)^3$ , where  $E_b$  is the surface binding energy] with  $E_b = 5.7$  eV [55]. Although the Sigmund-Thompson law is not strictly appropriate for ions, the quality of the fit indicates clearly that the emission of  $\text{Ag}^+$  is collisional (see section I.2.A.3). Other examples of atomic ions KED can be found in section II.A.1. In contrast, the energy spectrum of  $\text{C}_2\text{H}_3^+$  is narrow (FWHM  $\cong 3$  eV) and does not extend beyond 10 eV. As shown in the literature review, this behaviour is characteristic of polyatomic ions. The significant intensity observed for 'negative' apparent energies in the KED of  $\text{C}_2\text{H}_3^+$  can be attributed to fast metastable decay reactions occurring in the acceleration section of the spectrometer (see section II.A.2).

The evolution of the  $\text{C}_x\text{H}_y^+$  ions KED with decreasing ion hydrogen content ( $y$ ) is very intriguing. It is illustrated in Fig. 16 for the  $\text{C}_3\text{H}_y^+$  series. For fragments with similar masses ( $37 \leq m/z \leq 43$ ), the KED broadens markedly with increasing unsaturation (unsaturation effect). Although this effect becomes less pronounced with increasing carbon content ( $x$ ), it can be observed for each  $\text{C}_x\text{H}_y$  series up to  $m/z = 100$ .

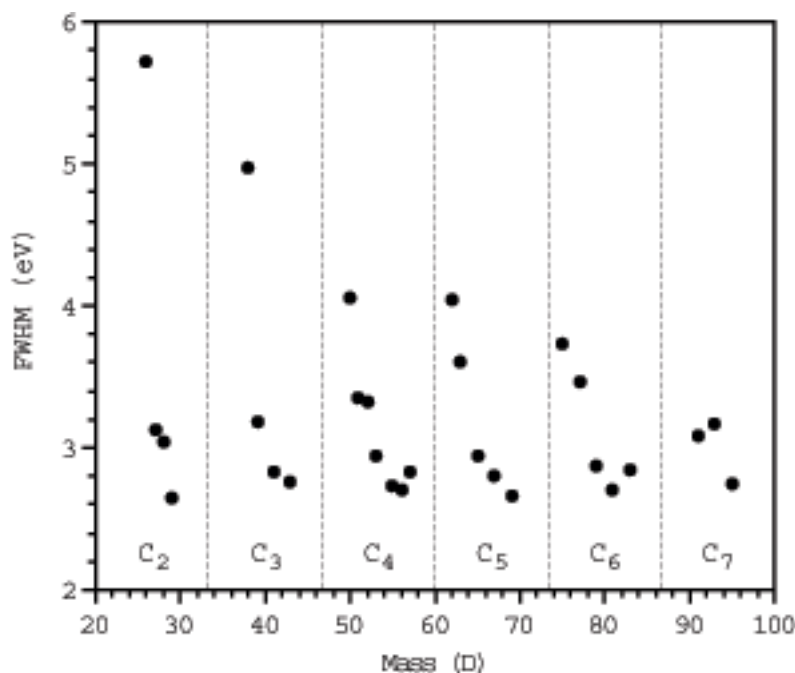


**Fig. 17.** FWHM of the distributions of hydrocarbon secondary ions sputtered from TC.

The modification of the KED shape with the ion unsaturation (and size) is reflected by the FWHM values (Fig. 17). In each  $C_xH_y$  series, the saturated hydrocarbon ions, characteristic of the TC molecule, have the thinnest distribution. In contrast, the less characteristic and more unsaturated ions have broader distributions.

On the other hand, Fig. 17 clearly shows that the spreading of the FWHMs decreases with increasing  $x$ . Thus, for a given  $y/x$  ratio, *the FWHM decreases with increasing ion mass (size effect)*.

Although the size effect was expected from the previous theoretical and experimental works, the unsaturation effect is difficult to interpret in the framework of the sputtering models presented in section I.2.A.3. This periodic variation is similar to the one reported by Papaléo et al. for fragment ions sputtered from PE and PS under 72.3 MeV  $^{127}I^{13+}$  primary ion bombardment [50]. Nevertheless, the variation discussed by Papaléo is deduced from the *radial* components of the secondary ions velocity, which does not allow a direct comparison with our data.

To explain this effect, we proposed an emission mechanism based on the initial transfer of momentum from the neighbouring atoms to the fragment precursor, in the surface region excited by the primary ion impact (Fig. 18 a). During the emission process, the internal energy excess of the precursor may be released by hydrogen elimination, leading to the generation of unsaturated ions (Fig. 18 b-c). The quantitative details are given in section II.A.1, but the main points of the process are summarised hereafter.

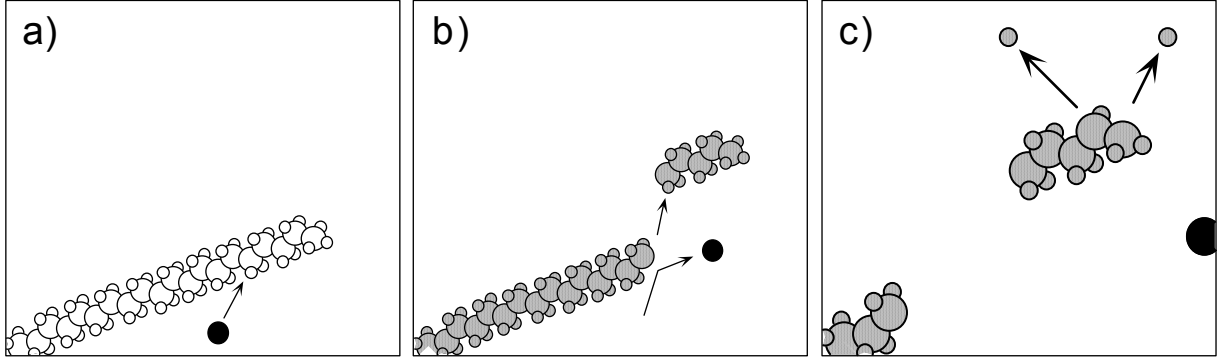


**Fig. 18.** Emission of a  $C_xH_y$  fragment. a) impact of a recoil atom with the fragment precursor; b) bond breaking and ejection of the precursor-like fragment in an excited state; c) decomposition of the excited fragment.

(i) The momentum is transferred to a carbon atom of the fragment, leading to a C-C bond-breaking (Fig. 18 a-b).

(ii) The remaining energy is distributed in the internal (vibration + rotation) and translational modes of the departing fragment precursor, according to Eq. (5) [74], where  $m$  is the mass of the impacted atom in the fragment,  $M$  is the total mass of the fragment,  $E$  is the total transferred energy,  $E_{\text{int}}$  is the internal energy and  $E_{\text{cm}}$  is the translational (centre-of-mass) energy.

$$E_{\text{cm}} = \frac{mE}{M} \quad (5) \quad E_{\text{int}} = \frac{(M-m)E}{M} \quad (5')$$

Eqs. (5) and (5') indicate that the internal energy fraction increases and that the kinetic energy fraction decreases with increasing fragment mass. A direct relation between  $E_{\text{cm}}$  and  $E_{\text{int}}$  can be deduced from these equations (Eq. 6).

$$E_{\text{cm}} = \frac{mE_{\text{int}}}{M-m} \quad (6)$$

For a given fragment, Eq. (6) evidences the correlation between the internal and kinetic energy fractions.

(iii) The internal energy excess  $E_{\text{int}}$  can be released by fast decomposition of the ion in the surface region (Fig. 18 c). Assuming that the departing ion dissociates by C-H bond breaking (hydrogen loss), its kinetic energy will be nearly unchanged. Indeed, it is reasonable to believe that the kinetic energy shared to the daughters will be proportional to their mass (fragmentation does not change the velocity). For a  $C_xH_y$  ion losing one hydrogen atom, the released kinetic energy will be less than 10 % of the total ion kinetic energy. By this mechanism, excited precursor ions relax by fragmentation in the surface region, giving rise to less characteristic, unsaturated ions with a high kinetic energy.

For the quantitative treatment, the internal energy excess released by hydrogen elimination can be approximated by the difference of formation energy ( $\Delta E_f$ ) between the reorganised ion and the precursor ion. Replacing  $E_{int}$  by this  $\Delta E_f$  in Eq. (6) allows to find a kinetic energy threshold  $E_{cm}^{min}$  for the reorganised ion. In general,  $\Delta E_f$  will be proportional to the number of lost hydrogen atoms, and the kinetic energy threshold  $E_{cm}^{min}$  will increase in parallel, accounting for the unsaturation effect observed in the KEDs. On the other hand, for a given internal energy excess,  $E_{cm}^{min}$  will decrease with increasing fragment mass  $M$  (Eq. 6). This dependence on  $1/M$  explains the above-mentioned size effect. Similarly, the consideration of several dissociation pathways with different  $\Delta E_f$  give minimum and maximum values  $E_{cm}^{min}$ ,  $E_{cm}^{max}$  for each reaction, i.e. for each fragment ion. Then, the average of these two calculated values,  $\langle E_{cm} \rangle$ , can be correlated with the experimental data.

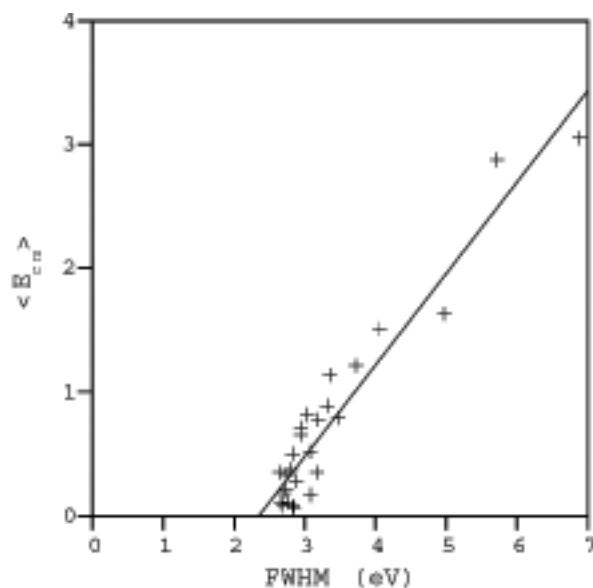


**Fig. 19.** Correlation between the calculated  $\langle E_{cm} \rangle$  and the FWHM of the  $C_xH_y^+$  ion distributions for TC adsorbed on silver.

The characteristic  $\langle E_{cm} \rangle$  values have been calculated for  $C_xH_y$  ions sputtered from TC (Fig. 19). Although there is a deviation from the linear regression, the correlation between  $\langle E_{cm} \rangle$  and the FWHM of the ion distributions is marked. The apparent FWHM threshold (2.5 eV) may be due to the combined action of two experimental artefacts: (i) the limited resolution of the energy slit (1.5 eV); (ii) the broadening of the distributions towards the low energy side caused by the distribution of metastables. In this respect, it is interesting to note that the metastable fraction (intensity fraction corresponding to 'negative' apparent energies) increases with decreasing unsaturation in the  $C_xH_y^+$  series (Fig. 16).

The full treatment has been achieved for hydrocarbon ions sputtered from tricosenoic acid in section II.A.1. In this case,  $\langle E_{cm} \rangle$  is clearly correlated with the median and FWHM of the experimental KEDs, too. In addition, the slope of the line is equal to 1 when the median of the distributions is used instead of the FWHM.

## Summary of the Results

The good correlation obtained between the calculated kinetic energy  $\langle E_{cm} \rangle$  and the characteristic energy width and median of the experimental KEDs is in favour of the proposed emission-fragmentation mechanism. Also, it shows the importance of hydrogen losses in the emission process. In this respect, it must be noticed that the easy elimination and recombination of hydrogen radicals during emission have been observed by Taylor and Garrison using molecular dynamics [85,86].

The unsaturation and size effects have been observed for adsorbed polymers, like PIB and PS, too. The periodic variation of the FWHMs is illustrated in Fig. 20 for PIB cast on silicon. In the case of polymers, the quantitative aspects of the model can not be directly applied, because the secondary ion emission requires two bond-breaking. More complicated sequences of events might be needed to provoke the sputtering of a molecular fragment (multiple collision, vibrational or electronic effects). For example, the preliminary creation of pendant radicals during the penetration of the primary ion in the polymer, followed by their ejection with the subsequent collision cascade would provide similar initial conditions than those considered in the above mechanism.

Although the described process might be too simple, the similarity of the observed effects is in favour of an identical sputtering mechanism for short molecule and polymer fragments, based on the initial momentum transfer to the fragment precursor and on the subsequent dissociation of the excited ejectum.

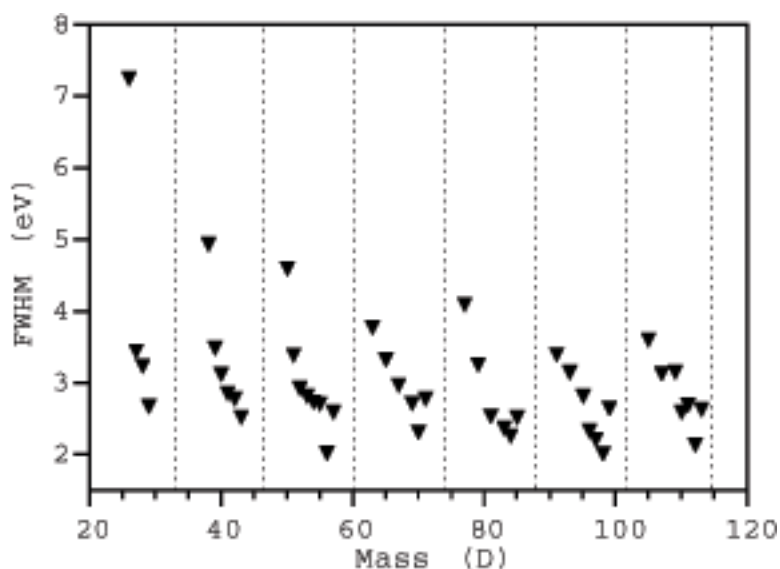


**Fig. 20.** FWHM of the distributions of hydrocarbon secondary ions sputtered from PIB.

#### I.4.A.5. Unimolecular dissociation of fragment ions in the vacuum

During the emission process of molecular secondary ions, the departing species receive both kinetic and internal energy, the latter being shared between the different vibration and rotation modes. If the polyatomic particle lays prior to emission in a region close to the primary impact point, where the deposited energy is high, the internal energy excess will probably cause its direct fragmentation (*vide supra*). On the other hand, if the received energy is lower, the internal energy may be absorbed in the rotation and vibration modes without fragmentation, resulting in the emission of the particle in an excited state. These excited molecular ions may then decompose during their time-of-flight in the spectrometer, which has important fundamental and analytical consequences.

Following the unimolecular reaction theory [109], the metastable decay of a parent ion can be described with a simple exponential equation:

$$Y_p(t) = Y^o \exp(-rt) \quad (7)$$

where  $Y^o$  is the initial number of parent ions. As recalled in section I.2.A.3, the constant ( $r$ ) in the exponential is the rate of dissociation and the half life of the metastable ion population ( $\tau_{1/2}$ ) is proportional to the inverse of  $r$ . The parameter governing the rate of dissociation of excited species is the excess of internal energy ( $E_{int}$ ) in the particle.

The number of daughter ions in time  $t$  can be easily obtained from Eq. (8) and its time derivative can be calculated by Eq. (9).

$$Y_d(t) = Y^o - Y_p(t) \quad (8)$$

$$\frac{dY_d(t)}{dt} = rY^o \exp(-rt) \quad (9)$$

With our ToF-SIMS, the daughter ions resulting from unimolecular dissociation of their metastable parents in the linear part of the spectrometer can be observed in the energy spectra of the secondary ions. Indeed, when they dissociate, the parents share their kinetic energy between the neutral and ion fragments in a proportion depending on the respective masses of these fragments. Consequently, the daughter ions originating from the dissociation process will be detected with a kinetic energy  $E_{acc} - \Delta E_{neutral}$ , lower than the kinetic energy of identical ions directly emitted from the surface.

In the remainder of this section, the results concerning the metastable decay of molecular ions sputtered from PIB, PBD and PS will be summarised and discussed.

##### *a) Metastable decay in the acceleration section*

For short lifetimes, typically in the range  $10^{-9}$  -  $10^{-7}$  s, the dissociation reaction occurs in the acceleration section of the ToF spectrometer. Then, the metastable ions

decompose before being completely accelerated (3 kV). These daughter ions having a kinetic energy deficit constitute a 'negative energy' tail in the KEDs. To illustrate this, the energy spectra of  $C_3H_5^+$  ( $m/z=41$ ) and  $C_4H_7^+$  ( $m/z=55$ ) sputtered from PIB are shown in Fig. 21. As was the case for  $C_xH_y$  ions ejected from TC (Fig. 16), the intensity remains significant for negative apparent energies, indicating the presence of unimolecular dissociation reactions in the vacuum. In principle, the simultaneous knowledge of the negative part of the KED and of the mass of the neutral fragment allows to deduce the lifetime of such metastable ions [118,119].

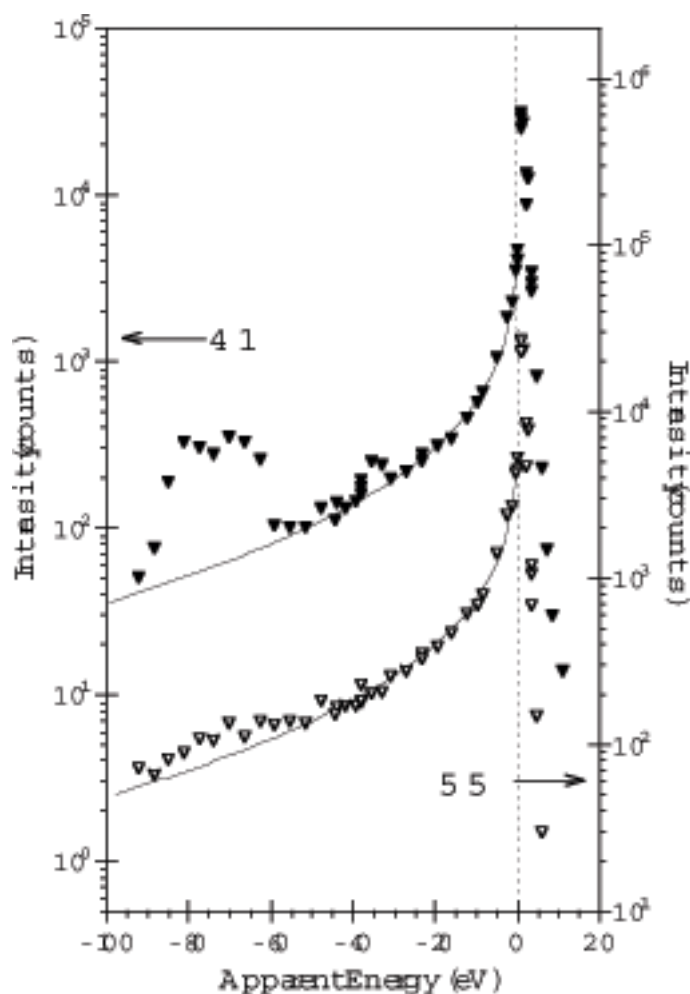


**Fig. 21.** KEDs of  $C_3H_5^+$  ( $m/z=41$ ) and  $C_4H_7^+$  ( $m/z=55$ ) sputtered from PIB. The solid line corresponds to the least square fit of the data by Eq. (12). [accelerating voltage  $V = 1500 V$ ].

Equations (8) and (9) can be used to explain the shape of the negative tails observed in Fig. 21. Nevertheless, one must be aware that this implies two severe hypotheses: (i) the decay of the considered parent occurs mainly via a single reaction, and not by several parallel reaction channels; (ii) the internal energy distribution of the parent ion is narrow and centred around a value  $E_{int}$  corresponding to a given rate  $r$ .

For an ion of mass  $m$  losing a neutral of mass  $\Delta m$  in the acceleration section of the spectrometer, the relation between the energy deficit  $\Delta E_k$  and the time-of-flight  $t$  at the dissociation point is described by Eq. (10), where  $e$  is the electron charge,  $l_{acc}$  is the length of the acceleration section and  $V$  is the accelerating voltage.

$$t = \frac{ml_{acc}}{eV} \left( \frac{2}{\Delta m} \right)^{1/2} \Delta E_k^{1/2} \quad (10)$$

Thus, the increment of energy  $d\Delta E_k$  corresponds to an increment of time :

$$dt = \frac{1}{2} \frac{ml_{acc}}{eV} \left( \frac{2}{\Delta m} \right)^{1/2} \Delta E_k^{-1/2} d\Delta E_k = \frac{1}{2} K \Delta E_k^{-1/2} d\Delta E_k \quad (11)$$

where  $K = \frac{ml_{acc}}{eV} \left( \frac{2}{\Delta m} \right)^{1/2}$ .

With these equivalences, one can calculate the derivative of the number of daughter ions as a function of the energy deficit  $\Delta E_k$  (Eq. 12)

$$\frac{dY_d}{d\Delta E_k} = \frac{dY_d}{dt} \times \frac{dt}{d\Delta E_k} = \frac{1}{2} KrY^o \Delta E_k^{-1/2} \exp(-rK\Delta E_k^{1/2}) \quad (12)$$

This derivative is the quantity observed in the negative part of the KEDs. Fitting the experimental data with Eq. (12) gives a very good agreement with the decaying baseline located between -100 and +0 eV in the KED of  $C_3H_5^+$  and  $C_4H_7^+$ , but it can not explain the peak at -75 eV in the distribution of  $C_3H_5^+$  (Fig. 21). It will be shown in the next paragraph that this peak is due to metastable decay in the drift region of the spectrometer.

The fraction of daughter ions produced in the acceleration section can be determined by integrating the 'negative energy' part of the KEDs for most of the secondary ions sputtered from PIB, PBD and PS cast on silicon. The results are reported in Fig. 22. On average, the fraction of ions produced by fast metastable decay increases with the mass of the daughter ion. This can not be explained by the fact that heavy parents spend a longer time in the acceleration section than lighter ones. Indeed, the reactions observed in the acceleration section are so fast that they occur completely in this section, for fast small ions as well as for slower heavy ions. The same trend has been reported by Zubarev and co-workers for secondary ions sputtered from a peptide mixture under 72 MeV,  $^{127}I^{13+}$  ion bombardment [54]. A possible explanation is that small ions, sputtered from the high deposited energy region, have already lost their internal energy excess by direct fragmentation during the emission process. In contrast, larger molecular ions, which are thought to be produced farther from the primary impact point, might be emitted without extensive fragmentation, but with a certain amount of internal energy leading to delayed decomposition.

## Summary of the Results

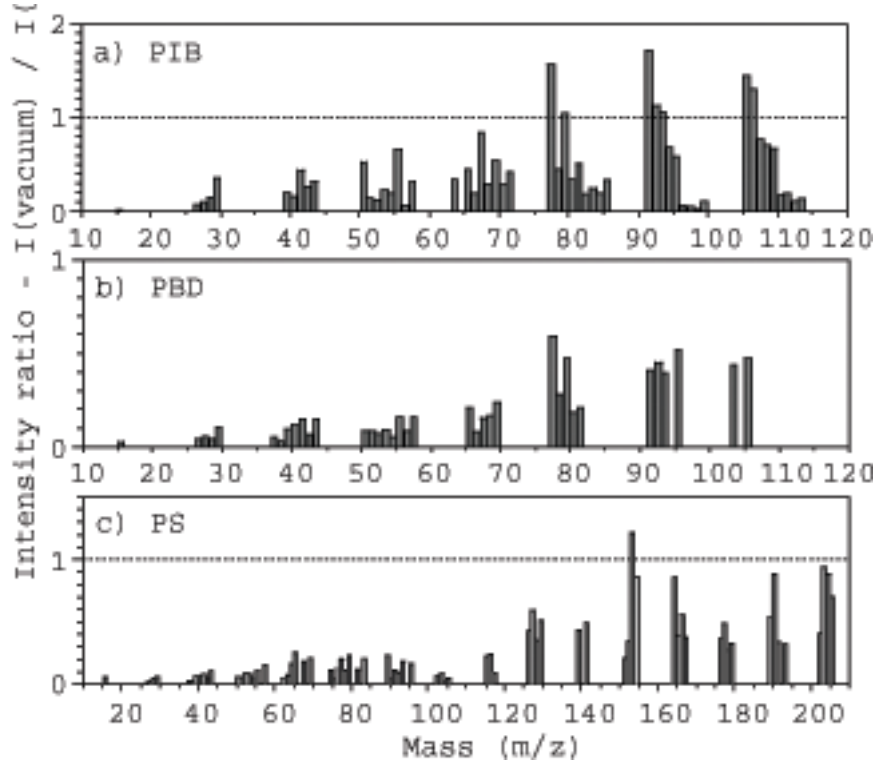


**Fig. 22.** Daughter ions produced in the acceleration section of the spectrometer. Ratio of the *number of ions produced in the vacuum per ion produced at the surface*.

The relative importance of the ion production by fast metastable decay follows the order of increasing hydrogen content of the polymers (PIB > PBD > PS). In the case of PIB, it is clear that the fraction of ions formed in the vacuum is very weak for characteristic ions ( $C_4H_8^+$ :  $m/z=56$ ,  $C_7H_{13}^+$ :  $m/z=97$  and  $C_7H_{14}^+$ :  $m/z=98$ ,  $C_8H_{15}^+$ :  $m/z=111$  and  $C_8H_{16}^+$ :  $m/z=112$ ). In the contrary, the ratio  $Y_{\text{metastable}} / Y_{\text{surface}}$  is larger than 1 for stable, aromatic secondary ions ( $C_6H_5^+$ :  $m/z=77$ ,  $C_7H_7^+$ :  $m/z=91$ ,  $C_8H_9^+$ :  $m/z=105$ ). Thus, for large molecular ions sputtered from PIB (above  $m/z=75$ ), the daughter ion fraction is inversely proportional to the ion yield.

### *b) Metastable decay in the field-free drift region*

For longer lifetimes, approximately  $10^{-6}$  -  $10^{-4}$  s, the parent ions decompose in the field-free drift section of the spectrometer preceding the first electrostatic analyser. In this case, the daughter ions of a given reaction have the same kinetic energy deficit, which is independent on the dissociation time because they are no longer accelerated in this section. Thus, they constitute a well-defined peak in the energy spectrum, and the mass of the neutral lost can be easily determined knowing the energy deficit (Eq. 13, see section II.A.2 for details).

$$\frac{\Delta m}{m} \frac{E_k}{\Delta E_k} = 1 \quad (13)$$

Fig. 23 shows the KED of several unsaturated ions observed in the mass spectra of PIB and PS. As was the case for  $C_3H_5^+$  sputtered from PIB (Fig. 21), beside the main peak in the positive part of the energy spectrum, these ion KEDs exhibit well-defined peaks at negative apparent energies. By Eq. (13), it is possible to assign these peaks. For PIB, the intense peak series in the negative apparent energy part corresponds to the daughter ions formed by the reaction  $C_xH_y^+ \rightarrow C_xH_{y-2}^+ + H_2$ . For PS, it is caused by the reaction  $C_xH_y^+ \rightarrow C_xH_{y-1}^+ + H$ . Conversely, the minor peaks with a lower energy deficit in the distributions of  $C_3H_3^+$  ( $m/z=39$ ) and  $C_5H_5^+$  ( $m/z=65$ ) sputtered from PIB are due to a single H loss, while the minor peak with a higher energy deficit in the distribution of  $C_8H_7^+$  ( $m/z=103$ ) sputtered from PS is due to a  $H_2$  loss.

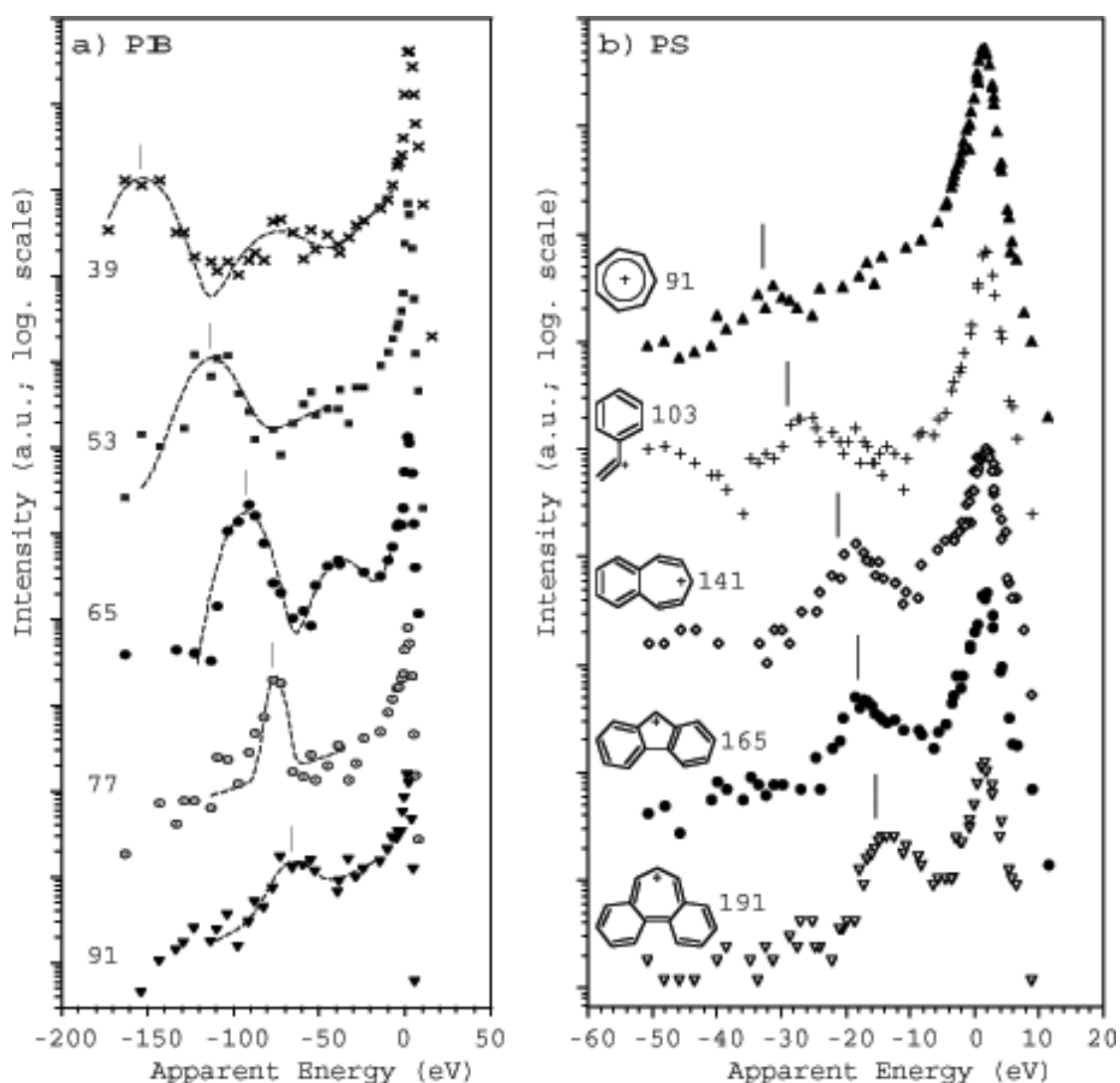


**Fig. 23.** KED of unsaturated molecular ions sputtered from PIB (a) and PS (b). (a) PIB: the vertical bars indicate the theoretical energy deficits for the reactions  $C_xH_y^+ \rightarrow C_xH_{y-2}^+ + H_2$ ; (b) PS: the vertical bars indicate the theoretical energy deficits for the reactions  $C_xH_y^+ \rightarrow C_xH_{y-1}^+ + H$ . [accelerating voltage  $V = 3000$  V]

## Summary of the Results

**Table 5.** Observed metastable decay reactions for molecular ions sputtered from PIB, PBD and PS. The relative daughter ion intensities are indicated in *italic*.

Metastable decay reactions	$Y_{\text{metastable}} / Y_{\text{surface}} \times 100$			
	$M_d$ (m/z)	PIB	PBD	PS
$C_3H_5^+ \rightarrow C_3H_3^+ + H_2$	39	<i>29</i>	-	-
$C_3H_4^+ \rightarrow C_3H_3^+ + H$	39	<i>7</i>	<i>5</i>	-
$C_3H_7^+ \rightarrow C_3H_5^+ + H_2$	41	<i>23</i>	-	-
$C_4H_7^+ \rightarrow C_4H_5^+ + H_2$	53	<i>17</i>	-	-
$C_4H_6^+ \rightarrow C_4H_5^+ + H$	53	-	<i>4</i>	-
$C_5H_7^+ \rightarrow C_5H_5^+ + H_2$	65	<i>73</i>	<i>53</i>	-
$C_5H_6^+ \rightarrow C_5H_5^+ + H$	65	<i>32</i>	<i>10</i>	-
$C_5H_8^+ \rightarrow C_5H_7^+ + H$	67	-	<i>9</i>	-
$C_6H_7^+ \rightarrow C_6H_5^+ + H_2$	77	<i>118</i>	<i>70</i>	-
$C_6H_6^+ \rightarrow C_6H_5^+ + H$	77	-	<i>13</i>	<i>4</i>
$C_6H_9^+ \rightarrow C_6H_7^+ + H_2$	79	<i>199</i>	<i>62</i>	-
$C_6H_8^+ \rightarrow C_6H_7^+ + H$	79	<i>37</i>	<i>22</i>	-
$C_7H_6^+ \rightarrow C_7H_5^+ + H$	89	-	-	<i>26</i>
$C_7H_9^+ \rightarrow C_7H_7^+ + H_2$	91	<i>91</i>	<i>46</i>	-
$C_7H_8^+ \rightarrow C_7H_7^+ + H$	91	-	<i>27</i>	<i>1</i>
$C_7H_{11}^+ \rightarrow C_7H_9^+ + H_2$	93	<i>61</i>	<i>26</i>	-
$C_8H_9^+ \rightarrow C_8H_7^+ + H_2$	103	-	<i>77</i>	<i>8</i>
$C_8H_8^+ \rightarrow C_8H_7^+ + H$	103	-	-	<i>3</i>
$C_8H_{11}^+ \rightarrow C_8H_9^+ + H_2$	105	-	<i>43</i>	-
$C_9H_9^+ \rightarrow C_9H_7^+ + H_2$	115	-	-	<i>20</i>
$C_9H_8^+ \rightarrow C_9H_7^+ + H$	115	-	-	<i>4</i>
<sup>a</sup> $C_{10}H_9^+ \rightarrow C_{10}H_8^+ + H$	128	-	-	<i>31</i>
<sup>a</sup> $C_{11}H_{10}^+ \rightarrow C_{11}H_9^+ + H$	141	-	-	<i>25</i>
<sup>a</sup> $C_{12}H_9^+ \rightarrow C_{12}H_8^+ + H$	152	-	-	<i>55</i>
<sup>a</sup> $C_{13}H_{10}^+ \rightarrow C_{13}H_9^+ + H$	165	-	-	<i>40</i>
<sup>a</sup> $C_{14}H_{11}^+ \rightarrow C_{14}H_{10}^+ + H$	178	-	-	<i>21</i>
<sup>a</sup> $C_{15}H_{12}^+ \rightarrow C_{15}H_{11}^+ + H$	191	-	-	<i>69</i>

<sup>a</sup> In these series, only the main ions are reported.

The metastable H and H<sub>2</sub> loss reactions observed for PIB, PBD and PS are summarised in Table 5. The ions produced by these reactions have often an aromatic structure. This is probably due to the particular stability of (poly)cyclic ions. In this respect, it is interesting to note that for unsaturated hydrocarbon polymers, intense molecular ions observed beyond m/z = 200 in the mass spectra are (poly)cyclic aromatic ions [349,350,351]. This is valid for PS, but also for PBD, poly(isoprene), etc. These ions

do not reflect the polymer chemical structure (even in the case of PS), and their emission needs a complex reorganisation of the precursor, involving multiple hydrogen losses. The fact that such large molecular ions may survive to multiple bond-breaking without fragmenting into much smaller ions indicates their high stability. This stability must act as a driving force in the metastable decay process, too.

Although H<sub>2</sub> loss is predominant for PIB and PBD secondary ions, it is minor for PS. In the case of PS, a single H loss is the main decay channel. For large (poly)cyclic daughter ions produced from PS, this may be explained because the heavy species leaving the surface are already aromatic or very unsaturated. Then, the simultaneous loss of two hydrogen atoms might be less probable, or it would lead to a structure which is no longer cyclic, due to the hydrogen deficit, and thus, less stable.

For PIB and PBD, important fractions of ions formed in the vacuum are observed below  $m/z = 100$ , while it occurs mostly for heavier ions with PS. Again, the secondary ions emitted from PS are already very unsaturated and stable, which should reduce the probability to decay by hydrogen losses. This explanation might account for the decreasing fraction of metastable decay with increasing polymer unsaturation in the acceleration section, too.

The results presented in this section show that, for hydrocarbon polymers, both metastable decay in the acceleration section and in the drift region are important ion formation channels. The amount of ions resulting from unimolecular dissociation reactions

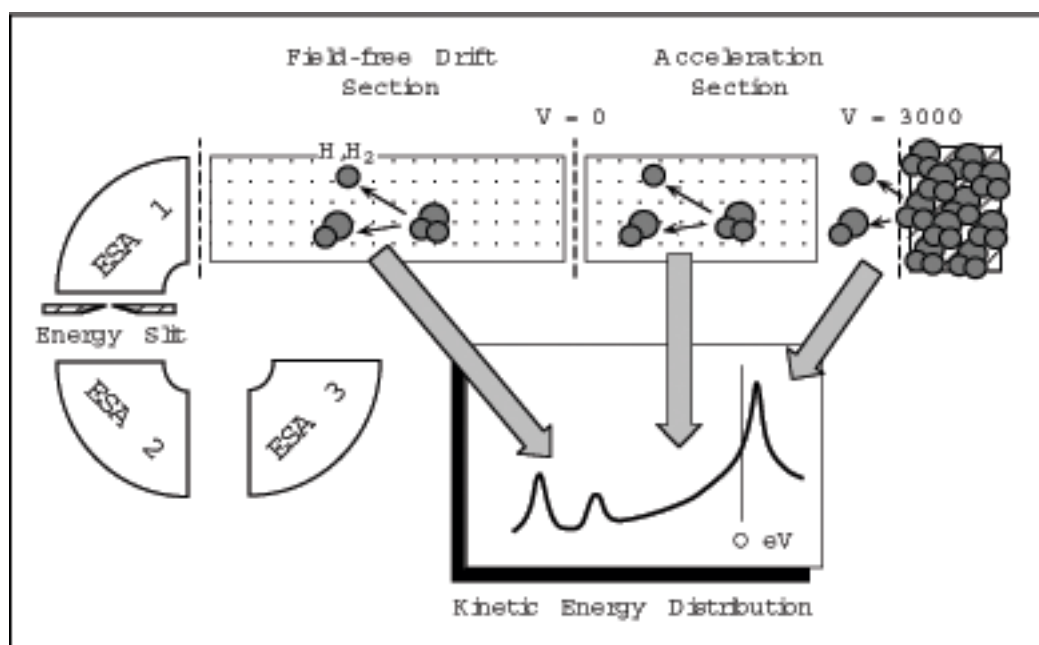


**Fig. 24.** Dissociation channels evidenced for molecular ions sputtered from hydrocarbon polymers (PIB, PBD, PS) and their relation with the KED. By order of increasing distance from the surface (decreasing internal energy): fragmentation in the surface region, dissociation in the acceleration section, H and H<sub>2</sub> loss in the field-free drift section.

## Summary of the Results

can be summarised by the total metastable fraction  $Y_{\text{metastable}} / (Y_{\text{surface}} + Y_{\text{metastable}})$ , which is equal to 26 % for PIB, 15 % for PBD and 15 % for PS.

To summarise this section, the different fragmentation channels evidenced for hydrocarbon molecular ions are described in Fig. 24: (i) direct fragmentation at the surface, corresponding to the main peak of the KED; (ii) fast metastable decay in the acceleration section of the spectrometer, explaining the regular intensity decrease in the 'negative energy' tail and (iii) loss of H and H<sub>2</sub> in the drift region of the spectrometer, leading to additional peaks for quantified energy deficits. These metastable decay reactions can be explained with simple arguments based on the unimolecular reactions theory.

### I.4.A.6. Emission of large parent ions from organic adsorbates

One of the most amazing effects in SIMS of organics is the emission of large intact molecules adsorbed on solid surfaces. A way to achieve high yields of large molecular ions in SIMS of organic materials and low molecular weight polymers is the cationisation of sputtered particles by complexation with metal substrate atoms. The discovery of this phenomenon is not recent [352]. Nevertheless, convincing explanations for cationised molecules and parent ion emission lack of experimental support. In the case of cationisation, the metal (Me) is thought to bring the positive charge to the neutral organic molecule (M), resulting in the formation of an organometallic complex ion of the kind  $(M+Me)^+$ . Three hypotheses are considered to explain the formation of these complexes [353]: (i) the complex is formed at the surface and is sputtered without fragmentation nor recombination (precursor model); (ii) the complex ion is formed in the selvedge by the recombination of a neutral molecule with a metal ion; (iii) the complex ion is formed from the metastable decay of larger  $M_xMe_y$  clusters.

For this thesis, the sputtering yield, KED and ion beam degradation behaviour of parent-like ions ejected from TSA, TC, DBA, TPN and PS oligomers have been measured and analysed. The details of this work are presented in section II.A.3. Hereafter, the attention will be focused on the parent-like ion KEDs.

The KED of the parent-like ions ejected from TC, DBA and PS oligomers are presented in Fig. 25. Several observations can be drawn from these curves:

(i) The maxima of the parent-like ion KEDs are in the region 0-2 eVs for TC and 2-4 eVs for PS and DBA. In addition, the KEDs of PS and DBA exhibit high energy tails expanding beyond 10 eV, which supports a collisional emission process. The KEDs are much thinner for cationised TC molecules. As shown in section II.A.3, the KEDs of TSA parent-like ions are very narrow and similar to those of TC. The higher mean kinetic energy of aromatic as compared to aliphatic molecular ions could be related to the better resistance of these ions against fragmentation.

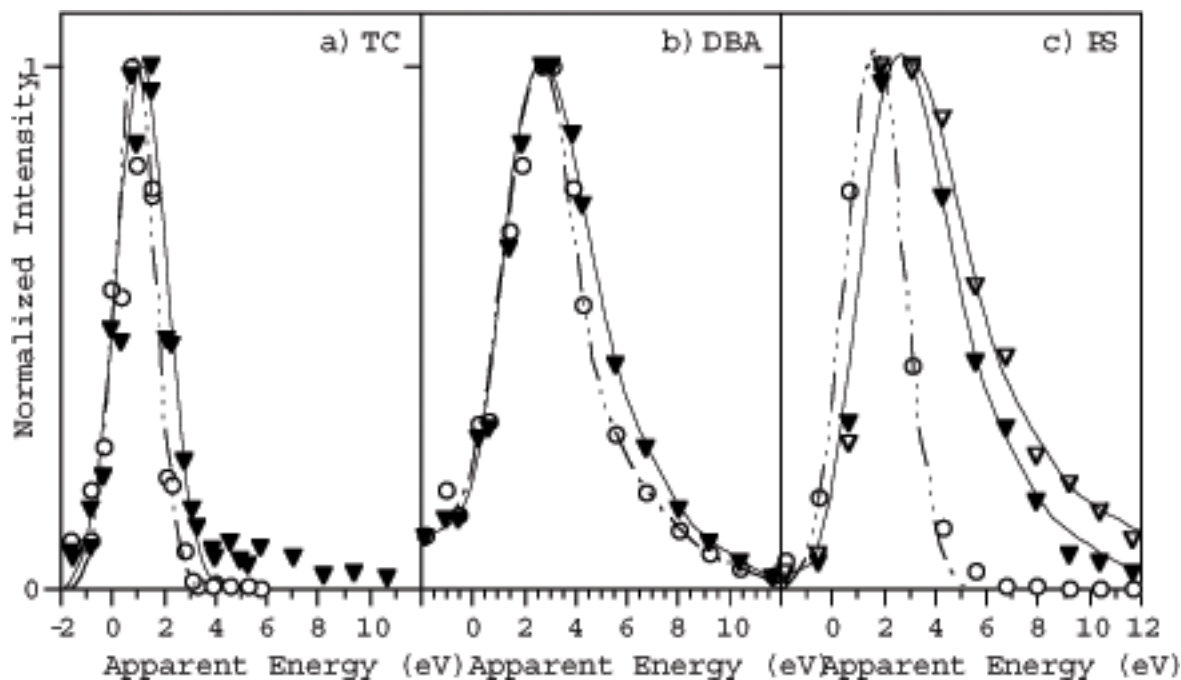


**Fig. 25.** KED of parent-like ions sputtered from TC, DBA and PS oligomers adsorbed on Ag. a) TC:  $C_{30}H_{60}^+$  ( $\circ$ );  $[C_{30}H_{60}]Ag^+$  ( $\blacktriangledown$ ); b) DBA:  $C_{22}H_{14}^+$  ( $\circ$ );  $[C_{22}H_{14}]Ag^+$  ( $\blacktriangledown$ ); c) PS:  $C_8H_8^+$  ( $\circ$ );  $[C_4H_9(C_8H_8)_nH]Ag^+$  for  $n=4$  ( $\blacktriangledown$ ) and  $n=12$  ( $\nabla$ ).

(ii) For DBA and PS, the slope of the high energy tails is close to the predictions of Urbassek ( $E^{-5}$ ) [75], Hoogerbrugge et al. ( $E^{-4.5}$ ) [76] and Haring et al. ( $E^{-4.5}$ ) [73] for the uncorrelated double collision process (see section I.2.A.3). In the case of TC, there is a change of slope in the high energy tail of the Ag-cationised molecule KED beyond 5 eV, which is not observed in the parent ion KED. After that point, the slope of the high energy tail is close to the one of the parent-like ions of PS and DBA. The change of slope suggests the contribution of two emission mechanisms, with different characteristic mean energies. Then, the high energy contribution could be collisional. For PS, the KEDs broaden and the high energy tails become softer with increasing oligomer size (from  $E^{-5}$  to  $E^{-3.5}$ ). This interesting effect will be investigated in details in the following.

(iii) In general, the Ag-cationised molecules are more energetic than the characteristic fragment and parent ions, as indicated by the shift of the maximum and/or by the width of the distribution (this effect is particularly marked for TPN, see section II.A.3).

(iv) Except for the negative apparent energy part, the KEDs of cationised DBA and PS molecules are very similar to each other, which is in favour of an identical emission mechanism.

(v) Unexpectedly, the metastable contribution is significant for parent-like ions, too. It is very important for DBA (>30%), lower for TC (~15%) and weak for PS parent-like

ions (<2.5%). Thus, a fraction of the parent-like ions is produced by the decomposition of larger  $M_xAg_y^+$  aggregates in the vacuum.

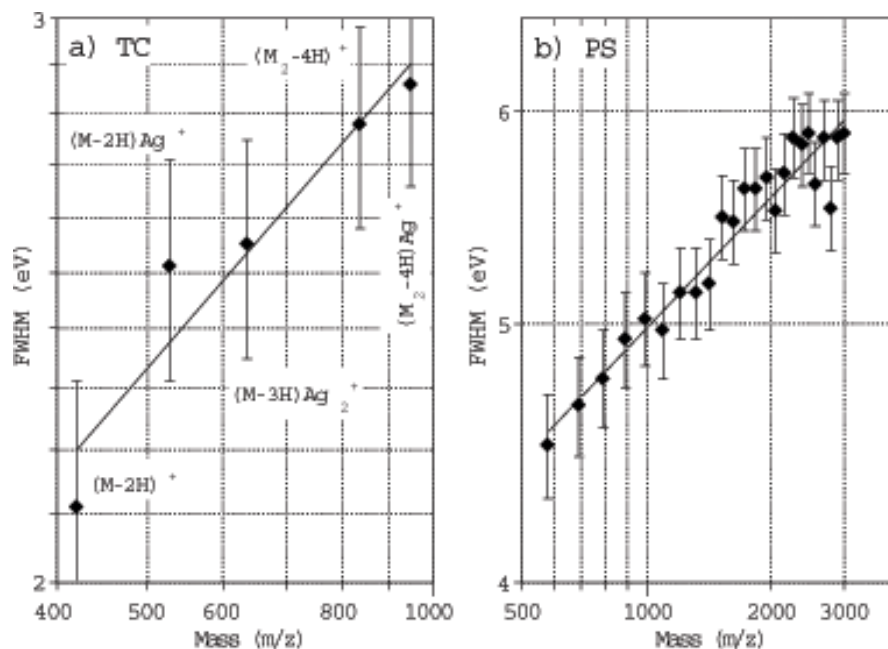


**Fig. 26.** FWHMs of the distributions of parent-like ions sputtered from a) TC and b) PS.

The evolution of the distribution FWHMs with the molecular ion sizes is informative, too (Fig. 26). For TC, the KED is broader for the dimer ion and Ag-cationised dimer than for the monomer homologues (Fig. 26a). The FWHM increases from 2 to 3 eV for masses in the range  $400 < m/z < 1000$ . It should be noted that this effect includes all the  $M_xAg_y^+$  ions indistinctly ( $0 \leq y \leq 2$ ). For Ag-cationised PS oligomers, which are *identical* from the chemical viewpoint, the effect is even more obvious (Fig. 26b). The FWHM varies from 4.5 to 6 eV for masses in the range  $500 < m/z < 3000$ .

The trends of Fig. 26 are contrary to the size effect observed for fragment ions (*vide supra*). Since only few results have been presented, the details of the discussion concerning large ions emission and cationisation will not be reported in this introductory part (the reader is invited to see section II.A.3 for this discussion). Instead, we will propose three arguments, based on these results, which lead us to think that a multiple collision process is required to explain the emission of large parent-like ions:

(i) In the case of Ag-cationised PS oligomers, a large number of ions have more than 5 eV kinetic energy (Fig. 25c). Suppose that the emission is caused by a single collision between a recoil Ag (C) atom and a carbon atom of the molecule. According to Eq. (6), to provide 5 eV kinetic energy, the internal energy transferred to the molecule by this localised impact should be as high as 200 eV for a PS oligomer with 4 repeat units. This is equivalent to the energy of all the C-C bonds of the molecule. For metal substrates, Garrison has

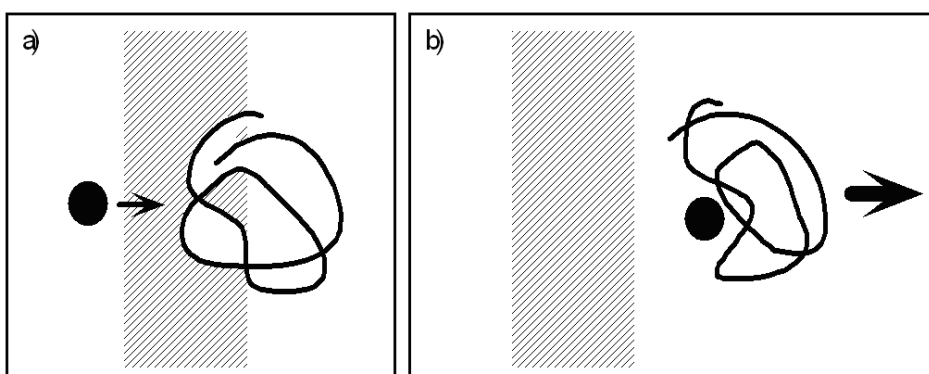


**Fig. 27.** PS oligomer emission and cationisation by the interaction with a recoil silver atom

argued that the heavy recoil atom might interact with several carbon atoms of the molecule [80]. If the interaction involves four carbon atoms, the internal energy is reduced to 50-60 eV. Even in these conditions, it is hard to believe that a localised, single impact may cause the emission of the molecule without fragmentation. This argument is valid for DBA and TPN, too.

(ii) Consider the hypothesis described in Fig. 27, i.e. the association of a silver atom with a PS oligomer as a result of the interaction between the moving silver atom and the oligomer at rest. In this case, the KED of the (M+Ag) aggregate can be calculated with simple mechanistic arguments on the basis of the recoil Ag atoms distribution, *if fragmentation is neglected*. In first approximation, the experimental KED of  $\text{Ag}^+$  can be used to model the Ag distribution. The initial interaction with one or more carbon atoms is

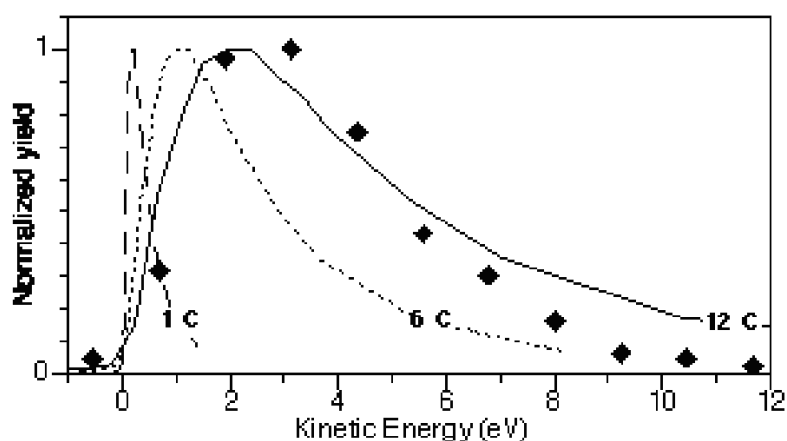


**Fig. 28.** Experimental KED of  $[\text{C}_4\text{H}_9(\text{C}_8\text{H}_8)_4\text{H}]\text{Ag}^+$  sputtered from PS (◆) and calculated distributions according to the scenario displayed in Fig. 27. The silver atom transfers a parallel momentum to 1, 6 or 12 carbon atoms.

easily taken into account in the calculation. The calculated distributions are shown in Fig. 28 in the case of an oligomer containing 4 repeat units. The results indicate that the kinetic energy provided by one silver atom is not sufficient to explain the KED of the Ag-cationised oligomer if the silver atom interacts with one and even six carbon atoms of the molecule. To obtain a sufficient kinetic energy for the aggregate, the initial interaction with *twelve* carbon atoms is needed. In fact, the concerted push of two or three substrate atoms is more probable.

(iii) In the single recoil impact hypothesis, the dependence of the mean kinetic energy as a function of the particle size should be as  $M^{-1}$  (Eq. 6). The observed dependence for Ag-cationised PS oligomers is  $M^{+0.16}$ . To reconcile these results, one should assume that the mean internal energy increases as  $M^{+1.16}$ , i.e. that the fragmentation threshold increases drastically with the particle mass, which, again, is improbable considering a fast and localised impact.

In conclusion, these results support a model in which the large organic molecules are pushed by the concerted action of several substrate atoms. Larger aggregates of the form  $M_xMe_y^+$  are sputtered too. Those having an internal energy excess may decay during their time-of-flight, giving rise to the delayed generation of  $M^+$  and  $(M+Me)^+$  parent-like ions in the vacuum.

#### I.4.A.7. Towards a comprehensive picture of molecular ion emission

Taking into account the results reported in sections I.4.A.4-6 and in the literature (section I.2.A.3), a tentative picture of thin organic layer sputtering, although speculative, may be sketched. The chronology of the different stages is displayed in Fig. 29 for short PS oligomers adsorbed on a heavy substrate. The energies indicated in Fig. 29a-c are typical values of the *kinetic energy per sputtered atom* measured for the considered processes.

First, the primary ion penetrates into the solid, creating a highly excited region around the impact point. In the early times of the collision cascades, only atomic or very small molecular ions may be emitted from this small excited volume, due to the high energies involved, which lead to the extensive fragmentation of the organic molecules (Fig. 29a).

When the excited volume has spread out and cooled down, less energetic recoils eject small and/or excited molecular fragments (and substrate atoms clusters) which may dissociate or rearrange to release their internal energy excess (hydrogen loss), keeping a rather high kinetic energy (Fig. 29b).

In the last stages of the cascades, large precursor-like fragments and intact molecules may be sputtered from farther away, probably with the concerted action of several substrate atoms (Fig. 29c).

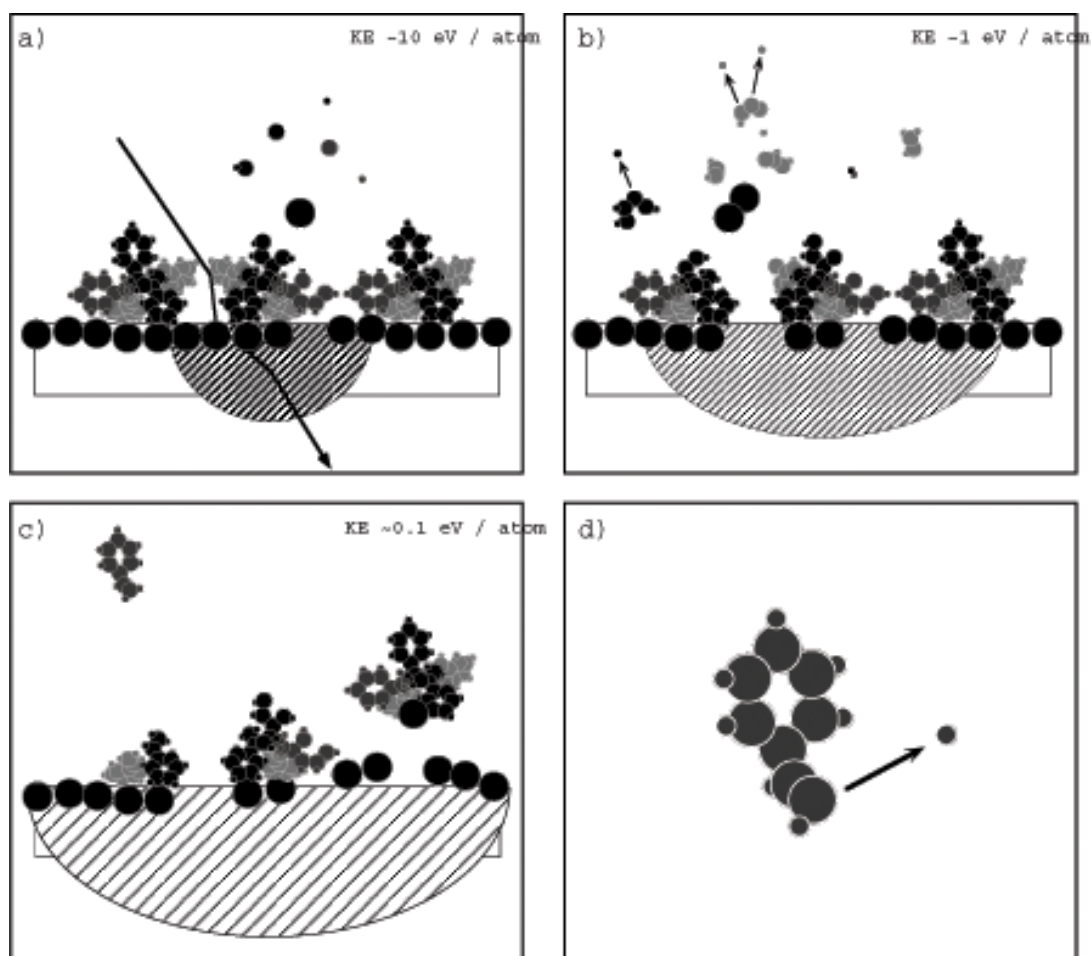


**Fig. 29.** Chronological picture of the different stages of sputtering for a thin layer of PS oligomers cast on a metal surface under keV ion bombardment. a) Penetration of the primary ion and emission of fast atomic ions; b) Expansion and cooling down of the excited volume; ejection of small and excited molecular fragments; c) Emission of precursor-like fragments and desorption of intact oligomers; d) Unimolecular dissociation of the excited secondary particles far away from the surface.

During their time-of-flight to the spectrometer, fragments, parents and clusters bearing an internal energy excess may decompose into smaller daughter particles, accounting for the negative tails in the measured KEDs (Fig. 29d).

In summary, the results suggest that atomic or little fragment ions, which have lost the memory of the organic molecule structure, are sputtered in the first stages of the collision cascades, from the region of the primary ion impact where the deposited energy is high. Instead, the precursor-like fragments and parent-like particles would be mainly produced when the cascade energy is much lower and at some distance from the primary impact point.

#### **I.4.A.8. Conclusion**

In this fundamental approach of secondary ion ejection from thin organic layers, we have shown that different ion emission mechanisms generate different KED shapes. Several processes could be evidenced : (i) low-energy emission of precursor-like fragments, reflecting the chemical structure of the organic molecules; (ii) emission of fragmented ions having a higher mean kinetic energy and a lower hydrogen content than the precursor; (iii) desorption of intact oligomers and molecules requiring the interaction with several recoil atoms, as witnessed by their rather high kinetic energies (iv) 'fast' ( $10^{-8}$  s) and 'slow' ( $10^{-5}$  s) metastable decay of excited molecular fragment, parent and cluster ions during their time-of-flight to the spectrometer.

With the TRIFT spectrometer, the sample is put at a high voltage (3000 V) in order to accelerate the departing secondary ions and the KED measurements are conducted using an energy filtering procedure. In this experiment, the slightest charging effect (1 V versus 3000 V) induces a drastic modification of the KED shape. Therefore, the KED measurements would not have been possible with thicker insulating layers or bulk polymers. Nevertheless, except the cationisation by substrate atoms, which is not observed with thicker layers for evident reasons, and, to a lesser extent, the emission of large parent-like ions, the other effects are likely to occur with thick films and bulk organic compounds. This is supported by the remarkable similarity between the relative and absolute molecular ion yields observed in the fingerprint region of the spectra for thin and thick coatings (provided that the layer is thick enough to avoid any substrate effect, see section II.A.2). In particular, the observation of the same satellite peaks in the mass spectra of thin layers and bulk polymers shows that identical metastable decay reactions occur in both cases.

By the detailed analysis of the mass spectrum, ion yield, KED and ion beam degradation data, rather general trends have been evidenced concerning the sputtering of molecular ions from thin organic layers. As already mentioned, some of these trends may be valid for thick films and bulk polymers, too. This wealth of data would not have been obtained without the various existing methods for thin layer elaboration, e.g. spin-coating, Langmuir-Blodgett and alternate polyelectrolyte physisorption. Owing to these techniques, high-quality model systems could be built up and studied from the viewpoint of the sputtering process. In the articles of sections II.A.1-3, all the results reviewed in this part of the thesis (and others) are presented in details, for various samples and preparation methods. The analysed samples and the types of result are indexed in Table 6.

In the second part of this thesis (referenced by a B letter), the approach will be reversed, since the unique analytical capabilities of ToF-SIMS will be used to investigate the structure of polyelectrolyte multilayers.

**Table 6.** Index of the results reported in the thesis (Part A). The corresponding section is indicated for each combination of sample and result type.

	Mass spectrum	Ion beam degradation	Substrate effect	Atomic ion KED	Fragment ion KED	Metastable decay	Parent-like ion KED
TSA	II.A.1.2	-	II.A.3.1	II.A.1.1 II.A.3.1	II.A.1.1 II.A.1.2	II.A.3.1	II.A.1.1 II.A.3.1
TC	I.4.A.4 II.A.3.1	II.A.3.1	II.A.3.1	II.A.3.1	I.4.A.4	II.A.3.1	I.4.A.6 II.A.3.1
DBA	II.A.2.1	-	-	II.A.3.1	II.A.2.1	II.A.2.1	I.4.A.6 II.A.3.1
TPN	II.A.3.1	II.A.3.1	II.A.3.1	II.A.3.1	-	II.A.3.1	II.A.3.1
PIB	II.A.1.4	II.A.1.4	-	II.A.1.4	I.4.A.4 II.A.1.4	I.4.A.5 II.A.1.4	-
PBD	-	-	-	-	-	I.4.A.5	-
PS 60000	II.A.2.1	-	II.A.2.1	II.A.1.4	II.A.1.4 II.A.2.1	I.4.A.5 II.A.2.1	-
PS 1100	II.A.3.1	-	-	II.A.3.1	II.A.3.1	II.A.3.1	I.4.A.6 II.A.3.1
PET	II.B.2.1	-	-	-	II.A.1.3	-	-
MV copolymer		-	-	II.A.1.3	II.A.1.3	-	-
Polyions P1 & P2	II.B.1.3	-	-	-	II.A.2.2	II.A.2.2	-

## **I.4.B. Surface analysis of alternate polyelectrolyte multilayers**

---

### **I.4.B.1. Introduction**

The study of thin organic films by ToF-SIMS is appropriate to get information concerning the layer structure and lateral homogeneity (phases, defects), the molecule bonding states, the surface chemical reactions, the effects of the environmental and preparation conditions, etc. It has proved to be useful for the study of Langmuir-Blodgett and self-assembled layers (section I.2.B.3).

In the following, results will be reported concerning the analysis of alternate polyelectrolyte multilayers by ToF-SIMS. Preliminary experiments combining surface analysis results in correlation with XRR and AFM data will lead to a quantitative determination of the information depths in XPS and ToF-SIMS. By this means, a quantitative evaluation of the organic multilayer thicknesses for uncharacterised samples will be possible using XPS or ToF-SIMS. The main interest for this development is that XPS and ToF-SIMS may give results for samples which cannot be treated by XRR and AFM (rough substrates, substrates which are indistinguishable from the coating by optical or mechanical means).

The unambiguous interpretation of the ToF-SIMS data measured for well-known samples deposited on model supports (silicon wafers) will constitute the basis for a more prospective investigation of the multilayer adsorption on 'real world' substrates (polymers). In this context, it will be shown that the combined use of ToF-SIMS and XPS brings a sufficiently large number of data to build up a convincing picture of the polyelectrolyte adsorption on polymers. In general, information will be gained about surface chemistry, multilayer structure, counterion binding, functionalisation and crosslinking reactions, lateral organisation of the layers, etc.

After a brief description of the samples and characterisation techniques, the results part will begin with the important issue of the information depth in XPS and ToF-SIMS (section I.4.B.4). The interpretation of the experiments conducted with multilayers built-up on silicon substrates will follow (section I.4.B.5). Finally, the adsorption of polyelectrolyte multilayers on polymer supports will be discussed at length (section I.4.B.6).

The results presented in this part of the thesis refer to the articles available in sections II.B.1-2.

### **I.4.B.2. Characterisation techniques**

The main characterisation tools used in this part of the thesis are ToF-SIMS and XPS. The principle and experimental setup of ToF-SIMS have been presented in section I.4.A.2.

In XPS, an X-Ray beam transfers its energy to the electrons of the atoms in the solid. Photoelectrons are ejected with a kinetic energy  $E_k$  which corresponds in first approximation to the excitation energy ( $h\nu$ ) minus the electron binding energy in the atom ( $E_b$ ) [354]. The direct measurement of  $E_k$  allows to find the characteristic binding energies of the photoelectrons emitted by the solid surface. These photoelectron lines indicate the nature of the atoms present at the surface. The quantitative fractions of these atoms can be determined by correcting the photoelectron line intensities with appropriate sensitivity factors. In addition, a fine chemical information can be deduced from the exact value of  $E_b$ , which is sensitive to the chemical environment of the atom (chemical shift). With this chemical shift, the surface functionalities can be quantified. Therefore, XPS is also called Electron Spectroscopy for Chemical Analysis (ESCA).

The XPS equipment used in this thesis is a SSI-X-Probe (SSX-100/206 from Fisons) [355] with an aluminium anode (10 kV, 11.5 mA) and a quartz monochromator. The photoelectrons are energy-discriminated by a hemispherical analyser and detected by a micro-channel plate. The angle of detection in the usual configuration is  $35^\circ$  with respect to the sample surface. The analysed surface is a spot of  $1.37 \text{ mm}^2$ . For this study, detailed scans of the main lines of each element found in the polyelectrolyte formulations were recorded. A Shirley type non-linear background subtraction was used [356], and the peaks were decomposed by using a least square routine assuming a Gaussian/Lorentzian (85/15) function. The XPS atomic percentages were calculated from the peak area of each element, corrected by the sensitivity factors proposed by the manufacturer (C 1s : 1.0, O 1s : 2.49, N 1s : 1.68, S 2p : 1.79 and Si 2p : 0.90).

### **I.4.B.3. Samples**

The chemical formulae of the polyelectrolytes used for the multilayer assemblies are displayed in Table 7. The PEI, PVS and PSS are commercial products from Aldrich Chemie. The poly(choline methacrylate) (PCM), the copolymer based on the PCM architecture (PCM COPO) and the different ionenes (I0, I6, I3, I3a, I10, I10a, I10p) have been synthesised in the chemistry department of the university (Dr. E. Wischerhoff and Pr. A. Laschewsky). The substrates were silicon, glass and various polymers including PP and PET. The glass and Si substrates were cleaned in a  $\text{H}_2\text{SO}_4/\text{H}_2\text{O}_2$  1:1 mixture for 20 min prior to deposition. The polyelectrolytes were first dissolved in water (0.02 mol/l) and the multilayers were made by dipping the substrates for 20 min into the polycation and polyanion solutions, alternatively (see section I.2.B.1). After each polyelectrolyte layer, the



samples were rinsed three times in milli-Q water (millipore). They were then dried in air. Most of the time, PEI was used as primer layer.

Assemblies constituted of piled up I3a and I10a polyampholyte layers were obtained via a two steps cycle (deposition + activation) [262]: first, the substrate was dipped in the I3 (I10) polycation solution; after this deposition step, the I3 (I10) layer was functionalised with a diazonium salt derived from sodium 2-amino-5-nitrobenzene-sulphonate, restoring a negatively-charged surface for the next adsorption step. By this way, I3a and I10a were synthesised 'on the layer'. Remarkably, this hybrid technique should lead to non-centrosymmetric coatings and a greater tendency to the alignment of the chromophore pendant groups is expected. This technique was also used to build-up multilayers with polyampholyte P1 (see sections I.4.A.3 for nomenclature and section II.B.1.3 for characterisation).

#### **I.4.B.4. Information depth in SIMS and XPS**

To interpret the SIMS and XPS data measured on organic coatings constituted of stratified layers as thin as 10 Å, a good knowledge of the information depth of the characterisation techniques is crucial. Indeed, although these techniques are said 'extremely surface sensitive', the depth through which the signal is integrated is of the same order of magnitude than the layer thickness for such ultrathin films (1 nm and 10 nm are often cited for the information depth in SIMS and XPS respectively). Therefore, preliminary experiments have been performed to gain quantitative indications concerning the photoelectron inelastic mean free path (XPS) and the secondary ion emission depth (SIMS) for these samples. This can be achieved by measuring the attenuation of the substrate photoelectrons (XPS) and ions (SIMS) within organic multilayers of well-known thickness. In this case, the determination of the sample thicknesses must rely on other methods (XRR and AFM in this work).

In XPS, the attenuation of the substrate photoelectrons in a film of uniform thickness  $d$  can be expressed by the Beer-Lambert law :

$$I_{XPS} = I_{XPS}^0 \exp(-d / \lambda_{XPS} \sin \theta) \quad (14)$$

where  $I_{XPS}$  is the detected intensity,  $I_{XPS}^0$  is the intensity emitted from the substrate,  $d$  is the layer thickness,  $\theta$  is the detection angle calculated with respect to the sample surface and  $\lambda_{XPS}$  is the inelastic mean free path of the substrate photoelectrons. Eq. (14) shows that the *absolute* intensity of the substrate photoelectrons is an exponential function of the organic layer thickness  $d$ .

## Summary of the Results

In Fig. 30a, the intensity of the Si 2p photoelectrons is shown as a function of the organic layer thickness  $d$  for different multilayer samples. The decay of the substrate signal is exponential and the best fit of the data by Eq. (14) gives a value of 47 Å for  $\lambda_{\text{XPS}}$ .

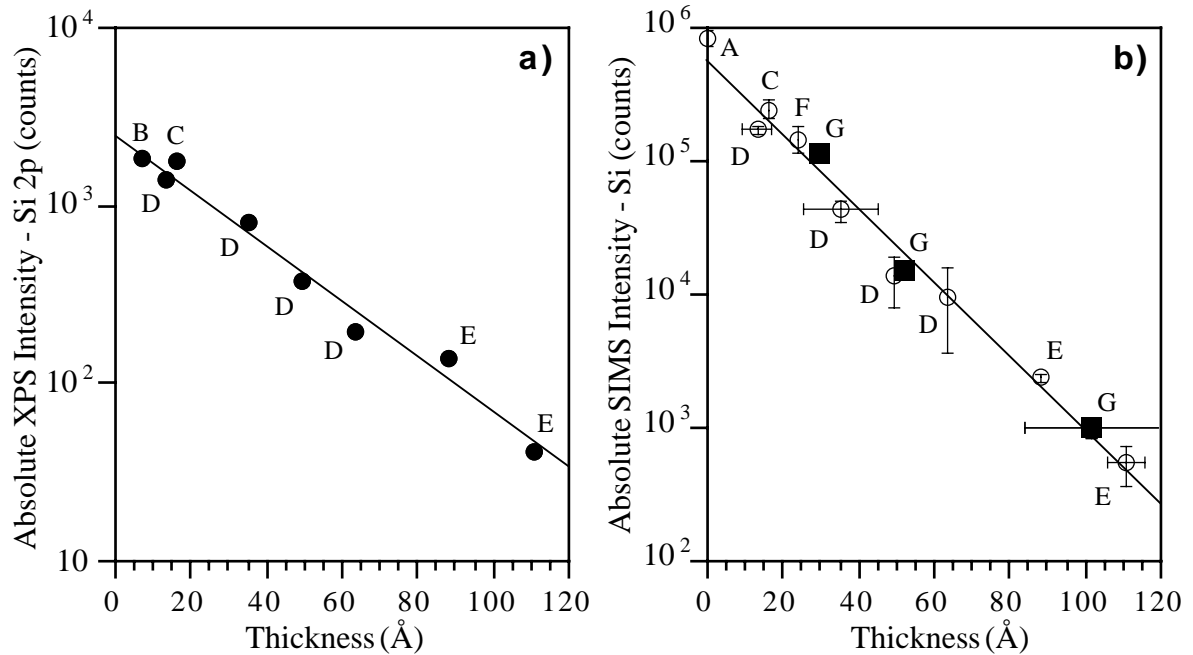


**Fig. 30.** Correlation between the substrate signals measured by XPS and ToF-SIMS and the multilayer thickness measured by XRR or AFM for various assemblies built-up on silicon substrates. The horizontal error bars correspond to the RMS roughness of the assemblies. The vertical error bar in SIMS is the standard deviation calculated with 3-5 data points measured on the same sample. a) XPS: Si 2p photoelectron line (crystalline Si); b) ToF-SIMS: Si<sup>+</sup> ion intensity.

*Samples:* **A:** silicon wafer; **B:** PEI primer layer; **C:** PEI/PVS; **D:** PEI/PVS/(I10a)<sub>x</sub> (1 ≤ x ≤ 4); **E:** PEI/(PVS/I10p)<sub>2</sub> and PEI/(PVS/I10p)<sub>3</sub>; **F:** PEI/PVS/I3a; **G:** PEI/(PVS/I0)<sub>y</sub> (y=3,6,9).

Although rather high, this value is in agreement with the literature [357,358]. It might be overestimated for the following reason: the multilayer thicknesses are measured in air, which means that the films are probably swollen with water during the measurement; in contrast, the XPS and SIMS measurements are performed under UHV (10<sup>-9</sup> torrs), where the films have lost their loosely bound water. Therefore, the measured thicknesses might be larger than the thicknesses experienced under UHV, resulting in an overestimation of  $\lambda_{\text{XPS}}$ . As described in the literature, the water uptake in the film can lead to a thickness increase of the order of 10 %, which is significant [222]. Nevertheless, the  $\lambda_{\text{XPS}}$  value determined by this means can be used in practice for thickness determination, knowing that the obtained values will rather reflect the sample thickness in air than the thickness really experienced under UHV. Taking into account the detection angle  $\theta$ , the calculated value of  $\lambda_{\text{XPS}}$  means that 95 % of the silicon signal would come from a thickness of 80 Å for a hypothetical organic layer with an homogeneous distribution of silicon atoms.

A similar correlation is reported in Fig. 30b for Si<sup>+</sup> secondary ions in SIMS. Remarkably, the intensity decrease is again exponential, allowing us to propose a similar empirical attenuation law as in XPS (Eq. 15).

$$I_{SIMS} = I_{SIMS}^0 \exp(-d / \lambda_{SIMS}) \quad (15)$$

In this equation,  $I_{SIMS}^0$  is the substrate ion intensity without any coating and  $\lambda_{SIMS}$  is defined as the *mean emission depth* of the ion. As the detection is conducted along the surface normal in the ToF-SIMS apparatus,  $\sin\theta = 1$  and this term can be neglected. For  $\lambda_{SIMS}$ , a value of 15.4 Å is found from the best fit of the data. If the silicon atoms were homogeneously distributed in a bulk organic layer with the same features, this  $\lambda_{SIMS}$  value would mean that 95 % of the signal comes from a thickness of 45 Å.

In the context of the collision cascade theory,  $\lambda_{SIMS}$  is the combination of two different factors: (i) the attenuation of the flux of moving substrate particles in the organic film and (ii) the extent of the collision cascade volume in the solid, which must be proportional to the range of the primary ions. In contrast with XPS, the penetration depth of the primary beam in the solid and the attenuation length of the secondary particles should not differ by orders of magnitude, as witnessed by the rather high value of  $\lambda_{SIMS}$ . Therefore, the attenuation of the primary beam must be a relevant parameter for the determination of  $\lambda_{SIMS}$ .

In ToF-SIMS, beside the atomic ion Si<sup>+</sup>, several molecular ions are sputtered from the silicon substrate. Among them, SiH<sup>+</sup>, SiOH<sup>+</sup>, SiO<sup>-</sup>, SiO<sub>2</sub><sup>-</sup> and SiO<sub>3</sub>H<sup>-</sup> constitute intense peaks in the mass spectra of bare silicon wafers. If the emission depths of these ions are different, it can be shown that the correlation between the absolute intensities of two of them must be expressed by a power law for a series of samples with different thicknesses (Eq. 16, see section II.B.1.1 for a detailed discussion).

$$I_{SIMS}^2 = I_{SIMS}^1 \lambda_{SIMS}^1 / \lambda_{SIMS}^2 \quad (16)$$

The correlations I(SiOH<sup>+</sup>) *versus* I(Si<sup>+</sup>) and I(SiO<sub>3</sub>H<sup>-</sup>) *versus* I(Si<sup>+</sup>) are shown in Fig. 31a-c for multilayer samples in which the surface roughness is weak with respect to the total coating thickness (less than 10%). These correlations are strongly non-linear and the data can be nicely fitted by power functions (full lines), which indicates that the emission depths of SiOH<sup>+</sup> and SiO<sub>3</sub>H<sup>-</sup> are different than that of Si<sup>+</sup>. The ratios  $\lambda_{SIMS}(\text{SiOH}^+) / \lambda_{SIMS}(\text{Si}^+)$  and  $\lambda_{SIMS}(\text{SiO}_3\text{H}^-) / \lambda_{SIMS}(\text{Si}^+)$  deduced from the fits are equal to 1.9 and 3.1, respectively. From these ratios, one can calculate the emission depths of SiOH<sup>+</sup> and SiO<sub>3</sub>H<sup>-</sup>, which are equal to 8.1 Å and 5 Å, respectively. This means that the intensity of SiO<sub>3</sub>H<sup>-</sup> (SiOH<sup>+</sup>) is reduced to 5% of its initial value with an organic overlayer of 15 Å (25 Å).

In section II.B.1.1, the emission depth values have been calculated with different sets of experimental data (in general, less data have been taken into account) and slightly

different values have been found. In general, the error due to the quality of the fits should not exceed 10% of the indicated values.

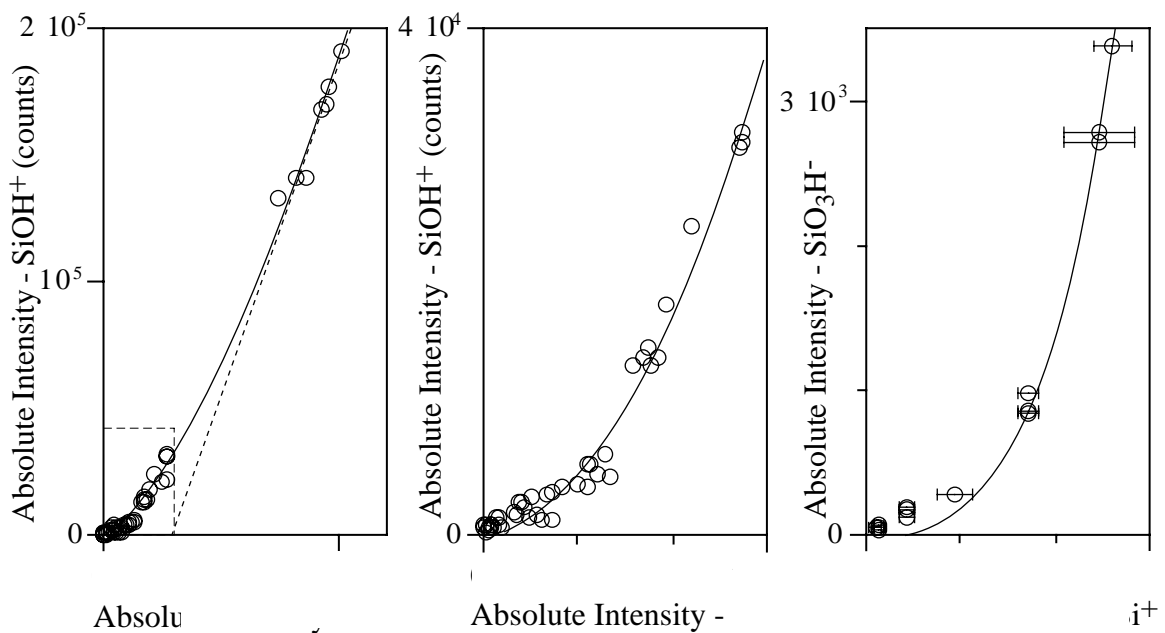


**Fig. 31.** Correlations between substrate ion absolute intensities in SIMS. a)  $I(\text{SiOH}^+)$  versus  $I(\text{Si}^+)$ ; b)  $I(\text{SiOH}^+)$  versus  $I(\text{Si}^+)$ , detail of a); c)  $I(\text{SiO}_3\text{H}^-)$  versus  $I(\text{Si}^+)$ . Full line: fit by Eq. (16).

The results of Fig. 31 show that the emission depth  $\lambda_{\text{SIMS}}$  is larger for atomic ions than for molecular ions. In addition,  $\lambda_{\text{SIMS}}$  decreases gradually with increasing ion size for the considered set of ions: the emission depth of  $\text{SiOH}^+$  and  $\text{SiO}_3\text{H}^-$  are 2 and 3 times smaller than the emission depth of  $\text{Si}^+$ , respectively. Therefore, molecular ions are more 'surface specific' than atomic ions, and this specificity increases with the size of the considered ion.

In contrast, if the coating thickness is strongly non-uniform, e.g. the sample grows by successive adsorption of thick patches on bare areas, a linear correlation will be expected between the substrate signal intensities. Indeed, in this case, the substrate signals, completely attenuated in the thick areas, will originate exclusively from the bare fraction of the surface, which should decrease with the adsorbed amount. A good example of this behaviour is shown in Fig. 32 for high molecular weight PIB adsorbed on silicon from solutions of different concentrations. In this case, the thickness (gyration radius) of the adsorbed coils should be much larger than the emission depth of the secondary ions. Thus, the measured substrate signal comes from uncovered areas, and the relationship between  $I(\text{SiOH}^+)$  and  $I(\text{Si}^+)$  is linear (slope = 1 in the double log plot).

In summary, the calibration of the XPS and SIMS information depth by the correlation with XRR and AFM data could be achieved. It allows us to determine the

thickness of uncharacterised samples deposited on various substrates. To do so, the following procedure can be applied: (i) the inelastic mean free path of other elements photoelectrons can be deduced from the value obtained for silicon by the empirical equation of Seah and Dench, where  $\rho$  is the substrate density [359]:

$$\lambda_{\text{XPS}} = 1/\rho (49/E_k^2 + 0.11E_k^{0.5}) \quad (17)$$

(ii) Knowing the inelastic mean free path for the substrate photoelectrons, the coating thickness can be determined by Eq. (14). (iii) The limited roughness of the multilayer can be qualitatively assessed by the correlation between the ToF-SIMS and XPS substrate signals.

Advantageously, this procedure can be applied for multilayers built-up on rough substrates and/or substrates which are similar to the polyelectrolytes from the optical and mechanical viewpoints (polymers), which is not the case of the thickness determination by XRR and AFM.

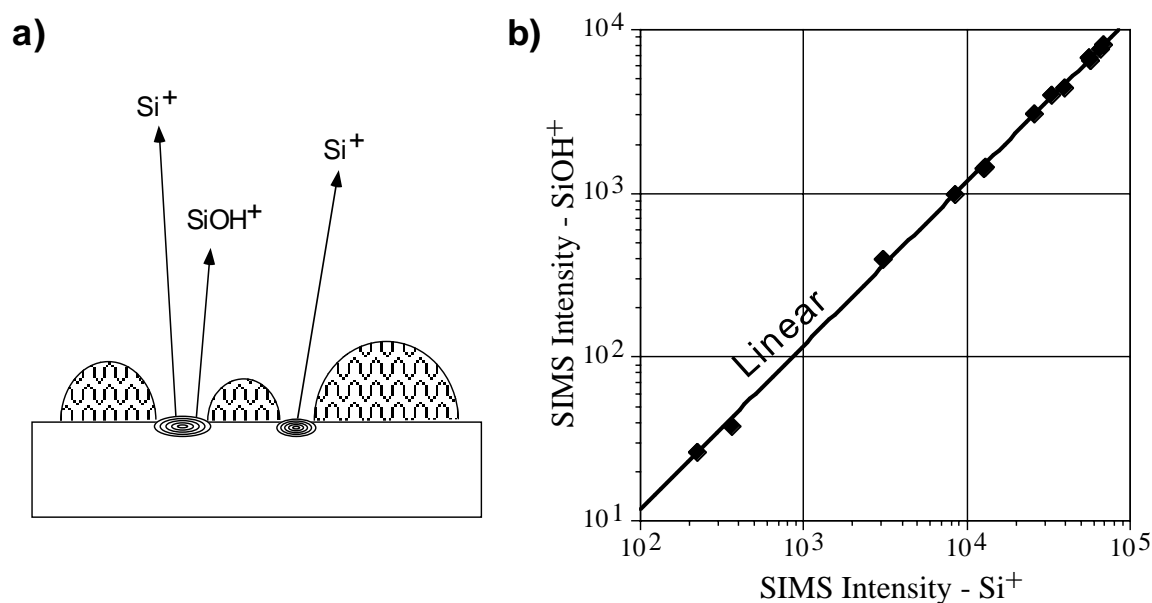


**Fig. 32.** a) Sample with an alternation of thick organic patches and bare substrate areas. b) Correlation  $I(\text{SiOH}^+)$  versus  $I(\text{Si}^+)$  for PIB cast on silicon from different solution concentrations.

#### 1.4.B.5. Adsorption of multilayers on silicon

The efficiency and reproducibility of the alternate polyelectrolyte adsorption have been first tested by building-up multilayers on the traditional silicon substrates, already well-documented in the literature. This verification step was very important since our investigations by ToF-SIMS constitute the first report in the area. In addition, the easy comparison with XRR, AFM and XPS data, already mentioned above, allows for an easier interpretation of the ToF-SIMS data. The extension of this basic study to 'exotic'

## Summary of the Results

polyelectrolyte systems synthesised in the chemistry department and to the application of the hybrid (deposition + activation) technique constitutes the more prospective part of the results related to the adsorption of multilayers on silicon.

In the remainder of this survey, the results obtained with a restricted number of polyelectrolyte assemblies will be presented in details, except when a direct comparison between different systems is needed to support the discussion or when the hybrid (deposition + activation) method is concerned. The chosen system will be the assembly PEI/(PSS/PCM)<sub>x</sub>. This type of assembly has been the most extensively studied during this thesis for several reasons: (i) PSS and PCM are two strong polyelectrolytes, which ensures a weak dependence of the number of charged sites with the pH of the solutions; (ii) These polymers are not too complex from the chemical viewpoint and, including the same polyanion, the PSS/PCM pair can be easily compared to the very well studied PSS/PAH pair. (iii) For comparison purpose, a series of PCM-based copolymers of increasing hydrophobicity was available, too, which will appear very interesting in the case of hydrophobic PP supports (PCM COPO). (iv) Due to their chemical structure, these polyelectrolytes exhibit highly characteristic peaks in the secondary ion mass spectra (*vide infra*), which is not expected in the case of PAH.

### *a) Mass spectra*

Reference spectra of PCM and PSS have been obtained by casting a droplet of the concentrated solution of these polymers (~0.1 mol/l) on a clean silicon wafer. These spectra are shown in Fig. 33a and 33b, respectively. The absence of silicon signals indicates that the deposited layer is thick with respect to the secondary ion emission depth. The most characteristic ions of PCM are clearly related to its pendant group (C<sub>2</sub>H<sub>4</sub>N<sup>+</sup>, C<sub>3</sub>H<sub>8</sub>N<sup>+</sup>, C<sub>5</sub>H<sub>12</sub>N<sup>+</sup>, C<sub>5</sub>H<sub>12</sub>NO<sup>+</sup>, C<sub>5</sub>H<sub>14</sub>NO<sup>+</sup>) and the monomer ion (*m/z*=172, not shown) constitutes a weak but significant peak. The only striking feature of the negative spectrum of 'bulk' PCM is the very high intensity of the bromine counterions (<sup>79</sup>Br<sup>-</sup> and <sup>81</sup>Br<sup>-</sup>).

The positive mass spectrum of PSS contains very few distinctive features: the intensities of unsaturated ions (*m/z*=39, 50, 51, 77, 91) are unexpectedly weak and the intensities of saturated hydrocarbons, rather pronounced. On the other hand, the positive spectrum is completely dominated by the sodium peak, corresponding to the counterion of PSS. The series of intense SO<sub>x</sub><sup>-</sup> peaks (0 ≤ *x* ≤ 3) in the negative spectrum is more characteristic.

When the PSS/PCM pair is deposited by alternate layer physisorption, the same characteristic peaks are observed. This is exemplified by the mass spectra of the assembly PEI/(PSS/PCM)<sub>4</sub> deposited on silicon (Fig. 34, see also section II.B.1.2). The positive mass spectrum reveals mainly the peaks corresponding to PCM and a weak silicon peak, while the negative spectrum is dominated beyond *m/z* = 40 by the SO<sub>x</sub><sup>-</sup> series mentioned above. This shows that the top layer of PCM does not prevent the emission of molecular ions from the

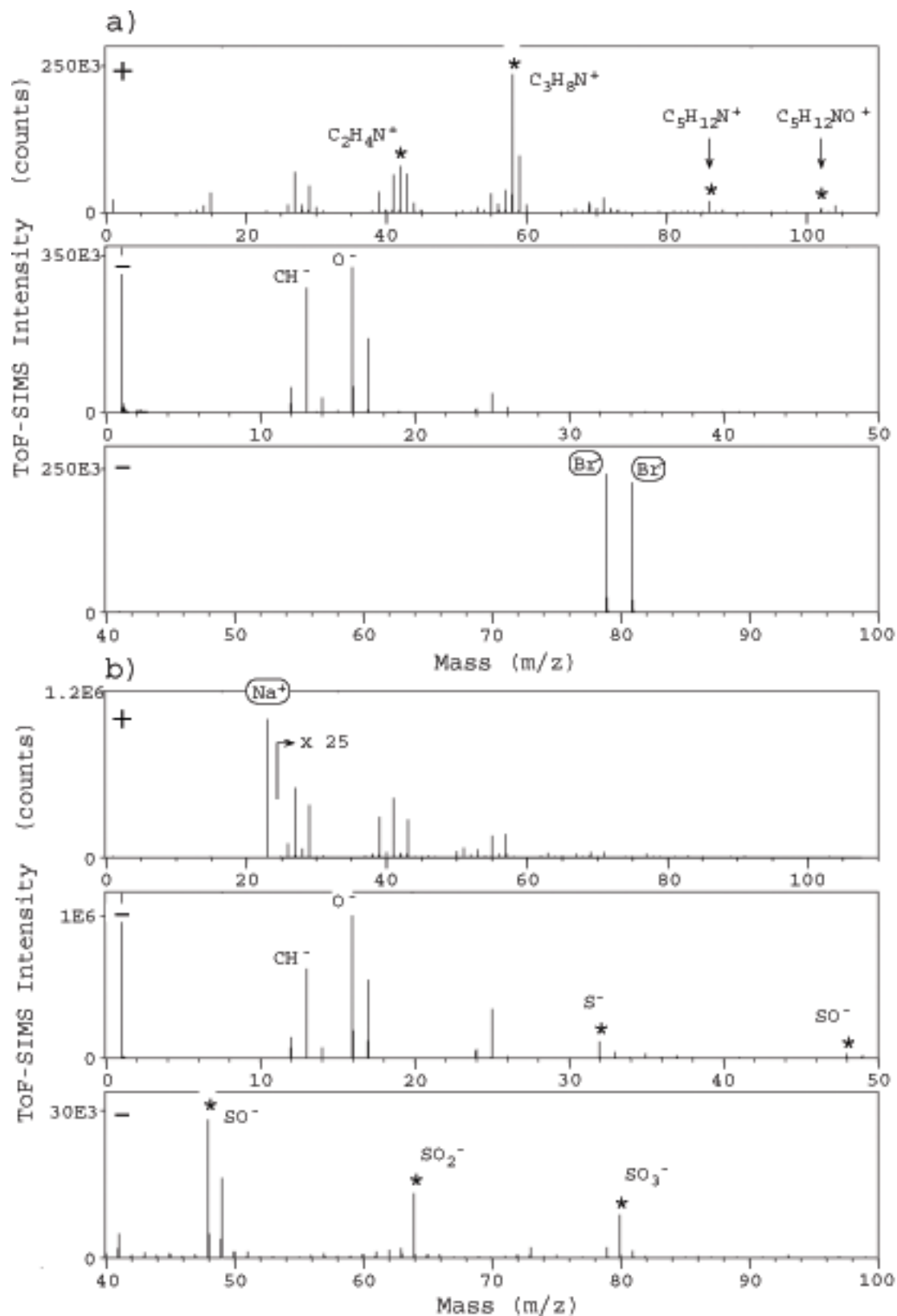


**Fig. 33.** Positive and negative secondary ion mass spectra of a) a thick layer of PCM cast on silicon; b) a thick layer of PSS cast on silicon.

## Summary of the Results

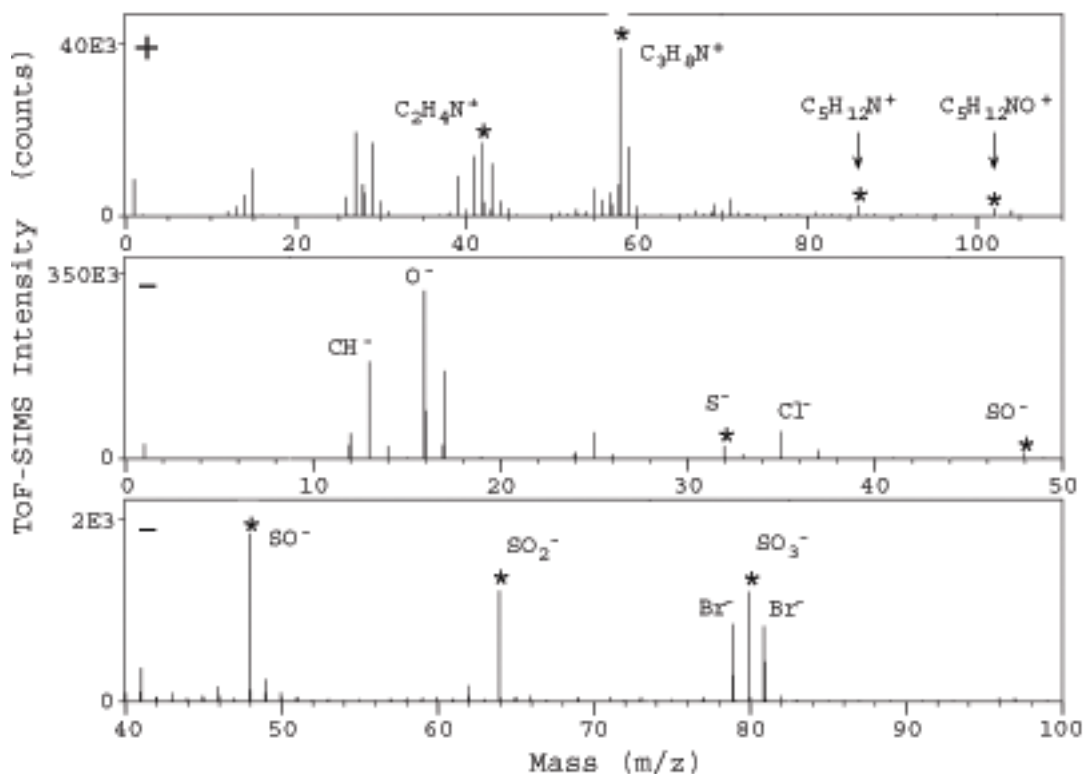


**Fig. 34.** Positive and negative secondary ion mass spectra of the sample PEI/(PSS/PCM)<sub>4</sub>.

underlying PSS layer. In the hypothesis of a stratified coating (as will be indicated by the evolution of the substrate ion intensities), two arguments can be proposed to explain this: (i) the top layer is very thin; (ii) the two polymers are strongly interdigitated. The second has been demonstrated for PSS/PAH layers. More information concerning this point will arise from the detailed study of similar multilayers with different layer numbers.

The more important difference between the spectra of Fig. 33 and Fig. 34 relates to the counterion intensities. Although  $\text{Na}^+$  dominates the positive spectrum of 'bulk' PSS, it is absent from the multilayer spectrum. Knowing the high sensitivity of ToF-SIMS to  $\text{Na}^+$ , this means that *the complexation is quantitative in the film*. In contrast, the Br counterions are present in the negative spectrum of the assembly, but their relative and absolute intensities are 50 times lower than that observed for 'bulk' PSS. The presence of these Br counterions is probably related to the overcompensation of the PSS negative charges by the positive charges of the PCM top layer. It is difficult to get a quantitative information from the much weaker relative intensity of the counterion peaks in the multilayer. Indeed, the very large peaks in the 'bulk' PSS are the result of the signal integration over a rather important depth, while the signal should come only from the last layer in the multilayer. Nevertheless, the results suggest that the overcompensation might be weaker than proposed in the literature. In the following, several evidences of the regular multilayer build-up will be presented.

## b) Multilayer build-up: substrate signals

In section I.4.B.4, a direct correlation between the substrate signal intensities and the thickness of the organic coating has been demonstrated. In addition, the emission depth  $\lambda$ SIMS appears insensitive to the exact chemistry of the polyelectrolytes, since all the data merge into one universal curve in Fig. 30. Therefore, the empirical Eq. (15) can be applied to determine the mean layer thickness of any kind of assembly.

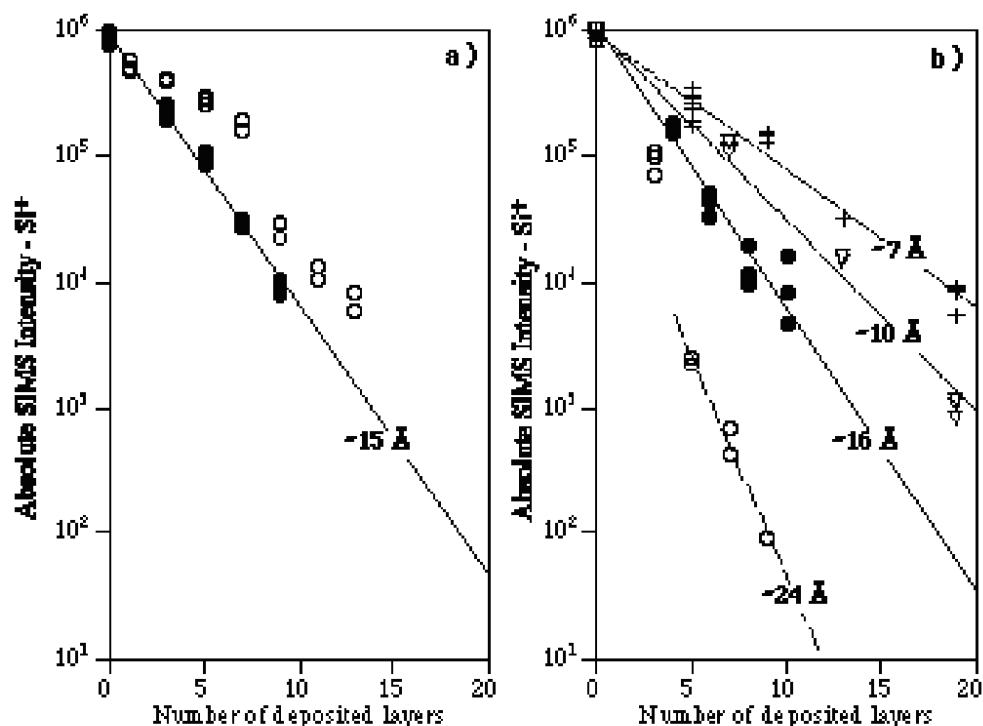


**Fig. 35.** Evolution of the substrate  $\text{Si}^+$  ion intensity with the layer number for: a)  $\text{PEI}/(\text{PSS}/\text{PCM})_x$  ( $\bullet$ );  $\text{PCM}/(\text{PSS}/\text{PCM})_x$  ( $\circ$ ); b)  $\text{PEI}/(\text{PVS}/\text{I6})_x$  and  $\text{I6}/(\text{PVS}/\text{I6})_x$  ( $+$ );  $\text{I0}/(\text{PVS}/\text{I0})_x$  ( $\nabla$ );  $\text{PEI}/\text{PVS}/(\text{I10a})_x$  ( $\bullet$ );  $\text{PEI}/(\text{PVS}/\text{I10p})_x$  ( $\circ$ ).

The expected decay of the substrate ion intensities as a function of the layer number can be easily tested in the case of the  $\text{PEI}/(\text{PSS}/\text{PCM})_x$  assemblies. It is illustrated in Fig. 35a. The decay of  $\text{Si}^+$  is an exponential function of the layer number. *If the coatings are stratified and homogeneous*, this means that the bilayer thickness does not change with the layer number, in contrast with the observations reported for several other systems in the literature [181]. Indications supporting the uniform thickness of the  $\text{PEI}/(\text{PSS}/\text{PCM})_x$  multilayers can be deduced from the correlation between XPS and SIMS signals, and between different substrate ion intensities (vide supra). They will be described in details in section II.B.1.2. The bilayer thickness for the  $\text{PSS}/\text{PCM}$  system, obtained by fitting the data with Eq. (15), is 15 Å. A similar value is given by the fit of the XPS measurements done with the same samples (section II.B.1.2).

## Summary of the Results

Interestingly, samples built up with a PCM primer layer instead of PEI [ $PCM/(PSS/PCM)_x$  assemblies] do not grow significantly with less than 7 deposited layers, which is probably due to the insufficient interaction between PCM and silicon (Fig. 35a). A posteriori, this justifies the use of a PEI primer layer in the assemblies.

The substrate ion intensity decay is displayed in Fig. 35b for several kinds of assemblies. Among them, the samples for which the thickness had been measured by XRR or AFM, have already been used to determine  $\lambda_{SIMS}$  in Fig. 30. Fig. 35b shows that the exponential decay is observed in most cases and that the mean bilayer thickness may vary significantly for different systems. The exception is the series of assemblies PEI/(PVS/I10p) $_x$  for which the intercept of the regression is lower than  $10^6$  counts. For this system, it has been shown by XRR that the top layer was thicker, which explains the shift of the intensities towards lower values [232]. In addition, the PEI/PVS/I10p multilayer exhibits an anomalous behaviour. Imaging SIMS performed on this sample revealed important lateral inhomogeneities of 5  $\mu\text{m}$  diameter (see section II.B.1.1). Thus, the substrate ions also constitute an efficient probe of the coating quality and homogeneity.

### *c) Multilayer build-up: coating signals*

The evolution, as a function of the deposition cycle number, of the XPS and SIMS intensities related to the coating gives interesting indications concerning the multilayer build-up, too. The XPS atomic fractions of sulphur (PSS) and of ionic nitrogen (PCM) are displayed in Fig. 36a. These fractions increase to a maximum value, in the range of 3-4 atomic percents. The slow increase of the nitrogen and sulphur fractions can be explained by the large inelastic mean free path of the photoelectrons. The high initial value of the sulphur fraction is probably due to the significant fraction of sulphur already observed on the bare substrates. The origin of this sulphur is the pre-treatment of the silicon wafers, prior to the multilayer deposition (see experimental section). The stoichiometric values for the PSS/PCM assembly, calculated from the number of atoms of each element present in the formulae (1:1 monomer), should be close to four percents for nitrogen and sulphur. Fig. 36a shows that the nitrogen fraction tends to this value, but not the sulphur fraction. The explanation of this behaviour could be related to the attenuation of the PSS photoelectrons in the top PCM layer.

The evolution of the SIMS intensities is shown in Fig. 36b and 36c for PSS and PCM secondary ions, respectively. The S-containing ions exhibit different behaviours: While the intensity of the sulphur  $^{34}\text{S}^-$  isotope increases regularly with increasing layer number, the saturation is reached earlier for the molecular ions  $\text{SO}_3^-$  (2-3 cycles) and  $\text{MpSS}^-$  (1 cycle). This can be easily interpreted with the hypothesis of the different emission depth found for atomic and molecular ions in section I.4.B.4. The results show clearly that the signal of  $^{34}\text{S}^-$  is integrated over the bulk of the sample, even with four bilayers, while the signal of the monomer ion ( $\text{MpSS}^-$ ) is integrated over one single layer. The  $\text{SO}_x^-$  ions exhibit intermediate behaviours.

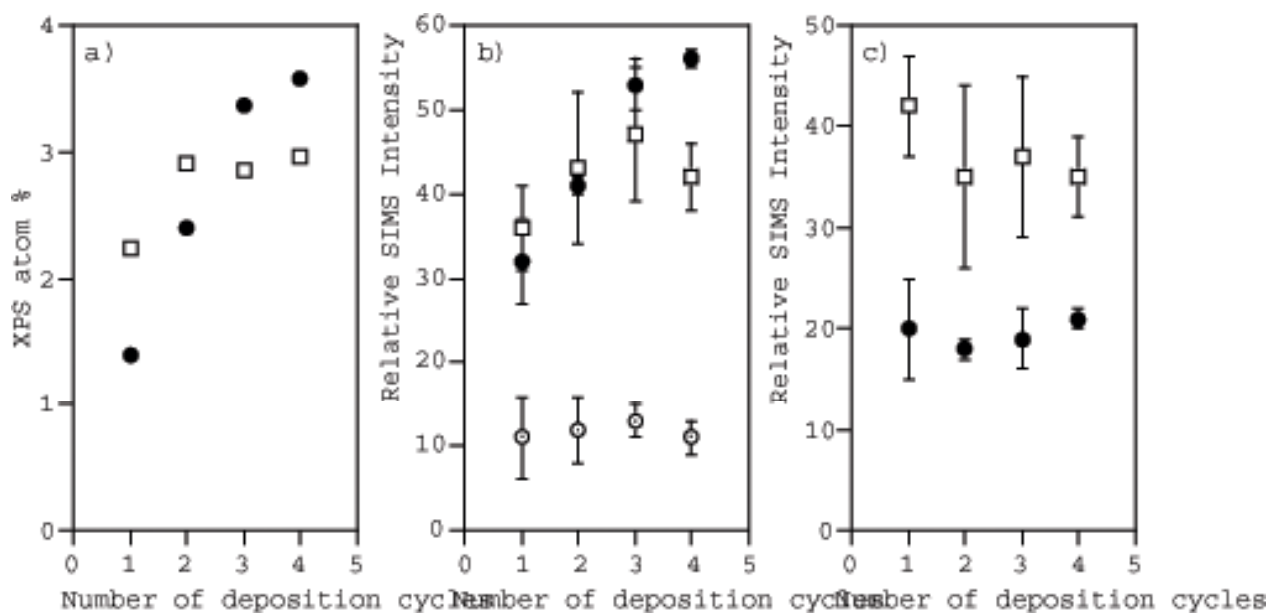


**Fig. 36.** PEI/(PSS/PCM)<sub>x</sub> multilayers. a) XPS atomic percentages of nitrogen (N<sup>+</sup>) (●) and sulphur (□) in the assemblies. b) SIMS relative intensities of the S-containing ions [ $I_{peak}/I(CH^+) \times 10^n$ ]: <sup>34</sup>S<sup>-</sup> (n=4) (●); SO<sub>3</sub><sup>-</sup> (n=3) (□); MPSS<sup>-</sup> (n=4) (○). c) SIMS relative intensities of the N-containing ions [ $I_{peak}/I(C_2H_3^+) \times 10^n$ ]: C<sub>3</sub>H<sub>8</sub>N<sup>+</sup> (n=1) (●); MPCM<sup>+</sup> (n=4) (□).

For all the PCM secondary ions, the saturation is obtained with one single deposition cycle (Fig. 36c). Thus, the information depth of the ions C<sub>3</sub>H<sub>8</sub>N<sup>+</sup>, C<sub>5</sub>H<sub>12</sub>N<sup>+</sup>, C<sub>5</sub>H<sub>12</sub>NO<sup>+</sup>, etc. is lower than the bilayer thickness. It will be shown in the following that the PSS/PCM deposition on PET substrates gives slightly different results.

#### d) Applications

In the context of the hybrid elaboration method described in the experimental section, several types of assemblies have been studied by ToF-SIMS and XPS. The effects of the activation reaction, as well as the regularity of the multilayer build-up have been tested. Detailed results are reported in section II.B.1.1 and II.B.1.2 for the assemblies PEI/PVS/(I10a)<sub>x</sub> and in section II.B.1.3 for another kind of polyampholyte system.

#### e) Summary

From the comparison between 'bulk' polyelectrolytes and multilayers fabricated by the step-by-step adsorption method, it is reasonable to conclude that the complexation of the polyelectrolytes in the multilayer is nearly quantitative. Indeed, the fraction of counterions remaining in the assemblies is negligible as compared to the 'bulk' polyelectrolyte layer. Moreover, it seems that the amount of counterions remaining in the top polyelectrolyte layer of the assemblies is weaker than that expected for a pronounced charge overcompensation.

## *Summary of the Results*

The validity of these results is reinforced by the very high sensitivity of the SIMS technique to sodium and bromine ions.

The exponential decay of the substrate ion intensities and the non-linear correlation between XPS and SIMS substrate signals and between different substrate ion intensities are in favour of a regular multilayer growth for the studied systems. In particular, the assemblies PEI/(PSS/PCM)<sub>x</sub>, with a constant bilayer thickness of ~15 Å, are good model systems for subsequent deposition on polymer substrates.

For the same multilayer system, the evolution of the characteristic XPS atomic fractions and SIMS intensities related to the coating, consistent with the calculated values for the PSS/PCM system, point to the good quality of the assemblies.

#### 1.4.B.6. Adsorption of multilayers on polymers

The investigation of multilayers adsorbed on model silicon supports has led to the determination of the information depth of SIMS and XPS. Moreover, indications about the composition of the layers, the mean layer thickness and homogeneity and the counterion binding have been gained by the combined use of these two techniques.

In the following, these developments will be used to study the polyelectrolyte adsorption on *uncharged* polymer substrates. For this purpose, several polymers have been chosen as possible substrates in order to verify the influence of different surface chemical groups on the adsorption process. Eight polymer supports have been tested: PP, PIB, PS, PET, poly(methyl methacrylate) (PMMA), poly(ethylene terephthalate-co-isophthalate), poly(2,6-dimethyl-p-phenylene oxide) and poly(ether imide). In the remainder of this section, we will present the pristine and modified polymer mass spectra and the influence of the adsorption on the substrate and coating signals. The particularly interesting case of PET supports will be addressed at length. In a more prospective attempt, we will propose the use of ion beam sputtering as a means to obtain patterned multilayers.

##### a) Overview of the polyelectrolyte adsorption on polymers

The positive ion mass spectra of pristine PIB, PET, PMMA, PS, Poly(2,6-dimethyl-p-phenylene oxide) and poly(ether imide) are displayed in Fig. 37. The spectra of PIB, PET, PMMA and PS are similar to those reported in the literature [278,360,361]. The total secondary ion intensity varies strongly with the polymer nature: there is a factor of ten between the total intensities measured for PS and PMMA, which shows the very different ion formation probabilities for these polymers. All the spectra exhibit characteristic fingerprint peaks in this mass range (indicated in Fig. 37), except for the poly(ether imide). In the case of poly(ether imide), the positive spectrum is mainly composed of uncharacteristic hydrocarbons, which is probably due to the very low formation probability of characteristic aromatic, nitrogen- and oxygen-containing ions from the polymer backbone. Although reference spectra for poly(ether imide) are missing, the same hydrocarbon pattern is observed in the spectra of poly(ether ether ketone) and poly(carbonate) [277]. For PMMA, poly(2,6-dimethyl-p-phenylene oxide) and poly(ether imide), more characteristic secondary ions can be found in the negative spectra (*PMMA*:  $\text{CH}_3\text{O}^-$ ,  $\text{C}_4\text{H}_3\text{O}_2^-$ ,  $\text{C}_9\text{H}_{13}\text{O}_4^-$ ; *poly(2,6-dimethyl-p-phenylene oxide)*:  $\text{C}_8\text{H}_8\text{O}_2^-$ ; *poly(ether imide)*:  $\text{CNO}^-$ ,  $\text{C}_{15}\text{H}_{15}\text{O}^-$ ).

These polymer supports have been dipped in the polyelectrolyte solutions in order to deposit seven consecutive layers, corresponding to the assembly PEI/(PSS/PCM)<sub>3</sub>. Except for PIB, the similarity between the modified polymer spectra is striking (Fig. 38). For the other substrates, the modified surface shows the fingerprint spectrum of PCM, as observed in Figs. 33 and 34. In agreement with the multilayer deposition on silicon (Fig. 34), the  $\text{Na}^+$  counterions are weak or absent from the positive spectra of Fig. 38. Similarly, the intensity of the bromine counterions is weak in the negative spectra of the modified polymer surfaces (not shown). In each case, the complexation between the alternate

## Summary of the Results

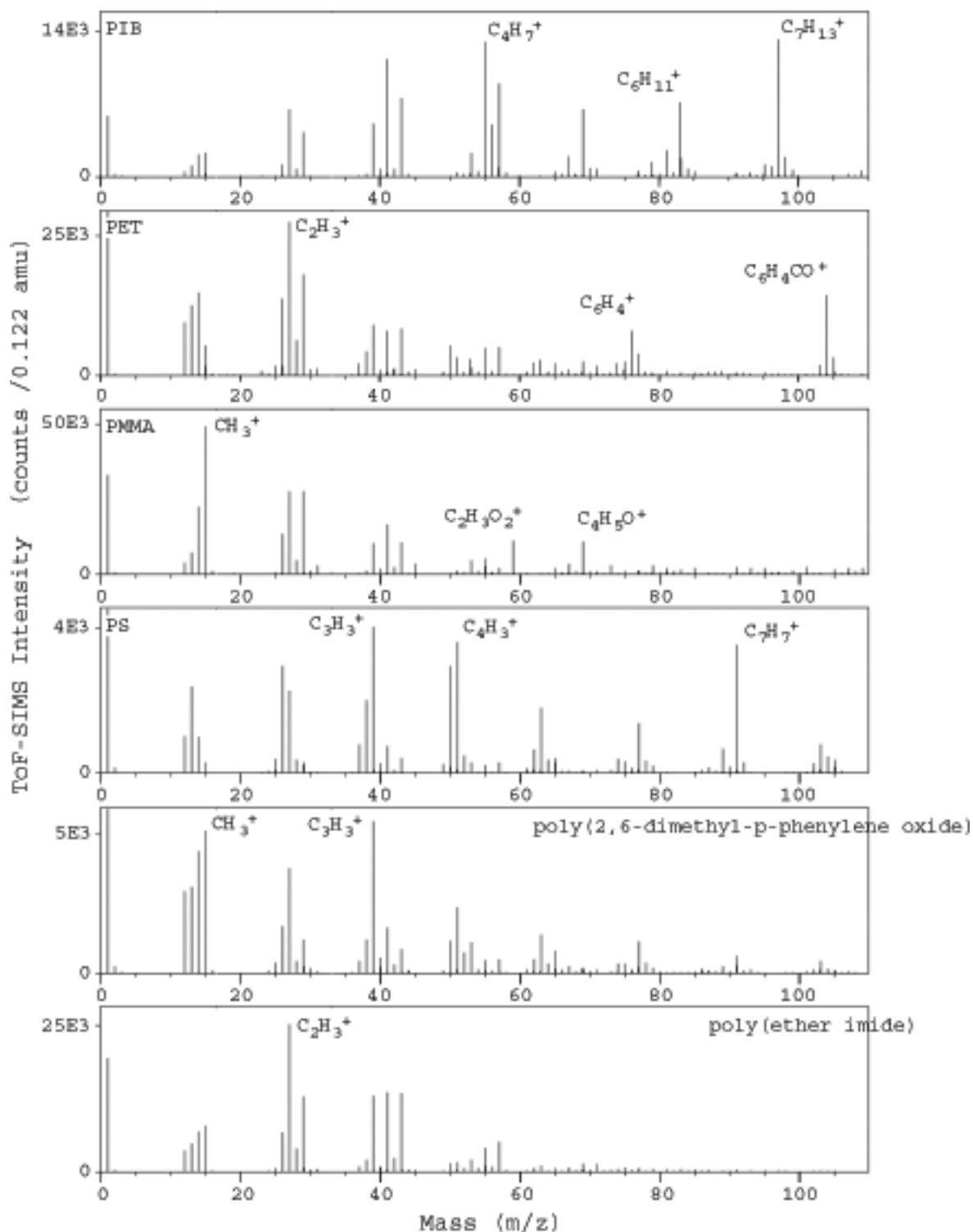


**Fig. 37.** Positive ion mass spectrum of some pristine polymer substrates used for the multilayer deposition.

polyelectrolyte chains is ensured. On the other hand, the total ion intensities are higher than that of pristine polymer substrates, and differ by a factor of 2 at the most (PIB excluded).

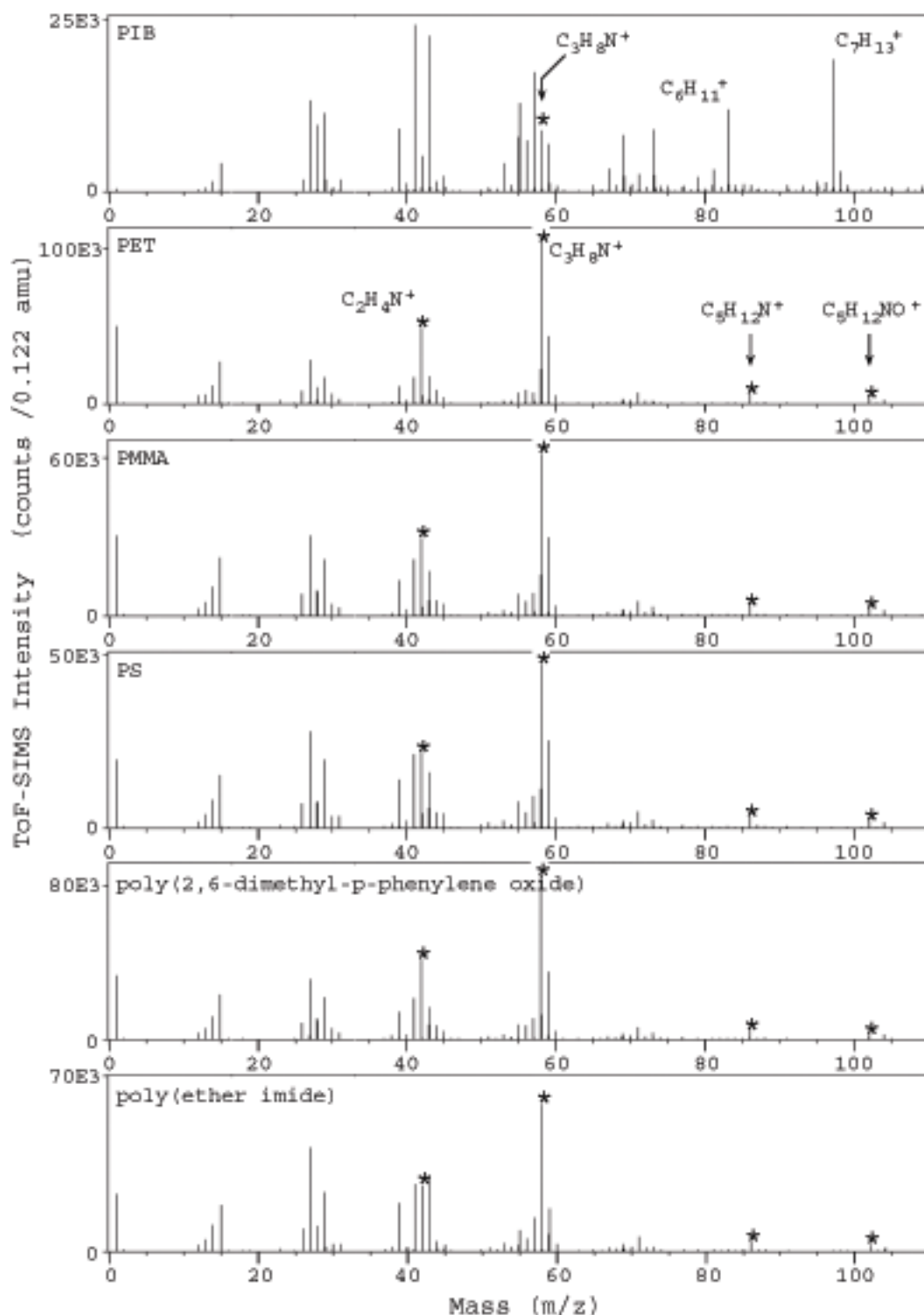


**Fig. 38.** Positive ion mass spectrum of the polymer substrates after deposition of seven polyelectrolyte layers (PEI/(PSS/PCM)<sub>3</sub>).

Although the modified polymer surfaces look identical to the modified silicon in most cases, this is not true for the aliphatic polyolefins, PIB and PP (see section II.B.2). For these polymers, the surface modification by polyelectrolytes does not shield the substrate ion emission:  $C_6H_{11}^+$  and  $C_7H_{13}^+$  remain dominant in the modified PIB spectrum, while

## Summary of the Results

$C_2H_3^+$  and  $C_3H_5^+$  dominate the modified PP spectrum (section II.B.2). For these polymers, a simple look at the SIMS spectra indicates that the multilayer deposition has failed. We will take advantage of this behaviour for the development of patterned polyelectrolyte surfaces (paragraph d).

The evolution of the more characteristic substrate ions, for the pristine and modified polymers (polymer + PEI/(PSS/PCM)<sub>3</sub>), is displayed in Fig. 39. The two extreme cases correspond to PET and PIB. As already observed in the mass spectra, the substrate intensities are not reduced by the polyelectrolyte adsorption for PIB, confirming the absence of multilayer growth. In contrast, the substrate ion intensities are reduced by a factor of ~400 in the coated PET. For the same polyelectrolyte layer number, the Si<sup>+</sup> intensity was reduced by a factor of ~30 in the case of silicon substrates. As the emission depth of molecular ions should be several times smaller than atomic ions, these ratios may not be directly compared. Nevertheless, the drastic intensity reduction suggests that the multilayer builds-up on PET. For the other polymers, the reduction is intermediate (factor of 10 to 30), which prevents any conclusion.

The surface compositions of the coated polymers, as determined by XPS, give complementary indications concerning the multilayer growth for these systems. They are reported in details in section II.B.2. The atomic fractions of ionic nitrogen and of sulphur, characteristic of the coating, are shown in Fig. 40 for the silicon and polymer substrates. For a hypothetical 'bulk' assembly of PSS and PCM with a 1:1 monomer stoichiometry, they

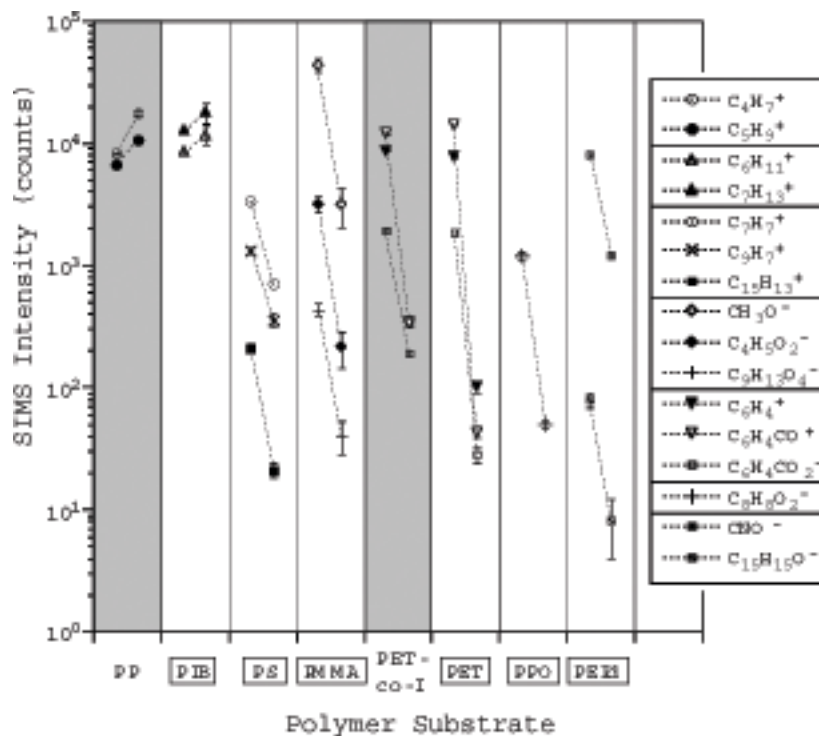


**Fig. 39.** Absolute intensity of the fingerprint ions of the polymer supports before and after coating with the multilayer PEI/(PSS/PCM)<sub>3</sub>.

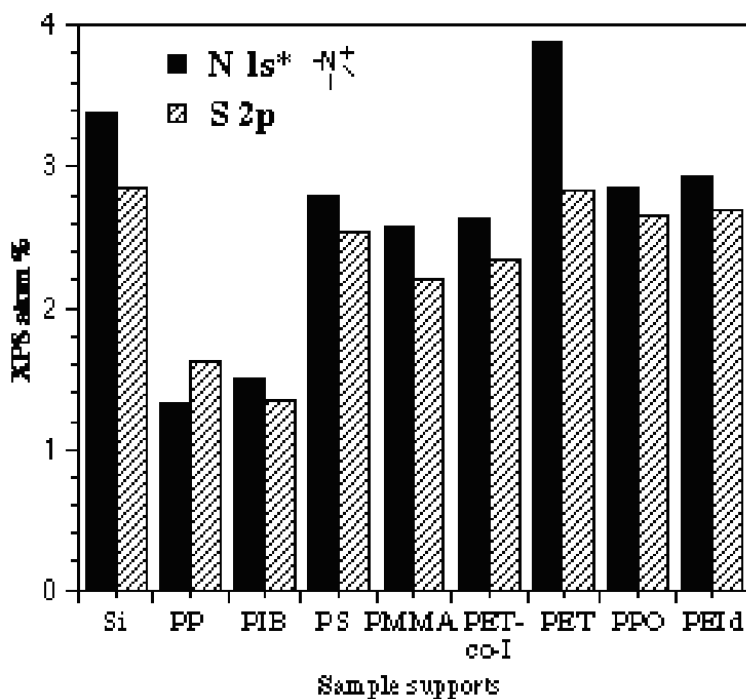


**Fig. 40.** Nitrogen ( $N^+$ ) and sulphur atomic fractions after coating with the multilayer PEI/(PSS/PCM)<sub>3</sub>.

should be close to 4 %. In contrast, these fractions are around 1.5 % for PP and PIB supports, confirming again the bad quality of the deposit for these samples. For the other polymer samples, the fractions are comparable to those measured on the coated silicon, suggesting that the multilayer growth has really started. The ionic nitrogen fraction is particularly high for the PET support, which is in perfect agreement with the ToF-SIMS results presented in Fig. 39.

#### b) PET supports

The adsorption of polyelectrolyte layers on uncharged PET exhibits particularly interesting features (Fig. 39-40). Therefore, the multilayer build-up on PET has been investigated in details (section II.B.2). To complement the results of Fig. 40, Fig. 41 shows the variation of the same atomic fractions (S,  $N^+$ ) as a function of the number of polyelectrolyte layers adsorbed on PET. The corresponding evolution for silicon substrates (Fig. 36a) is also recalled in Fig. 41. For PET, these fractions increase regularly with the layer number. The ionic nitrogen fraction clearly tends to the value calculated for the stoichiometric PSS/PCM complex, while the sulphur remains slightly lower, as it was observed for silicon supports, too. On average, the ionic nitrogen fraction is also higher for coated PET than for coated silicon with the same layer number.

These data confirm that a significant amount of fresh polyelectrolyte is adsorbed at each step during the deposition on PET. The gradual increase of the nitrogen ( $N^+$ ) and sulphur fractions for coated PET samples supports the hypothesis of stratified multilayer build-up.

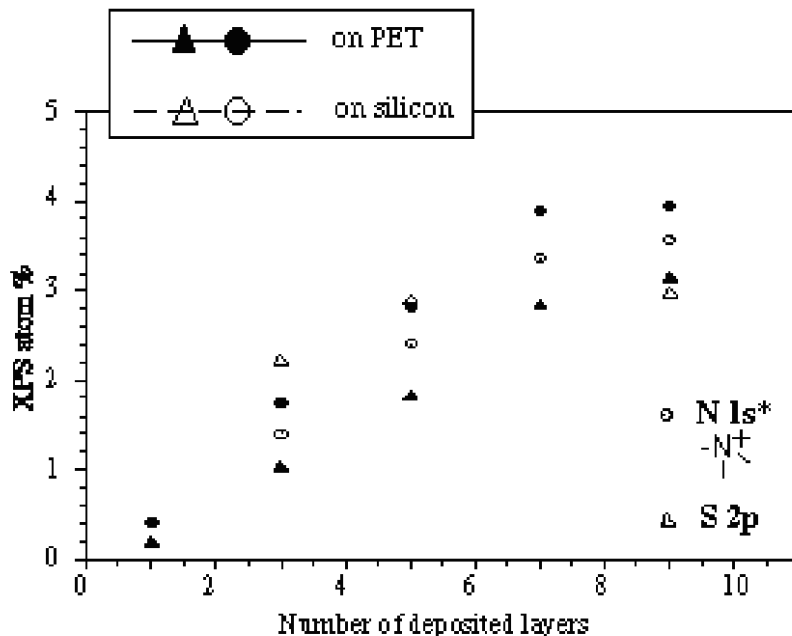


**Fig. 41.** Nitrogen ( $N^+$ ) and sulphur atomic fractions as a function of the polyelectrolyte layer number for PET coated with the multilayer PEI/(PSS/PCM)<sub>x</sub>. Comparison with coated silicon supports.

The parallel variation of the XPS substrate signals is informative, too (see section II.B.2 for ToF-SIMS). The evolution of the C 1s ( $O=C-O$ ) atomic fraction corresponding to the PET support is presented in Fig. 42. The inelastic mean free path of the C 1s photoelectrons can be calculated with the relation of Seah and Dench (Eq. 17), by the procedure described at the end of section I.4.B.4. It is equal to 43 Å. *In the hypothesis of uniform layer thickness*, the evolution of the substrate photoelectron intensities should be exponential, as observed for silicon substrates (section II.B.1.2). The fit of the data by an exponential function in Fig. 42 gives a mean layer thickness of 12 Å, which is larger than the mean layer thickness measured on silicon (~7.5 Å). In addition, the curve is not strictly exponential, suggesting different layer thicknesses for the successive layers. As shown in Fig. 42, the first deposited layers would have a thickness close to 5 Å, while the thickness of the last would reach 16 Å. The comparison with the multilayer build-up on silicon, where the hypothesis of identical layer thicknesses was the most probable, suggests a different growth process.

It is important to note that the correlation between SIMS and XPS substrate intensities is strongly non linear in the case of PET supports, too (section II.B.2). Therefore, a predominant effect of the multilayer roughness can be excluded.

The ToF-SIMS intensities of the characteristic secondary ions sputtered from the coating complement the XPS results (Fig. 43a-b). To illustrate this, Fig. 43a shows the variation of the  $C_3H_8N^+$  ion intensity, related to both PEI and PCM polyelectrolytes. After a plateau for the PEI and PEI/PSS samples, this ion intensity increases to a second

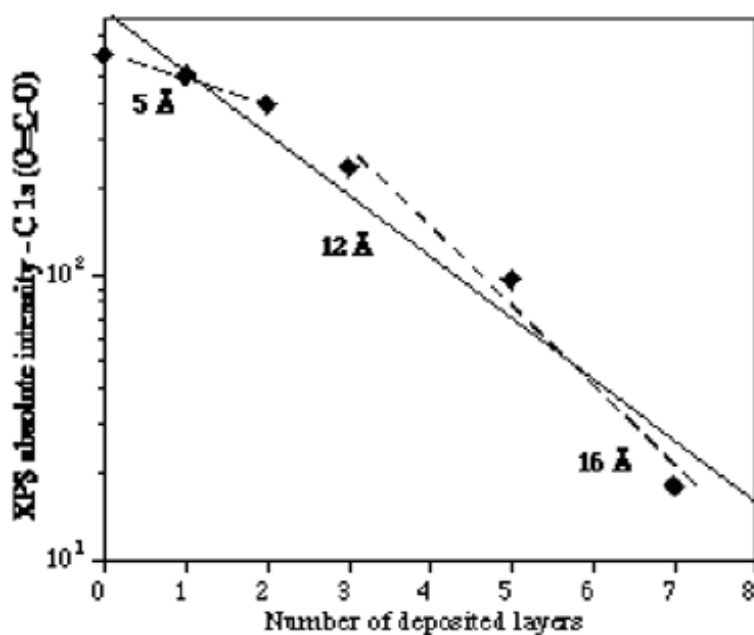


Fig. 42. Carbon (O=C-O) fraction related to the PET support. Variation as a function of the polyelectrolyte layer number for the multilayer PEI/(PSS/PCM)<sub>x</sub>.

plateau, reached with two PSS/PCM layers. The intermediate value observed for the PEI/PSS/PCM assembly indicates that the first PCM layer is not thick enough to obtain the saturation of this ion intensity. As mentioned above, a predominant effect of the roughness is improbable.

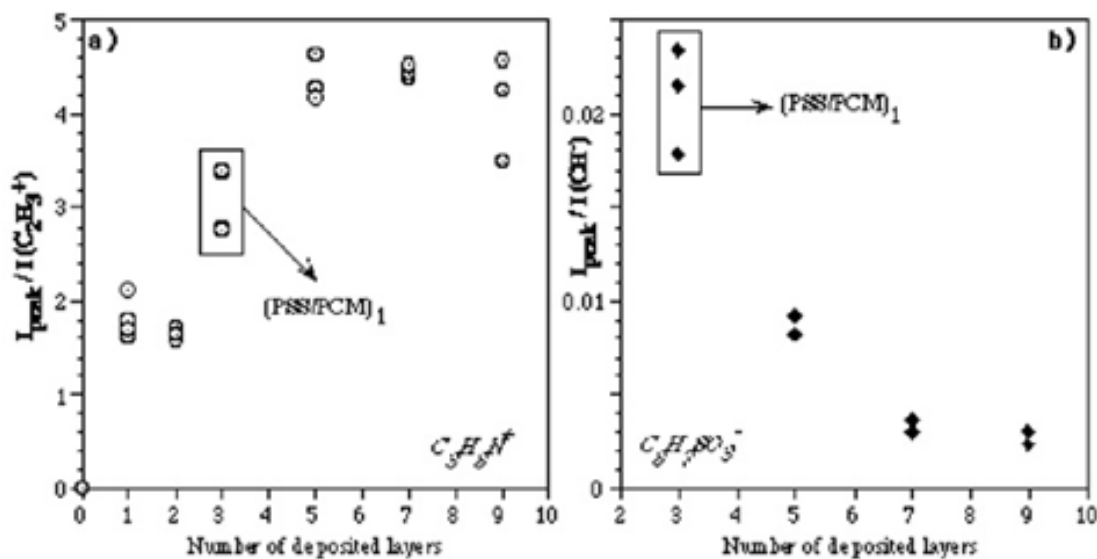


Fig. 43. Evolution of the intensity of selected secondary ions sputtered from PET coated with the multilayer PEI/(PSS/PCM)<sub>x</sub>. [Primary ions: Cs<sup>+</sup>, 11 keV].

## Summary of the Results

The parallel evolution of the PSS monomer intensity ( $M_{\text{PSS}^-}$ ) is intriguing, too (Fig. 43b). For  $\text{PEI}/(\text{PSS}/\text{PCM})_x$  assemblies with increasing  $x$ , the PSS monomer intensity *decreases* regularly. Again, this was not observed for the polyelectrolyte adsorption on silicon substrates. To explain this behaviour, one must assume that the attenuation of the PSS monomer intensity in the top PCM layer increases with the layer number  $x$ . This is in complete agreement with the proposed increase of the successive polyelectrolyte layer thickness, deduced from the decay of the PET photoelectron intensities.

More complete ToF-SIMS and XPS results obtained for the multilayer build-up on PET are presented in section II.B.2. In contrast with silicon supports, all the experimental evidences point to a mechanism of multilayer growth in which the layer thickness increases at each deposition step. The fact that an equilibrium thickness is not reached within four deposition cycles is not in contradiction with the literature [181]. Moreover, the important amount of material deposited per adsorption step, assessed by the combined use of ToF-SIMS and XPS, shows that PET is a very interesting polymer candidate for the alternate polyelectrolyte multilayer build-up.

To explain the polyelectrolyte adsorption on PET, one must assume that strong non-electrostatic interactions take place, leading to the deposition of the primer PEI layer. Indeed, with a PEI solution kept at  $\text{pH}=1$ , the few carboxylic acid residues present at the surface of the PET are not dissociated, and the number of negative charges should be very weak. Instead, hydrogen bonding between the nitrogen atoms of PEI and the carbonyl groups of PET might play an important role. On the other hand, the improved adsorption observed on PS with respect to the aliphatic polyolefins indicates that hydrogen bonding is only part of the explanation. The results suggest that the polyelectrolyte charged groups develop a preferential interaction with the electron-rich functionalities of the support in general (carbonyl, benzene ring). The role of hydrophobic interactions might be important, too.

In the next paragraphs, the case of aliphatic polyolefins will be briefly discussed.

### *c) PP supports*

It has been shown that the deposition of the multilayer  $\text{PEI}/(\text{PSS}/\text{PCM})_x$  on PP and PIB is problematic. To overcome this problem, a copolymer based on PCM, but including long alkyl pendant residues, was designed (PCM COPO). The use of PCM COPO as primer layer improves the polyelectrolyte adsorption, especially if it is used as polycation instead of PCM in the subsequent deposition cycles, too. Good results have also been obtained with a primer PCM COPO layer and a cationic coloured ionene in the subsequent deposition cycles. The UV/vis, XPS and ToF-SIMS data will be presented in section II.B.2.

In fact, PCM COPO compatibilises the apolar PP support with the hydrophilic polyelectrolytes. Therefore, the use of hydrophobic interactions to anchor the first deposited layers on the PP substrate is an interesting strategy, avoiding the surface modification of PP by other techniques.

In another set of experiments, assemblies with a photocrosslinkable copolymer as polycation (P2 in Table 4) have been deposited on PP [261]. The crosslinking reaction was assessed by the disappearance of the characteristic peaks of the photoreactive residues in ToF-SIMS. These ions were used to trace the residual non-crosslinked groups, after UV irradiation [261]. In addition, it was shown that the assemblies based on the photoreactive polycation exhibit improved mechanical and solvent resistances.

*d) Future developments: ion beam patterning*

Patterned polyelectrolyte multilayers have been fabricated by Whitesides and co-workers using micro-contact printing [260]. In this paragraph, we will present a preliminary work which aims at creating multilayers with a lateral pattern by means of ion beam sputtering. In this method, chemical inhomogeneities are created on the polymer substrate by scanning the ion beam on the surface with a high fluence, well beyond the static SIMS limit (Fig. 44). Although not completely understood, the effects of the ion beam bombardment are manifold: implantation of primary atoms, creation of radicals in the solid, unsaturation, cross-linking, etc.

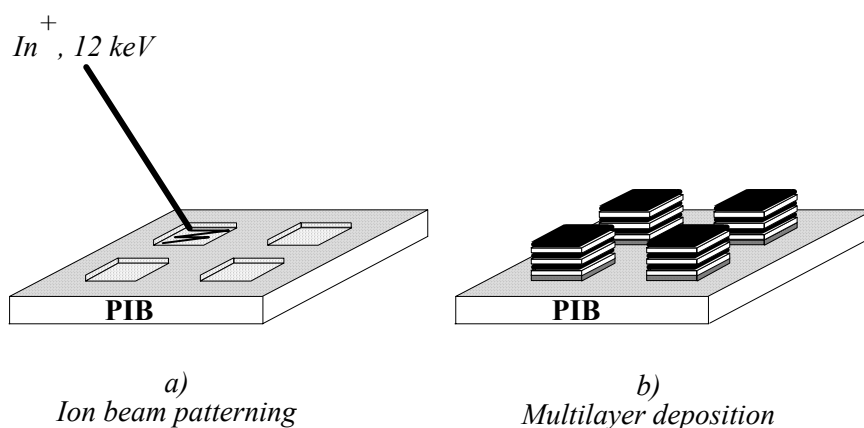


**Fig. 44.** Ion beam patterning of a PIB spin-coated film a) and multilayer deposition on the modified areas b).

As shown by the results obtained with PS supports (section I.4.B.6), the presence of unsaturation in the substrate favours polyelectrolyte adsorption. Therefore, a positive effect of the ion beam modification on the multilayer build-up is expected. In addition, the high reactivity of the bombarded surfaces might also lead to an improved oxidation when returning to air and water, which is also in favour of a better adsorption.

To form the pattern, the following strategy is used: (i) a polymer known as *bad* support for the polyelectrolyte multilayer build-up is chosen (PIB); (ii) it is spin-coated on a silicon support; (iii) after that, a well-resolved pattern is created using a high fluence  $\text{In}^+$ , 12 keV bombardment in pre-defined areas ( $10^{16}$  ions/cm<sup>2</sup>) (Fig. 44a); (iv) finally, the patterned sample is successively dipped into polycation and polyanion solutions, in order to obtain a multilayer (Fig. 44b).

## Summary of the Results

After bombardment, a primer layer of PEI and three bilayers of the PSS/PCM pair have been deposited on the modified PIB sample. Imaging SIMS has been used to verify the effects of the ion beam bombardment and multilayer deposition. The results are shown in Figs. 45a-j. The initial pattern (before the multilayer deposition) is revealed by the implanted indium ions (Fig. 45a). Concerning the deposition step, Figs. 45b-j indicate that the polyelectrolyte adsorption occurs preferentially on the modified areas. Indeed, the intensity related to the ions sputtered from PCM (Figs. 45d and 45g), from PSS (Figs. 45i and 45g) and from the counterions of PCM (Fig. 45h) is at least two times higher in the pre-bombarded areas. The corresponding depletion of intensity in the image of the PIB characteristic ions is due to the ion beam degradation, rather than to the multilayer deposition (Fig. 45c). Therefore, no conclusion can be drawn concerning the layer thickness. The different intensity distribution appearing in the total ion images shows that the contrast observed in the other images is not due to the sample topography, although this topography exists (Figs. 45b and 45f). Finally, the linescans drawn across the PCM and PSS images confirm the important intensity increase in the pre-bombarded regions. Nevertheless, the intensity threshold corresponding to the pristine PIB areas shows that polyelectrolyte chains adsorb to some extent on the PIB, too. This was expected from the previous measurements reported in section I.4.B.6.

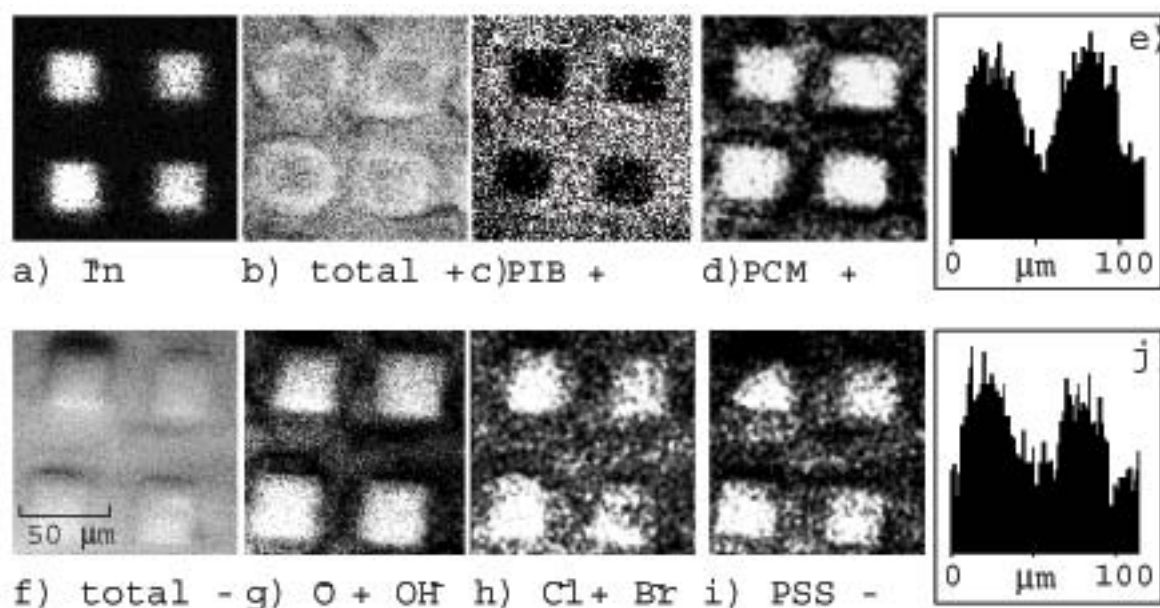


**Fig. 45.** Multilayer deposition on ion beam patterned PIB. *Before polyelectrolyte adsorption:* a) Implanted indium. *After polyelectrolyte adsorption, positive ions:* b) total ion image; c)  $C_6H_{11}^+$  and  $C_7H_{13}^+$ ; d)  $C_3H_8N^+$ ,  $C_5H_{12}N^+$ ,  $C_5H_{12}NO^+$  and  $C_5H_{14}NO^+$  (PCM); e) horizontal intensity profile through the bottom squares of image d); *negative ions:* f) total ion image; g) oxygen and hydroxyl ions; h) counterions of PEI and PCM;  $SO_2^-$ ,  $SO_3^-$  and monomer ion of PSS; j) horizontal intensity profile through the bottom squares of image i).

*e) Summary*

By a combined ToF-SIMS and XPS study, we have shown that the adsorption of polyelectrolyte multilayers on uncharged polymers is feasible, and that the amount of polyelectrolyte deposited in the first layers is comparable to the results obtained with silicon supports, except for the PP and PIB substrates.

The data reported for polymer substrates have been interpreted without ambiguity, owing to the calibration of the information depths in static SIMS and XPS (section I.4.B.5), and to the study of multilayer deposition on silicon (section I.4.B.6).

Based on the comparison with silicon supports, the detailed analysis of the substrate and coating signals has led to propose a different mechanism of multilayer growth in the case of PET substrates. With PET, the results point to a non-linear increase of the layer thickness in the first deposited layers.

In the case of aliphatic polyolefins, different primer polyelectrolyte layers (including a photocrosslinkable polycation) have been used to compatibilise the apolar polymers with the hydrophilic polyelectrolytes used for the multilayer assembly (section II.B.2).

Finally, it has been demonstrated that the poor adsorption observed in the case of aliphatic polyolefins is an advantage for the development of ion beam patterned surfaces with selective polyelectrolyte multilayer adsorption.

#### **I.4.B.7. Conclusion**

In the more applied part of these notes, polyelectrolyte multilayers have been investigated by the combined use of ToF-SIMS and XPS. On the one hand, the detailed analysis of well-characterised multilayer samples by means of surface techniques has given a new insight into the origin of the information acquired in ToF-SIMS. For instance, it has been shown that the emission depth of atomic secondary ions ( $\text{Si}^+$ ) is close to 15 Å, i.e. that the layer thickness probed by these ions may be as large as 50 Å in the case of polyelectrolyte multilayers. Remarkably, the information depth of molecular ions is much smaller, making these ions more surface specific. These results can be intuitively understood considering that energetic atomic species may easily propagate through the solid before the emission, while moving molecular species would directly fragment and remain in the solid.

On the other hand, the study of  $\text{PEI}/(\text{PSS}/\text{PCM})_x$  multilayers adsorbed on silicon has led to interesting conclusions: (i) the complexation of the polyelectrolytes in the multilayer is nearly quantitative; (ii) the fraction of counterions remaining in the top polyelectrolyte layer of the assemblies is weak; (iii) the  $\text{PEI}/(\text{PSS}/\text{PCM})_x$  assemblies form good quality multilayers, with a regular bilayer thickness of 15 Å when deposited on silicon; (iv) the

## Summary of the Results

functionalisation of polycations I10 and P2 performed on the layer via the (deposition + activation) technique (sections II.B.1.1 and II.B.1.3) and the multilayer build-up with these polyelectrolytes have been assessed.

The know-how gained by the study conducted with model substrates could be successfully transposed for the investigation of multilayers adsorbed on polymer supports: (i) multilayers can be adsorbed on uncharged polymer supports like PET; (ii) the results indicate that the growth of the PEI/(PSS/PCM)<sub>x</sub> assemblies is non-linear for the first ten deposited layers on PET; (iii) the deposition is much more problematic on aliphatic polyolefins (PP and PIB); (iv) this can be overcome by the use of hydrophobic or crosslinkable polycation layers instead of PEI and PCM. (v) For PIB supports, preliminary results have been obtained showing the preferential polyelectrolyte adsorption on ion beam bombarded areas. This could be verified by Imaging SIMS.

The experiments and results discussed above are described in details through the articles presented in sections II.B.1-2. The analysed samples and properties are indexed in Table 8 for sake of clarity.

**Table 8.** Index of the results reported in the thesis (Part B). The corresponding section is indicated for each combination of sample and result type.

	Substrate		Mass spectra	Layer thickness	Chemical reaction	Imaging SIMS
	silicon	polymer				
bare substrates	II.B.1.2	II.B.2	II.B.1.2 II.B.2	-	-	-
PEI/(PSS/PCM) <sub>x</sub>	II.B.1.2	II.B.2	II.B.1.2	II.B.1.2	-	I.4.B.6.
PCM COPO/ (PSS/PCM COPO) <sub>x</sub>	-	II.B.2	-	-	-	-
PEI/(PVS/I0) <sub>x</sub> PEI/(PVS/I6) <sub>x</sub>	I.4.B.4	-	-	I.4.B.5	-	-
PEI/(PVS/I10p) <sub>x</sub>	II.B.1.1 II.B.1.2	-	-	-	-	II.B.1.1.
PEI/PVS/(I10a) <sub>x</sub>	II.B.1.1 II.B.1.2	-	II.B.1.1	II.B.1.2	II.B.1.1	-
PEI/PSPM/(P1a) <sub>x</sub>	II.B.1.3	-	II.B.1.3	II.B.1.3	II.B.1.3	-



# I.5.

---

## Concluding remarks

---

### I.5.1. Conclusion

This thesis has explored two major topics : A) the development of a complex characterisation technique (ToF-SIMS) and (B) the elaboration of a new kind of materials (polymers with a polyelectrolyte multilayer coating). By the combination of these two elements, several advances in both fields have been achieved.

From the viewpoint of the characterisation method, a fundamental study involving a variety of organic coatings and substrates has been carried out. The obtained results can be seen as the prerequisite for a smart and realistic interpretation of the data related to complex organic multilayers.

First, the analysis of the secondary ion KEDs constitutes a powerful method to gain information about the emission processes in SIMS of organic layers. Among them, the following mechanisms have been identified and explained: the emission of low-energy, precursor-like species (i), of faster and strongly dehydrogenated ions (ii), of rather energetic cationised oligomers and molecules (iii), as well as the metastable decay of excited ejecta (iv). Our phenomenological model based on the concept of internal energy-dependent fragmentation of excited ejecta accounts for the periodic variation of the hydrocarbon ion kinetic energy (i-ii). On the other hand, a multiple collision process is the more appropriate to fit the observed kinetic energies in the case of large parent-like ions (iii). Finally, the observed metastable decay processes can be interpreted with the formalism of the unimolecular reaction theory. These advances may be integrated in a comprehensive picture of the sputtering event.

By the use of polyelectrolyte multilayer samples of well-known thicknesses, the information depth of atomic and molecular ions have been determined. For  $\text{Si}^+$ ,  $\text{SiOH}^+$  and  $\text{SiO}_3\text{H}^-$ , 95 % of the substrate ion intensity is lost with organic coatings of 45 Å, 25 Å and 15 Å thickness, respectively. This result indicates that the surface specificity of the sputtered ions is proportional to their size.

In a second stage, the fundamental knowledge deduced from the yields and KED measurements, ion beam degradation and substrate effect studies has been applied to the investigation of polyelectrolyte multilayers.

In a preliminary phase, multilayers deposited on model silicon substrates have been used to establish the SIMS results, in combination with other characterisation techniques. For the PSS/PCM system, this analysis shows that multilayers grow regularly, with a mean thickness of 15 Å per bilayer and that the complexation of the layers is nearly quantitative. The intensity variation of the polyelectrolyte secondary ions suggests that the layers are interdigitated. For the other systems, activation and cross-linking chemical reactions could also be assessed by ToF-SIMS.

Remarkably, the multilayer build-up occurs on uncharged polymer substrates, too. Except for aliphatic hydrocarbons (PP and PIB), the secondary ion intensities related to the polymer supports are drastically reduced with only three PSS/PCM deposition cycles, which is comparable to the case of silicon. Therefore, PET, PS, PMMA and more complicated polymers including various chemical functionalities constitute interesting substrates for the multilayer deposition. For PET, the deposited amount of polyelectrolyte increases with the layer number, and the more realistic interpretation involves the increase of the layer thickness at each step, rather than the irregular deposition of polymer patches. Interestingly, the bilayer thickness would reach 30 Å after 3 deposition cycles, which is two times the thickness measured on silicon. For PP and PIB supports, better quality layers can be obtained using more hydrophobic polyelectrolytes, as demonstrated by UV/vis, XPS and ToF-SIMS measurements. In practice, the limited adsorption on aliphatic polyolefins can be advantageously used to design patterned multilayers, too.

The adsorption of polyelectrolyte multilayers on these 'real-world' supports extends the field of application of these materials. In this respect, adequate multilayer coatings will provide well-defined properties to the polymer substrates, e.g. improved gas barrier properties, particular optical features (refractive index, anisotropy, coloration), specific biorecognition capability, improved biocompatibility, better protection against UV radiations, good electrical conductivity, etc.

## I.5.2. Outlook

---

Although new approaches have been developed, many question marks and unexplored regions remain in the different fields covered by these notes.

Concerning the sputtering processes, our data should be compared to molecular dynamics results obtained with similar samples. The collisional character of most of the emission processes, indicated by the KEDs in several cases, suggests that this approach is the more appropriate to model the keV ion induced emission of secondary ions. Experimentally, the nature, yield and kinetic energy distribution of ions sputtered from similar organic molecules adsorbed with different bond strength and orientations on the substrate would provide new data for the comparison with simulation results. On the other hand, the *ejection time distribution* of the secondary species might tell us whether the proposed picture (section I.4.A.7) is consistent with the facts. Indications about this parameter could be extracted from the peak resolution obtained for mass spectra acquired with a narrow energy passband (without the energy dispersion, the time of ejection might become a major parameter giving rise to time-of-flight differences). The effects of the primary beam energy (from keV to MeV) should be investigated, too.

In the applied part of the thesis, the adsorption of polyelectrolyte layers on uncharged polymers has been demonstrated. To carry on this work, mechanical and chemical tests should be performed on similar samples. In addition, more details concerning the structure of the layers are desirable. The investigation of the modified supports by near-field microscopies would certainly bring complementary information.

From the viewpoint of the applications, the use of functional assemblies with specific properties (conducting layers, diffusion barriers, biologically active layers) and the development of patterned surfaces are promising.

---

## References

- [1] R. S. Taylor, available on the web at the following address: [http://galilei.chem.psu.edu/Research\\_org.html](http://galilei.chem.psu.edu/Research_org.html)
- [2] W. R. Grove, *Philos. Mag.* 5 (1853) 203.
- [3] E. Goldstein, *Verh. Dtsch. Phys. Ges.* 4 (1902) 237.
- [4] J. J. Thomson, *Philos. Mag.* 20 (1910) 752.
- [5] R. Behrisch, in: *Sputtering by Particle Bombardment I*, ed. R. Behrisch (Springer Verlag, Berlin, 1981) p. 1.
- [6] J. T. Trauger, *Science* 226 (1984) 337.
- [7] R. E. Johnson and B. U. R. Sundqvist, *Physics Today* 45/3 (1992) 28.
- [8] K. Roessler, in: *Solid-State Astrophysics*, Elsevier (Amsterdam, 1991) p. 197
- [9] O. Auciello, in: *Ion Bombardment Modification of Surfaces, Fundamentals and Applications*, eds. O. Auciello and R. Kelly, Elsevier (Amsterdam, 1984) p. 435.
- [10] A. Benninghoven, F. G. Rüdener and H. W. Werner, *Secondary Ion Mass Spectrometry*, Wiley (New York, 1987) p.699.
- [11] A. Benninghoven, *Chem. Phys. Lett.*, 6 (1970) 616.
- [12] D. F. Torgerson, R. P. Skowronski, R. D. Macfarlane, *Biochem. Biophys. Res. Commun.* 60 (1974) 616.
- [13] R. D. Macfarlane, D. F. Torgerson, *Science* 191 (1976) 920.
- [14] A. Benninghoven, D. Jaspers, W. Sichtermann, *Appl. Phys* 11 (1976) 35.
- [15] B. T. Chait and K. G. Standing, *Int. J. Mass Spectrom. Ion Phys.* 40 (1981) 185.
- [16] D. Briggs, in: *Practical Surface Analysis, Vol. 2 - Ion and Neutral Spectroscopy*, ed. D. Briggs and M. P. Seah, Wiley (New York, 1992) p. 367.
- [17] A. Benninghoven, *Angew. Chem. Int. Ed. Engl.* 33 (1994) 1023.
- [18] R. D. Short, A. P. Ameen, S. T. Jackson, D. J. Pawson, L. O'Toole and A. J. Ward, *Vacuum* 44 (1993) 1160.
- [19] J. C. Vickerman and A. J. Swift, in: *Surface Analysis - The Principal Techniques*, ed. J. Vickerman, Wiley (New York, 1997) p. 135.
- [20] P. Bertrand and L. T. Weng in: *Surface Characterization, A User's Sourcebook*, eds. D. Brune, R. Hellborg, H. J. Whitlow, O. Hunderi, Wiley (New York, 1997) p. 335.
- [21] R. W. Odom, in: *Microscopic and Spectroscopic Imaging of the Chemical State*, ed. M. D. Morris, Marcel Dekker, Inc. (New York, 1993) p. 345.
- [22] T. R. Lundquist, *Surf. Sci.* 90 (1979) 548.
- [23] M. J. Vasile, *Phys. Rev. B* 29 (1984) 3785.
- [24] A. Wucher and H. Oechsner, *Surf. Sci.* 199 (1988) 567.
- [25] J. K. Norskov and B. I. Lundqvist, *Phys. Rev. B* 19 (1979) 5661.
- [26] M. L. Yu, in: *Sputtering by Particle Bombardment III*, eds. R. Behrisch and K. Wittmaack (Springer Verlag, Berlin, 1991) p. 91.
- [27] P. A. W. van der Heide, *Surf. Sci. Lett.* 302 (1994) L312.
- [28] G. Blaise and G. Slodzian, *Rev. Phys. Appl.* 8 (1973) 105.
- [29] M. A. Rudat and G. H. Morrison, *Surf. Sci.* 82 (1979) 549.
- [30] A. Benninghoven, F. G. Rüdener and H. W. Werner, *Secondary Ion Mass Spectrometry*, Wiley (New York, 1987).
- [31] R. A. Brizzolara and C. B. Cooper, *Nucl. Ins. Meth. Phys. Res. B* 43 (1989) 136.
- [32] S. R. Coon, W. F. Calaway, M. J. Pellin, G. A. Curlee, J. M. White, *Nucl. Ins. Meth. Phys. Res. B* 82 (1993) 329.
- [33] A. Wucher, M. Wahl, H. Oechsner, *Nucl. Ins. Meth. Phys. Res. B* 82 (1993) 337.

## References

- 
- [34] Z. Ma, W. F. Calaway, M. J. Pellin, E. I. von Nagy-Felsobuki, Nucl. Ins. Meth. Phys. Res. B 94 (1994) 197.
- [35] G. Betz and W. Husinsky, Nucl. Ins. Meth. Phys. Res. B 102 (1995) 281.
- [36] E. Vietzke, A. Refke, V. Philipps, M. Hennes, J. Nucl. Mater. 241 (1997) 810.
- [37] L. Kelner and S. P. Markey, Int. J. Mass Spectrom. Ion Proc. 59 (1984) 157.
- [38] L. Kelner and T. C. Patel, in: SIMS V proceedings, Springer. Ser. Chem. Phys. 44 (1986) p. 494.
- [39] G. J. Q. van der Peyl, W. J. van der Zande, R. Hoogerbrugge, P. G. Kistemaker, Adv. Mass Spectrom. 10 (1986) 1511.
- [40] R. Hoogerbrugge, W. J. Van Der Zande and P. G. Kistemaker, Int. J. Mass. Spectrom. Ion Proc. 76 (1987) 239.
- [41] R. Hoogerbrugge and P. G. Kistemaker, Nucl. Ins. Meth. Phys. Res. B 18 (1987) 600.
- [42] R. A. Haring, R. Pedrys, D. J. Oostra, A. Haring and A. E. de Vries, Nucl. Ins. Meth. Phys. Res. B 5 (1984) 483.
- [43] E. Pedrys, D. J. Oostra, R. A. Haring, L. Calcagno, A. Haring, A. E. de Vries, Nucl. Ins. Meth. Phys. Res. B 17 (1986) 15.
- [44] G. Gillen, Int. J. Mass Spectrom. Ion Processes 105 (1991) 215.
- [45] D. Briggs and A. B. Wootton, Surf. Interface Anal. 4 (1982) 109.
- [46] A. Brown and J. C. Vickerman, Surf. Interface Anal. 8 (1986) 75.
- [47] I. S. Gilmore and M. P. Seah, Surf. Interface Anal. 23 (1995) 191.
- [48] R. A. Zubarev, U. Abeywarnna, P. Hakansson, P. Demirev and B. U. R. Sundqvist, Rapid Commun. Mass Spectrom. 10 (1996) 1966.
- [49] R. M. Papaléo, G. Brinkmalm, D. Fenyő, J. Eriksson, H.-F. Kammer, P. Demirev, P. Hakansson and B.U.R. Sundqvist, Nucl. Ins. Meth. Phys. Res. B 91 (1994) 667.
- [50] R. M. Papaléo, P. Demirev, J. Eriksson, P. Hakansson and B.U.R. Sundqvist, Phys. Rev. B 54 (1996) 3173.
- [51] R. M. Papaléo, P. Demirev, J. Eriksson, P. Hakansson and B.U.R. Sundqvist, R. E. Johnson, Phys. Rev. Lett. 77 (1996) 667.
- [52] S. Della Negra, O. Becker, R. Cotter, Y. Le Beyec and E. A. Schweikert, Phys. Rev. Lett. 60 (1988) 948.
- [53] C. T. Reimann, in: Fundamental Processes in Sputtering of Atoms and Molecules, Matematisk-fysiske Meddelelser 43; ed. P. Sigmund, (Copenhagen, 1993) p. 351.
- [54] R. Zubarev, Ph.D. Thesis: Mass Spectrometry of Biopolymers Based on Ion-Induced Desorption (Uppsala, 1997).
- [55] P. Sigmund, in : Sputtering by Particle Bombardment I, ed. R. Behrisch (Springer Verlag, Berlin, 1981) p. 9.
- [56] S. J. Pachuta and R. J. Cooks, Chem. Rev. 87 (1987) 647.
- [57] M. W. Thompson, Philos. Mag. 18 (1968) 377.
- [58] P. Sigmund, Phys. Rev. 184 (1969) 383.
- [59] W. Hofer, in : Sputtering by Particle Bombardment III, eds. R. Behrisch and K. Wittmaack (Springer Verlag, Berlin, 1991) p. 15.
- [60] G. Betz and K. Wien, Int. J. Mass Spectrom. Ion Proc. 140 (1994) 1.
- [61] N. Winograd and B. Garrison, in Ion Spectroscopies for Surface Analysis; Ed.: A. W. Czanderna and D. M. Hercules, Plenum Press (New York, 1991) p. 58.
- [62] A. Benninghoven, Surf. Sci. 35 (1973) 427.
- [63] H. Oechsner and W. Gerhard, Surf. Sci. 44 (1974) 480.
- [64] G. P. Können, A. Tip and A. E. de Vries, Rad. Effects 26 (1975) 23.
- [65] F. Honda, G. M. Lancaster, Y. Fukuda, J. W. Rabalais, J. Chem. Phys 69 (1978) 4931.
- [66] G. M. Lancaster, F. Honda, Y. Fukuda, J. W. Rabalais, J. Am. Chem. Soc. 101 (1979) 1951.
- [67] P. T. Murray and J. W. Rabalais, J. Am. Chem. Soc. 103 (1981) 1007.

- [68] A. Benninghoven, in *Ion Formation from Organic Solids*, Springer Series in Chemical Physics 25; Ed. A. Benninghoven, Springer-Verlag (Berlin, 1983) p. 77.
- [69] A. W. Kolfshoten, R. A. Haring, A. Haring and A. E. de Vries, *J. Appl. Phys.* 55 (1984) 3813.
- [70] R. G. Orth, H. T. Jonkman, J. Michl, *J. Am. Chem. Soc.* 104 (1982) 1834.
- [71] K. Snowdon, *Nucl. Ins. Meth. Phys. Res. B9* (1985) 132.
- [72] K. Snowdon, R. Hentschke, W. Heiland, P. Hertel, *Z. Phys. A* 318 (1984) 261.
- [73] R. A. Haring, H. E. Rosendaal and P. C. Zalm, *Nucl. Instr. and Meth. B28* (1987) 205.
- [74] H. M. Urbassek, *Nucl. Instr. and Meth. B18* (1987) 587.
- [75] H. M. Urbassek, *Rad. Eff. Def. Solids* 109 (1989) 293.
- [76] R. Hoogerbrugge and P. G. Kistemaker, *Nucl. Ins. and Meth. B21* (1987) 37.
- [77] B. V. King, I. S. T. Tsong, S. H. Lin, *Int. J. Mass Spectrom. Ion Processes* 78 (1987) 341.
- [78] S. H. Lin, I. S. T. Tsong, A. R. Ziv, M. Szymonski and C. M. Loxton, *Phys. Scr. T6* (1983) 106.
- [79] G. J. Leggett and J. C. Vickerman, *Int. J. Mass Spectrom. Ion Proc.* 122 (1992) 281.
- [80] B. J. Garrison, *J. Am. Chem. Soc.* 104 (1982) 6211.
- [81] B. J. Garrison, *Int. J. Mass. Spectrom. Ion Phys.* 53 (1983) 243.
- [82] R. S. Taylor, C. L. Brummel, N. Winograd, B. J. Garrison, J. C. Vickerman, *Chem. Phys. Lett.* 233 (1995) 575.
- [83] B. H. Sakakini, N. Dunhill, C. Harendt, B. Steeples, J. C. Vickerman, *Surf. Sci.* 189/190 (1987) 211; B. H. Sakakini, I. A. Ransley, C. F. Oduoza, J. C. Vickerman, M. A. Chesters, *Surf. Sci.* 271 (1992) 227.
- [84] R. S. Taylor and B. J. Garrison, *Chem. Phys. Lett.* 230 (1994) 495.
- [85] R. S. Taylor and B. J. Garrison, *J. Am. Chem. Soc.* 116 (1994) 4465.
- [86] R. S. Taylor and B. J. Garrison, *Langmuir* 11 (1995) 1220.
- [87] R. S. Taylor and B. J. Garrison, *Int. J. Mass Spectrom. Ion Processes* 143 (1995) 225.
- [88] D. Briggs, *Surf. Interface Anal.* 15 (1990) 734.
- [89] I. S. Bitensky and E. S. Parilis, *Nucl. Ins. Meth. Phys. Res. B21* (1987) 26.
- [90] I. S. Bitensky, *Nucl. Ins. Meth. B83* (1993) 110.
- [91] R. E. Johnsson, B. U. R. Sundqvist, A. Hedin, D. Fenyö, *Phys. Rev. B40* (1989) 49.
- [92] A. Hedin, P. Hakansson, M. Salehpour, B. U. R. Sundqvist, *Phys. Rev. B35* (1987) 7377.
- [93] S. S. Wong, F. W. Röllgen, *Nucl. Ins. and Meth. B14* (1986) 436.
- [94] B. U. R. Sundqvist, *Nucl. Instr. and Meth. B48* (1990) 517.
- [95] J. C. Vickerman, A. Brown, N. M. Reed, in: *Secondary Ion Mass Spectrometry: Principles and Applications*, Clarendon Press (Oxford, 1989) p. 62.
- [96] M. L. Yu, in: *Sputtering by Particle Bombardment III*; Eds. R. Behrisch and K. Wittmaack (Springer Verlag, Berlin, 1991) p. 91.
- [97] G. Blaise and A. Nourtier, *Surf. Sci.* 90 (1979) 495.
- [98] G. Slodzian, *Surf. Sci.* 48 (1975) 161.
- [99] P. Williams, *Surf. Sci.* 90 (1979) 588.
- [100] G. E. Thomas, *Rad. Eff.* 31 (1977) 185.
- [101] C. Plog and W. Gerhard, *Surf. Sci.* 152/153 (1985) 127.
- [102] C. A. Andersen and J. R. Hinthorne, *Anal. Chem.* 45 (1973) 1421.
- [103] M. L. Yu and K. Mann, *Phys. Rev. Lett.* 57 (1986) 1476.
- [104] A. Wucher, M. Wahl, H. Oechsner, in: *Secondary Ion Mass Spectrometry, SIMS IX proceedings*; Eds. A. Benninghoven, Y. Nihei, R. Shimizu, H. W. Werner, Wiley (New York, 1994) p. 100.
- [105] A. Benninghoven, W. Lange, M. Jirikowsky, D. Holtkamp, *Surf. Sci.* 123 (1982) L721.
- [106] A. M. Spool, P. H. Kasai, *Macromolecules* 29 (1996) 1691.
- [107] G. J. Leggett, in: *The Wiley Static SIMS Library*, Wiley (New York, 1996) p. 19.

## References

- 
- [108] J. B. Pallix, U. Schuhle, C. H. Becker, D. L. Huestis, *Anal. Chem.* 61 (1989) 805.
- [109] W. Forst, *Theory of Unimolecular Reactions*, Ac. Press, New York (1973).
- [110] Y. Gotkis, M. Oleinikova, M. Naor and C. Lifshitz, *J. Phys. Chem* 97 (1993) 12282.
- [111] K. G. Standing, W. Ens and R. Beavis, in *Ion Formation from Organic Solids*, Springer Series in Chemical Physics 25; Ed. A. Benninghoven, Springer-Verlag (Berlin, 1983) p. 107.
- [112] B. Schueler, R. Beavis, W. Ens, D. E. Main, X. Tang and K. G. Standing, *Int. J. Mass Spectrom. Ion Proc.* 92 (1989) 185.
- [113] X. Tang, W. Ens, N. Poppe-Schriemer and K. G. Standing, in *Methods and Mechanisms for Producing Ions from Large Molecules*; Eds. K. G. Standing and W. Ens, Plenum Press (New York, 1991) p. 139.
- [114] H. Feld, A. Leute, D. Rading, A. Benninghoven, M. P. Chiarelli and D. M. Hercules, *Anal. Chem.* 65 (1993) 1947.
- [115] D. F. Barofsky, G. Brinkmalm, P. Hakansson, B. U. R. Sundqvist, *Int. J. Mass Spectrom. Ion Processes* 131 (1994) 283.
- [116] B. Schueler, R. Beavis, G. Bolbach, W. Ens, D. E. Main and K. G. Standing, *SIMS V*, Springer Series Chem. Phys. 44 (1986) 57.
- [117] W. Begemann, K. H. Meiwes-Broer and H. O. Lutz, *Phys. Rev. Lett.* 56 (1986) 2248.
- [118] N. K. Dzhemilev, A. M. Goldenberg, I. V. Veryovkin, S. V. Verkhoturov, *Nucl. Instr. and Meth. B114* (1996) 245.
- [119] A. D. Bekkerman, N. K. Dzhemilev, S. V. Verkhoturov, I. V. Veryovkin, A. Adriaens, *EMAS'97 proceedings, Microchimica Acta*, in press.
- [120] R. H. Tredgold, *Order in Thin Organic Films*, Cambridge University Press (Cambridge, 1994).
- [121] A. Laschewsky, in: *Polymer-Solid Interfaces: From Model to Real Systems*, ICPSI 2 proceedings, Eds. J. J. Pireaux, J. Delhalle, P. Rudolf, Presses Universitaires de Namur (Namur, 1998) p. 245.
- [122] G. Wegner, *Ber. Bunsenges. Phys. Chem.* 95 (1991) 1326; G. Wegner, *Thin Solid Films* 216 (1992) 105.
- [123] A. Ulman, *Chem. Rev.* 96 (1996) 1533.
- [124] G. Decher, in: *Polymer Materials Encyclopedia*, Vol. 6, Ed.: J. C. Salamone, CRC Press (Boca Raton, 1996) p. 4540.
- [125] W. Knoll, *Curr. Opinion Coll. Interface Sci.* 1 (1996) 137.
- [126] A. Kubono, N. Okui, K. Tanaka, S. Umemoto, T. Sakai, *Thin Solid Films* 199 (1991) 385.
- [127] R. d'Agostino, in *Plasma Processing of Polymers*, NATO ASI Series E - Vol. 346; eds.: R. d'Agostino, P. Favia and F. Fracassi, Kluwer Academic Publishers (Dordrecht, 1997) p. 3.
- [128] A. Chilkoti, B. D. Ratner, D. Briggs, *Anal. Chem* 63 (1991) 1612.
- [129] V. K. Agarwal, Y. Igasaki, H. Mitsuhashi, *Thin Solid Films* 33 (1976) L31.
- [130] A. Benninghoven in *Ion Formation from Organic Solids*, Springer Series in Chemical Physics 25; Ed. A. Benninghoven, Springer-Verlag (Berlin, 1983) p. 72; W. Lange, D. Holtkamp, M. Jirikowsky and A. Benninghoven, *ibid.*, p.124.
- [131] M. Sano, Y. Lvov, T. Kunitake, *Annu. Rev. Mater. Sci.* 26 (1996) 153.
- [132] M. Sano, M. Wada, A. Miyamoto, S. Yoshimura, *Thin Solid Films* 284-285 (1996) 249.
- [133] M. Ahlers, W. Müller, A. Reichert, H. Ringsdorf, J. Venzmer, *Angew. Chem. Int. Ed. Engl.* 29 (1990) 1269.
- [134] M. Whitesides, J. P. Mathias, C. T. Seto, *Science* 254 (1991) 1312.
- [135] J. D. Swalen, D. L. Allara, J. D. Andrade, E. A. Chandross, S. Garoff, J. Israelachvili, T. J. McCarthy, R. Murray, R. F. Pease, J. F. Rabolt, K. J. Wynne, H. Yu, *Langmuir* 3 (1987) 932.

- [136] G. Decher, B. Lehr, K. Lowack, Y. Lvov, J. Schmitt, *Biosensors and bioelectronics* 9 (1994) 677
- [137] Y. Sun, X. Zhang, C. Sun, B. Wang, J. Shen, *Macromol. Chem. Phys.* 197 (1996) 147.
- [138] M. Onda, Y. Lvov, K. Ariga, T. Kunitake, *Journal of Fermentation and Bioengineering* 82 (1996) 502.
- [139] C. Nicolini, *Thin Solid Films* 284-285 (1996) 1.
- [140] T. Kunitake, *Thin Solid Films* 284-285 (1996) 9.
- [141] D. H. Reinhoudt, A. M. A. van Wageningen, B.-H. Huisman, in *Physical Supramolecular Chemistry*, NATO ASI Series C - Vol. 485; eds.: L. Echegoyen and A. E. Kaifer, Kluwer Academic Publishers (Dordrecht, 1996) p. 1.
- [142] A. Laschewsky, E. Wischerhoff, S. Denzinger, H. Ringsdorf, A. Delcorte, P. Bertrand, *Chem. Eur. J.* 3 (1997) 34.
- [143] Th. M. Cooper, A. L. Campbell, R. L. Crane, *Langmuir* 11 (1995) 2713.
- [144] Y. Lvov, G. Decher, G. Sukhorukov, *Macromolecules* 26 (1993) 5396.
- [145] G.B. Sukhorukov, H. Mohwald, G. Decher, Y.M. Lvov, *Thin Solid Films* 284-285 (1996) 220.
- [146] J.D. Hong, K. Lowack, J. Schmitt, G. Decher, *Prog. Colloid & Polym. Sci.* 93 (1993) 98.
- [147] Y. Lvov, K. Ariga, T. Kunitake, *Chem. Lett.* 12 (1994) 2323.
- [148] Y. Lvov, K. Ariga, I. Ichinose, T. Kunitake, *J. Am. Chem. Soc.* 117 (1995) 6117.
- [149] W. Kong, X. Zhang, M. L. Gao, H. Zhou, W. Li, J. C. Shen, *Macromol. Rapid Commun.* 15 (1994) 405.
- [150] Y. Lvov, K. Ariga, I. Ichinose, T. Kunitake, *Thin Solid Films* 284-285 (1996) 797.
- [151] R. Kayushina, Y. Lvov, N. Stepina, V. Belayev, Y. Khurgin, *Thin Solid Films* 284-285 (1996) 246.
- [152] F. Caruso, K. Niikura, D. N. Furlong, Y. Okahata, *Langmuir*, 13 (1997) 3427.
- [153] E. Brynda, M. Houska, *J. Colloid Interface Sci.* 183 (1996) 18
- [154] Y. Lvov, H. Haas, G. Decher, H. Möhwald, A. Mikhailov, B. Mtchedlishvily, E. Morgunova, B. Vainshtein, *Langmuir* 10, (1994) 4232.
- [155] Y. Lvov, H. Haas, G. Decher, H. Mohwald, A. Kalachev, *J. Phys. Chem.* 97 (1993) 12835.
- [156] G. B. Sigal, C. Bamdad, A. Barberis, J. Strominger, G. M. Whitesides, *Anal. Chem.* 68 (1996) 490.
- [157] A. R. Bishop and R. G. Nuzzo, *Curr. Opinion Coll. Interface Sci.* 1 (1996) 127.
- [158] M. Ferreira, J.H. Cheung, M.F. Rubner, *Thin Solid Films* 244 (1994) 806.
- [159] J.H. Cheung, A.F. Fou, M.F. Rubner, *Thin Solid Films* 244 (1994) 985.
- [160] A. C. Fou, M. F. Rubner, *Macromolecules* 28 (1995) 7115.
- [161] A. C. Fou, O. Onitsuka, M. Ferreira, M. F. Rubner, *J. of Appl. Phys.* 79 (1996) 7501.
- [162] O. Onitsuka, A. C. Fou, M. Ferreira, B. R. Hsieh, M. F. Rubner, *J. of Appl. Phys.* 80 (1996) 4067.
- [163] J. Tian, C.-C. Wu, M. E. Thompson, J. C. Sturm, R. A. Register, M. J. Marsella, T. M. Swager, *Adv. Mater.* 7 (1995) 395.
- [164] J. K. Lee, D. S. Yoo, E. S. Handy, M. F. Rubner, *Appl. Phys. Lett.* 69 (1996) 1686.
- [165] D. Yoo, J.-K. Lee, M. F. Rubner, *Mat. Res. Soc. Symp. Proc.* 413 (1996) 395.
- [166] A. Wu, T. Fujuwara, M. Jikei, M.-A. Kakimoto, Y. Imai, T. Kubota, M. Iwamoto, *Thin Solid Films* 284/285 (1996) 901.
- [167] F. Saremi, G. Lange, B. Tieke, *Adv. Mater.* 8 (1996) 923.
- [168] K. Ariga, Y. Lvov, T. Kunitake, *J. Am. Chem. Soc.* 119 (1997) 2224.
- [169] K. Kajikawa, T. Yamada, S. Yokoyama, S. Okada, H. Matsuda, H. Nakanishi, M.-A. Kakimoto, Y. Imai, H. Takezoe, A. Fukuda, *Langmuir* 12 (1996) 580.
- [170] X. Wang, S. Balasubramanian, L. Li, X. Jiang, D. Sandman, M. F. Rubner, J. Kumar, S. K. Tripathy, *Macromol. Rapid Commun.* 18 (1997) 451.

## References

- 
- [171] Y. Lvov, S. Yamada, T. Kunitake, *Thin Solid Films* 300 (1997) 107.
- [172] A. Laschewsky, E. Wischerhoff, M. Kauranen, A. Persoons, *Macromolecules* 30 (1997) 8304.
- [173] L. M. Siewierski, W. J. Brittain, S. Petrash, M. D. Foster, *Langmuir* 12, (1996) 5838.
- [174] S. B. Roscoe, S. Yitzchaik, A. K. Kakkar, T. J. Marks, Z. Xu, T. Zhang, W. Lin, G. K. Wong, *Langmuir* 12 (1996) 5338.
- [175] S. B. Roscoe, A. K. Kakkar, T. J. Marks, A. Malik, M. K. Durbin, W. Lin, G. K. Wong, P. Dutta, *Langmuir* 12 (1996) 4218.
- [176] M. Maskus, J. Tirado, J. Hudson, R. Bretz, H. D. Abruna, in *Physical Supramolecular Chemistry*, NATO ASI Series C - Vol. 485; eds.: L. Echegoyen and A. E. Kaifer, Kluwer Academic Publishers (Dordrecht, 1996) p. 337.
- [177] L. S. Miller, A. M. McRoberts, D. J. Walton, I. R. Peterson, D. A. Parry, C. G. D. Sykesud, A. L. Newton, B. D. Powell, C. A. Jasper, *Thin Solid Films* 284-285 (1996) 927.
- [178] P. Stroeve, V. Vasques, M. A. N. Coelho, J. F. Rabolt, *Thin Solid Films* 284/285 (1996) 708.
- [179] X. Yang, S. Johnson, J. Shi, T. Holesinger, B. Swanson, *Sensors and Actuators B* 45 (1997) 87.
- [180] G. Decher, J. Reibel, A. Ditterich, H. Ringsdorf, H. Poths, R. Zentel, *Ber. Bunsen-Ges. Phys. Chem.* 97 (1993) 1386.
- [181] Y. Lvov, G. Decher, *Crystallography Reports* 39 (1994) 628.
- [182] K. B. Blodgett, *J. Am. Chem. Soc.* 57 (1935) 1007; K. B. Blodgett and I. Langmuir, *Phys. Rev.* 51 (1937) 964.
- [183] J. A. Zasadzinski, R. Viswanathan, L. Madsen, J. Garnæs, D. K. Schwartz, *Science* 263 (1994) 1726.
- [184] A. Laschewsky, H. Ringsdorf, G. Schmidt, *Thin Solid Films* 134 (1985) 153.
- [185] S. Yokoyama, M. Kakimoto, Y. Imai, *Langmuir* 10 (1994) 4594.
- [186] P. Hendlinger, A. Laschewsky, P. Bertrand, A. Delcorte, R. Legras, B. Nysten, D. Möbius, *Langmuir* 13 (1997) 310.
- [187] L. Netzer and J. Sagiv, *J. Am. Chem. Soc.* 105 (1983) 675.
- [188] R. Banga, J. Yarwood, A. M. Morgan, B. Evans, J. Kells, *Thin Solid Films* 284/285 (1996) 261.
- [189] R. Maoz, S. Matlis, E. DiMasi, B. M. Ocko, J. Sagiv, *Nature* 384 (1996) 150.
- [190] H. Lee, L. J. Kepley, H. G. Hong, T. E. Mallouk, *J. Am. Chem. Soc.* 110 (1988) 618.
- [191] H. E. Katz, G. Scheller, T. M. Putvinski, M. L. Schilling, W. L. Wilson, C. E. D. Chidsey, *Science* 254 (1991) 1485.
- [192] R. G. Nuzzo and D. L. Allara, *J. Am. Chem. Soc.* 105 (1983) 4481.
- [193] M. D. Porter, T. B. Bright, D. L. Allara, C. E. D. Chidsey, *J. Am. Chem. Soc.* 109 (1987) 3559.
- [194] T. Kim, R. M. Crooks, M. Tsen, L. Sun, *J. Am. Chem. Soc.* 117 (1995) 3963.
- [195] F. Sun, D. G. Castner, G. Mao, W. Wang, P. McKeown, D. W. Grainger, *J. Am. Chem. Soc.* 118 (1996) 1856.
- [196] Ch. Jung, O. Dannenberger, Y. Xu, M. Buck, M. Grunze, *Langmuir* 14 (1998) 1103.
- [197] O. Cavalleri, A. Hirstein, J.-P. Bucher, K. Kern, *Thin Solid Films* 284-285 (1996) 392.
- [198] G. Nelles, H. Schönherr, M. Jaschke, H. Wolf, M. Schaub, J. Küther, W. Tremel, E. Bamberg, H. Ringsdorf, H.-J. Butt, *Langmuir* 14 (1998) 808.
- [199] T. Ishida, S. Yamamoto, W. Mizutani, M. Motomatsu, H. Tokumoto, H. Hokari, H. Azehara, M. Fujihira, *Langmuir* 13 (1997) 3261.
- [200] T. Ishida, M. Hara, I. Kojima, S. Tsuneda, N. Nishida, H. Sasabe and W. Knoll, *Langmuir* 14 (1998) 2092.

- [201] C. D. Tidwell, S. I. Ertel, B. D. Ratner, B. J. Tarasevich, S. Atre, D. L. Allara, *Langmuir* 13 (1997) 3404.
- [202] D. A. Hutt and G. J. Leggett, *Langmuir* 13 (1997) 2740.
- [203] D. L. Allara and R. G. Nuzzo, *Langmuir* 1 (1985) 45; D. L. Allara and R. G. Nuzzo, *Ibid.* 52.
- [204] R. K. Iler, *J. Colloid Interface Sci.* 21 (1966) 569.
- [205] G. Decher and J. D. Hong, *Makromol. Chem. Macromol. Symp.* (1991) 321.
- [206] G. Decher and J. D. Hong, *Ber. Bunsenges. Phys. Chem.* 95 (1991) 1430.
- [207] G. Decher, J. D. Hong, J. Schmitt, *Thin Solid Films* 210/211 (1992) 831.
- [208] J. Schmitt, T. Grünwald, G. Decher, P. S. Pershan, K. Kjaer, M. Lösche, *Macromolecules* 26 (1993) 7058.
- [209] J. H. Fendler, *Chem. Mater* 8 (1996) 1616.
- [210] H. G. M. van de Steeg, M. A. Cohen Stuart, A. D. Keizer, B. H. Bijsterbosch, *Langmuir* 8 (1992) 2538.
- [211] N. G. Hoogeveen, M. A. Cohen Stuart, G. J. Fleer, *J. Colloid Interface Sci.* 182 (1996) 133.
- [212] F. Th. Hesselink, in: *Adsorption from solutions at solid/liquid interfaces*, Eds.: G. D. Parfitt and C. H. Rochester, Academic Press (New York, 1983) p. 377.
- [213] N. G. Hoogeveen, M. A. Cohen Stuart, G. J. Fleer, *J. Colloid Interface Sci.* 182 (1996) 146.
- [214] P. Berndt, K. Kurihara, T. Kunitake, *Langmuir* 8 (1992) 2486.
- [215] K. Lowack and C. A. Helm, *Macromolecules* 31 (1998) 823.
- [216] P. Linse, *Macromolecules* 29 (1996) 326.
- [217] T. P. Russell, *Mat. Sci. Rep.* 5 (1990) 171.
- [218] G. Decher, J. Schmitt, *Prog. Colloid Polym. Sci.* 89 (1992) 160.
- [219] Y. Lvov, G. Decher, H. Möwähld, *Langmuir* 9 (1993) 481.
- [220] A. Tronin, Y. Lvov, C. Nicolini, *Colloid Polym. Sci.* 272 (1994) 1317.
- [221] D. Korneev, Y. Lvov, G. Decher, J. Schmitt, S. Yaradaikin, *Physica B* 213&214 (1995) 954.
- [222] G. Decher, Y. Lvov, J. Schmitt, *Thin Solid Films* 244 (1994) 772.
- [223] J. J. Ramsden, Y. M. Lvov, G. Decher, *Thin Solid Films* 254 (1995) 246.
- [224] G. Decher, *Science* 277 (1997) 1232.
- [225] Y. Lvov, H. Haas, G. Decher and H. Möhwald, *J. Phys. Chem.* 97 (1993) 12835.
- [226] F. Caruso, K. Niikura, D. N. Furlong, Y. Okahata, *Langmuir* 13 (1997) 3422.
- [227] M. Onoda and K. Yoshino, *Jpn. J. Appl. Phys.* 34 (1995) L260.
- [228] J.-K. Lee, D. Yoo, M. F. Rubner, *Chem. Mater.* 9 (1997) 1710.
- [229] J. W. Baur, P. Besson, S. A. O'Connor, M. F. Rubner, *Mat. Res. Soc. Symp. Proc. Vol. 413* (1996) 583.
- [230] K. Araki, M. J. Wagner, M. S. Wrighton, *Langmuir* 12 (1996) 5393.
- [231] G. J. Kellogg, A. M. Mayes, W. B. Stockton, M. Ferreira, M. F. Rubner, S. K. Satija, *Langmuir* 12 (1996) 5109.
- [232] X. Arys, A. M. Jonas, B. Laguitton, R. Legras, A. Laschewsky, E. Wischerhoff, *Prog. Org. Coatings* 34 (1998) 108.
- [233] A. Laschewsky, B. Mayer, E. Wischerhoff, X. Arys, A. M. Jonas, *Ber. Bunsenges. Phys. Chem.* 100 (1996) 1033.
- [234] E. R. Kleinfeld and G. S. Ferguson, *Science* 265 (1994) 370.
- [235] G. Mao, Y. Tsao, M. Tirrell, H. T. Davis, V. Hessel, H. Ringsdorf, *Langmuir* 9 (1993) 3461.
- [236] G. Mao, Y. Tsao, M. Tirrell, H. T. Davis, V. Hessel, J. van Esch, H. Ringsdorf, *Langmuir* 10 (1994) 4174.
- [237] G. Mao, Y. Tsao, M. Tirrell, H. T. Davis, V. Hessel, H. Ringsdorf, *Langmuir* 11 (1995) 942.
- [238] F. Saremi, E. Maassen, B. Tieke, G. Jordan, W. Rammensee, *Langmuir* 11 (1995) 1068.
- [239] M. Gao, X. Kong, X. Zhang, J. Shen, *Thin Solid Films* 244 (1994) 815
- [240] X. Zhang, M. Gao, X. Kong, Y. Sun, J. Shen, *J. Chem. Soc., Chem. Com.* 15 (1994) 1055.

## References

- [241] M. Gao, M. Gao, X. Zhang, Y. Yang, B. Yang, J. Shen, *J. Chem. Soc., Chem. Com.* 15 (1994) 2777.
- [242] N. A. Kotov, I. Dekany, J. H. Fendler, *J. Phys. Chem.* 99 (1995) 13065.
- [243] M. Gao, X. Zhang, B. Yang, F. Li, J. Shen, *Thin solid films* 284-285 (1996) 242.
- [244] Y. Sun, E. Hao, X. Zhang, B. Yang, J. Shen, L. Chi, H. Fuchs, *Langmuir* 13 (1997) 5168.
- [245] K. Ariga, Y. Lvov, M. Onda, I. Ichinose, T. Kunitake, *Chem. Lett.* (1997) 125.
- [246] I. Ichinose, H. Tagawa, S. Mizuki, Y. Lvov, T. Kunitake, *Langmuir* 14 (1998) 187.
- [247] S. W. Keller, H.-N. Kim, T. E. Mallouk, *J. Am. Chem. Soc.* 116 (1994) 8817.
- [248] S. W. Keller, S. A. Johnson, E. S. Brigham, E. H. Yonemoto, T. E. Mallouk, *J. Am. Chem. Soc.* 117 (1995) 12879.
- [249] D. Cochín, M. Passmann, G. Wilbert, R. Zentel, E. Wischerhoff, A. Laschewsky, *Macromolecules* 30 (1997) 4775.
- [250] S. Watanabe, S. L. Regen, *J. Am. Chem. Soc.* 116 (1994) 8855.
- [251] V. V. Tsukruk, F. Rinderspacher, V. N. Bliznyuk, *Langmuir* 13 (1997) 2171.
- [252] G. Decher, M. Eckle, J. Schmitt, B. Struth, *Curr. Opinion Coll. Interface Sci.* 3 (1998) 32.
- [253] G. Kim, R. J. Farris, T. J. McCarthy, *Polymer Prepr. Am. Chem. Soc. Polym. Chem. Div.* 38 (1997) 672.
- [254] M. C. Hsieh, R. J. Farris, T. J. McCarthy, *Polymer Prepr. Am. Chem. Soc. Polym. Chem. Div.* 38 (1997) 670.
- [255] M. C. Hsieh, R. J. Farris, T. J. McCarthy, *Macromolecules* 30 (1997) 8453.
- [256] J.-M. Leväsalmi and T. J. McCarthy, *Macromolecules* 30 (1997) 1752.
- [257] W. Chen and T. J. McCarthy, *Macromolecules* 30 (1997) 78.
- [258] N. A. Kotov, S. Magonov, E. Tropsha, *Chem. Mater.* 10 (1998) 886.
- [259] L. A. Godinez, R. Castro, A. E. Kaifer, *Langmuir* 12 (1996) 5087.
- [260] P. T. Hammond and G. M. Whitesides, *Macromolecules* 28 (1995) 7569.
- [261] A. Laschewsky, E. Wischerhoff, P. Bertrand, A. Delcorte, *Macromol. Chem. Phys.* 198 (1997) 3239.
- [262] A. Laschewsky, B. Mayer, E. Wischerhoff, X. Arys, P. Bertrand, A. Delcorte, A. Jonas, *Thin Solid Films* 284-285 (1996) 334.
- [263] X. Wang, S. Balasubramanian, L. Li, X. Jiang, D. J. Sandman, M. F. Rubner, J. Kumar, S. K. Tripathy, *Macromol. Rapid Commun.* 18 (1997) 451.
- [264] W. B. Stockton and M. F. Rubner, in *Proc. of the MRS fall meeting 1994, Solid State Ionics IV*, 369 (1994) 587.
- [265] L. Wang, Z. Wang, X. Zhang, J. Shen, L. Chi, H. Fuchs, *Macromol. Rapid commun.* 18 (1997) 509.
- [266] Y. Shimazaki, M. Mitsuishi, S. Ito, M. Yamamoto, *Langmuir* 13 (1997) 1385.
- [267] G. B. Sukhorukov, G. Decher, J. Schmitt, *J. Am. Chem. Soc.*, submitted.
- [268] G. B. Sukhorukov, J. Schmitt, G. Decher, *Ber. Bunsenges. Phys. Chem.* 100 (1996) 948.
- [269] R. V. Klitzing and H. Möhwald, *Langmuir* 11 (1995) 3554.
- [270] R. V. Klitzing and H. Möhwald, *Thin Solid Films* 284-285 (1996) 352.
- [271] F. Caruso, E. Donath, H. Möhwald, *J. Phys. Chem. B* 102 (1998) 2011.
- [272] V. Charlier, A. Laschewsky, B. Mayer, E. Wischerhoff, *Macromol. Symp.* 126 (1997) 105.
- [273] A. Benninghoven, A. Müller, *Surf. Sci.* 39 (1973) 416.
- [274] W. Lange, M. Jirikowsky, A. Benninghoven, *Surf. Sci.* 136 (1984) 419.
- [275] M. Jirikowsky, D. Holtkamp, P. Klüsener, M. Kempken, A. Benninghoven, *Surf. Sci.* 182 (1987) 576.
- [276] N. M. Reed and J. C. Vickerman, in: *Surface Characterization of advanced polymers*; Eds.: L. Sabbatini and P. G. Zamboni, VCH (Weinheim, 1993) p.83.

- [277] D. Léonard, Ph.D. Thesis: Application of Secondary Ion Mass Spectrometry to Plasma Treated Polymer Surface Characterization in Correlation with Plasma Characterization, (Louvain-la-Neuve, 1996) p. 249.
- [278] J. C. Vickerman, D. Briggs, A. Henderson, The Wiley Static SIMS Library, Wiley (New York, 1996).
- [279] D. Brandl, Ch. Schoppmann, Ch. Tomaschko, M. Schurr, H. Voit, *Thin Solid Films* 256 (1995) 220.
- [280] J. H. Wandass and J. A. Gardella Jr., *J. Am. Chem. Soc.* 107 (1985) 6192.
- [281] J. H. Wandass, R. L. Schmitt, J. A. Gardella Jr., *Appl. Surf. Sci.* 40 (1989) 85.
- [282] R. W. Johnson Jr., J.-X. Li, P. A. Cornelio-Clark, J. A. Gardella Jr., in: *Secondary Ion Mass Spectrometry, SIMS VIII proceedings*; Eds. A. Benninghoven, K. T. F. Janssen, J. Tümpner, H. W. Werner, Wiley (New York, 1992) p. 293.
- [283] P. A. Cornelio and J. A. Gardella, *J. Vac. Sci. Technol. A* 8 (1990) 2283.
- [284] M. B. Clark and J. A. Gardella Jr., *Anal. Chem.* 62 (1990) 870.
- [285] P. A. Cornelio-Clark and J. A. Gardella Jr., *Langmuir* 7 (1991) 2279.
- [286] P. A. Cornelio-Clark and J. A. Gardella Jr., *Langmuir* 7 (1991) 2454.
- [287] J.-X. Li and J. A. Gardella Jr., *Anal. Chem.* 66 (1994) 1032.
- [288] J.-X. Li, J. A. Gardella Jr., P. J. McKeown, *Appl. Surf. Sci.* 90 (1995) 205.
- [289] G. Bolbach, R. Beavis, S. Della-Negra, C. Deprun, W. Ens, Y. Lebeyec, D. E. Main, B. Schueler, K. G. Standing, *Nucl. Ins. Meth. Phys. Res. B* 30 (1988) 74.
- [290] R. Galéra, J. C. Blais, G. Bolbach, *Int. J. Mass Spectrom. Ion Processes* 107 (1991) 531.
- [291] G. Bolbach, M. Plissonier, R. Galéra, J. C. Blais, *Thin Solid Films* 210/211 (1992) 524.
- [292] R. Galéra, G. Bolbach, O. Bouloussa, J. C. Blais, in: *Secondary Ion Mass Spectrometry, SIMS VIII proceedings*; Eds. A. Benninghoven, K. T. F. Janssen, J. Tümpner, H. W. Werner, Wiley (New York, 1992) p. 21.
- [293] G. Bolbach, J. C. Blais, S. Clémendot, A. Barraud, *Nucl. Ins. Meth. Phys. Res. B* 88 (1994) 180.
- [294] S. Clémendot, H. Perez, G. Derost, A. Ruaudel-Teixier, A. Barraud, G. Bolbach, J. C. Blais, H. Roulet, G. Dufour, G. Dagoury, *Thin Solid Films* 244 (1994) 895.
- [295] B. Hagenhoff, M. Deimel, A. Benninghoven, H.- U. Siegmund, D. Holtkamp, *J. Phys. D: Appl. Phys.* 25 (1992) 818.
- [296] B. Hagenhoff, A. Benninghoven, H.- U. Siegmund, D. Holtkamp, *Thin Solid Films* 210/211 (1992) 601.
- [297] B. Hagenhoff, H.- U. Siegmund, A. Benninghoven, in: *Secondary Ion Mass Spectrometry, SIMS VIII proceedings*; Eds. A. Benninghoven, K. T. F. Janssen, J. Tümpner, H. W. Werner, Wiley (New York, 1992) p. 289.
- [298] A. Benninghoven, *Angew. Chem. Int. Ed. Engl.* 33 (1994) 1023.
- [299] R. Linton, V. Guarisco, J. J. Lee, B. Hagenhoff, A. Benninghoven, *Thin Solid Films* 210/211 (1992) 565.
- [300] K. M. Leufgen, H. Rulle, A. Benninghoven, M. Sieber, H.-J. Galla, *Langmuir* 12 (1996) 1708.
- [301] K. M. Leufgen, H. Rulle, M. Sieber, H.-J. Galla, A. Benninghoven, in: *Secondary Ion Mass Spectrometry, SIMS X proceedings*; Eds. A. Benninghoven, B. Hagenhoff, H. W. Werner, Wiley (New York, 1997) p. 957.
- [302] H. Rulle, D. Rading, A. Benninghoven, in: *Secondary Ion Mass Spectrometry, SIMS X proceedings*; Eds. A. Benninghoven, B. Hagenhoff, H. W. Werner, Wiley (New York, 1997) p. 153.
- [303] S. Seki, H. Sumiya, H. Tamura, in: *Secondary Ion Mass Spectrometry, SIMS IX proceedings*; Eds. A. Benninghoven, Y. Nihei, R. Shimizu, H. W. Werner, Wiley (New York, 1994) p. 488.

## References

- 
- [304] M. Kudo, N. Ogura, S. Yamada, Y. Ichinohe, S. Yoshida, T. Watanabe, T. Hoshi, K. Endo, in: Secondary Ion Mass Spectrometry, SIMS XI proceedings; Eds. G. Gillen, R. Lareau, J. Bennett, F. Stevie, Wiley (New York, 1998) p. 472.
- [305] T. Hoshi, S. Yoshida, T. Watanabe, Y. Ichinohe, K. Endo, Z. Liu, M. Kudo in: Secondary Ion Mass Spectrometry, SIMS XI proceedings; Eds. G. Gillen, R. Lareau, J. Bennett, F. Stevie, Wiley (New York, 1998) p. 475.
- [306] M. Kudo, S. Yamada, S. Yoshida, T. Watanabe, T. Hoshi, Appl. Surf. Sci. (1996) 129.
- [307] T. Hoshi, S. Yamada, S. Yoshida, T. Watanabe, M. Kudo, in: Secondary Ion Mass Spectrometry, SIMS X proceedings; Eds. A. Benninghoven, B. Hagenhoff, H. W. Werner, Wiley (New York, 1997) p. 255.
- [308] J. F. Elman, D. H.-T. Lee, J. T. Koberstein, Langmuir 11 (1995) 2761.
- [309] Y. Li, J. Huang, R. T. McIver Jr., J. C. Hemminger, J. Am. Chem. Soc. 114 (1992) 2428.
- [310] M. J. Tarlov and J. G. Newman, Langmuir 8 (1992) 1398.
- [311] C. D. Frisbie, J. R. Martin, R. R. Duff Jr., M. S. Wrighton, J. Am. Chem. Soc. 114 (1992) 7142.
- [312] E. W. Wollman, D. Kang, C. D. Frisbie, I. M. Lorkovic, M. S. Wrighton, J. Am. Chem. Soc. 116 (1994) 4395.
- [313] C. D. Frisbie, E. W. Wollman, M. S. Wrighton, Langmuir 11 (1995) 2563.
- [314] T. J. Gardner, C. D. Frisbie, M. S. Wrighton, J. Am. Chem. Soc. 117 (1995) 6927.
- [315] M. J. Tarlov, D. R. F. Burgess Jr., G. Gillen, J. Am. Chem. Soc. 115 (1993) 5305.
- [316] G. Gillen, J. Bennett, M. J. Tarlov, D. R. F. Burgess Jr., Anal. Chem. 66 (1994) 2170.
- [317] G. Gillen, S. Wight, J. Bennett, M. J. Tarlov, Appl. Phys. Lett. 65 (1994) 534.
- [318] G. Gillen, S. Robertson, M. Tarlov, T. Herne, in: Secondary Ion Mass Spectrometry, SIMS X proceedings; Eds. A. Benninghoven, B. Hagenhoff, H. W. Werner, Wiley (New York, 1997) p. 831.
- [319] G. J. Leggett, M. C. Davies, D. E. Jackson, S. J. B. Tender, J. Chem. Soc. Faraday Trans. 89 (1993) 179.
- [320] G. J. Leggett, M. C. Davies, D. E. Jackson, S. J. B. Tender, J. Phys. Chem. 97 (1993) 5348.
- [321] D. A. Hutt, E. Cooper, G. J. Leggett, J. Phys. Chem. B 102 (1998) 174.
- [322] B. Hagenhoff, A. Benninghoven, J. Spinke, M. Liley, W. Knoll, Langmuir 9 (1993) 1622.
- [323] B. Hagenhoff, M. Deimel and A. Benninghoven, in: Secondary Ion Mass Spectrometry, SIMS IX proceedings; Eds. A. Benninghoven, Y. Nihei, R. Shimizu, H. W. Werner, Wiley (New York, 1994) p. 792.
- [324] C. Simon, F. Saldi, H.-N. Migeon and J. Mielczarski, in: Secondary Ion Mass Spectrometry, SIMS X proceedings; Eds. A. Benninghoven, B. Hagenhoff, H. W. Werner, Wiley (New York, 1997) p. 759.
- [325] H. Luo, S. A. Miller, R. G. Cooks, S. J. Pachuta, Int. J. Mass Spectrom. Ion Proc. 174 (1998) 193.
- [326] D. A. Offord, C. M. John, J. H. Griffin, Langmuir 10 (1994) 761.
- [327] D. A. Offord, C. M. John, M. R. Linford, J. H. Griffin, Langmuir 10 (1994) 883.
- [328] J.-C. Canry and J. C. Vickerman, in: Secondary Ion Mass Spectrometry, SIMS X proceedings; Eds. A. Benninghoven, B. Hagenhoff, H. W. Werner, Wiley (New York, 1997) p. 623.
- [329] J.-C. Canry and J. C. Vickerman, in: European Conference on Applications of Surface and Interface Analysis, ECASIA 95 proceedings; Eds. H. J. Mathieu, B. Reihl, D. Briggs, Wiley (New York, 1996) p. 903.
- [330] C. G. Worley, E. P. Enriquez, E. T. Samulski, R. W. Linton, Surf. Interface Anal. 24 (1996) 59.
- [331] F. Sun, D. G. Castner, G. Mao, W. Wang, P. McKeown, D. W. Grainger, J. Am. Chem. Soc. 118 (1996) 1856.

- [332] W. Wang, D. G. Castner, D. W. Grainger, *Supramol. Sci.* 4 (1997) 83.
- [333] D. Rading, R. Kersting, A. Benninghoven, in: *Secondary Ion Mass Spectrometry, SIMS XI proceedings*; Eds. G. Gillen, R. Lareau, J. Bennett, F. Stevie, Wiley (New York, 1998) p. 455.
- [334] D. E. Riederer, R. Chatterjee, S. W. Rosencrance, Z. Postawa, T. D. Dunbar, D. L. Allara and N. Winograd, *J. Am. Chem. Soc.* 119 (1997) 8089.
- [335] D. E. Riederer, S. W. Rosencrance, R. Chatterjee, T. D. Dunbar, D. L. Allara and N. Winograd, in: *Secondary Ion Mass Spectrometry, SIMS X proceedings*; Eds. A. Benninghoven, B. Hagenhoff, H. W. Werner, Wiley (New York, 1997) p. 965.
- [336] K. S. S. Liu, J. C. Vickerman, B. J. Garrison, in: *Secondary Ion Mass Spectrometry, SIMS XI proceedings*; Eds. G. Gillen, R. Lareau, J. Bennett, F. Stevie, Wiley (New York, 1998) p. 443.
- [337] W. J. Van Ooij and A. Sabata, in: *Silanes and other coupling agents*; Ed. K. L. Mittal, VSP (Utrecht, 1992) p. 323.
- [338] D. Wang, F. R. Jones, P. Denison, in: *Silanes and other coupling agents*; Ed. K. L. Mittal, VSP (Utrecht, 1992) p. 345.
- [339] B. Hagenhoff, A. Benninghoven, K. Stoppek-Langner, J. Grobe, *Adv. Mater.* 6 (1994) 142.
- [340] G. Egbers, D. Rading, K. Stoppek-Langner, J. Grobe, A. Benninghoven, in: *Secondary Ion Mass Spectrometry, SIMS X proceedings*; Eds. A. Benninghoven, B. Hagenhoff, H. W. Werner, Wiley (New York, 1997) p. 763.
- [341] K. Reihls, R. Aguiar Colom, S. Gleditzsch, M. Deimel, B. Hagenhoff, A. Benninghoven, *Appl. Surf. Sci.* 84 (1995) 107.
- [342] H. van der Wel, E. van der Sluis-van der Voort, N. P. Willard, *Surf. Interface Anal.* 21 (1994) 455.
- [343] B. W. Schueler, *Microsc. Microanal. Microstruct.* 3 (1992) 119.
- [344] A. Delcorte, L. T. Weng and P. Bertrand, *Nucl. Instr. and Meth. B100* (1995) 213.
- [345] J.-B. Lhoest, J.-L. Dewez and P. Bertrand, *Nucl. Instr. and Meth. B105* (1995) 322.
- [346] TRIFT analyser operator's guide, Physical Electronics, Inc.
- [347] B. W. Schueler, private communication.
- [348] D. Léonard, P. Bertrand, A. Scheuer, R. Prat, J. Hommet, J. Le Moigne and J. P. Deville, *J. Adhesion Sci. Technol.* 10 (1996) 1165.
- [349] W. J. Van Ooij and R. H. G. Brinkhuis, *Surf. Interface Anal.* 11 (1988) 430.
- [350] D. Briggs, *Surf. Interface Anal.* 15 (1990) 734.
- [351] L. T. Weng, P. Bertrand, W. Lauer, R. Zimmer and S. Buseti, *Surf. Interface Anal.* 23 (1995) 879.
- [352] H. Grade, N. Winograd, R. G. Cooks, *J. Am. Chem. Soc.* 99 (1977) 7725.
- [353] B. Hagenhoff, in: *The Wiley Static SIMS Library*, Eds. J. C. Vickerman, D. Briggs, A. Henderson; Wiley (New York, 1996) p. 39.
- [354] D. Briggs and M. P. Seah, *Practical Surface Analysis by Auger and X-Ray Photoelectron Spectroscopy*, Wiley (New York, 1983).
- [355] L. T. Weng, G. Vereecke, M. J. Genet, P. Bertrand and W. E. E. Stone, *Surf. Interface Anal.* 20 (1993) 179 and L. T. Weng, G. Vereecke, M. J. Genet, P. G. Rouxhet, J. H. Stone-Masui, P. Bertrand and W. E. E. Stone, *Surf. Interface Anal.* 20 (1993) 193.
- [356] D. A. Shirley, *Phys. Rev. B5* (1972) 4709.
- [357] T. J. Horr, J. Ralston, R. St. C. Smart, *Coll. Surf. A* 92 (1994) 277.
- [358] J. D. Andrade, in: *Surface and Interfacial Aspects of Biomedical Polymers*, Plenum Press (New York, 1985) p. 105.
- [359] M. P. Seah and W. A. Dench, *Surf. Interface Anal.* 1 (1979) 2.
- [360] D. Briggs, A. Brown, J. C. Vickerman, *Handbook of Static Secondary Ion Mass Spectrometry (SIMS)*, Wiley, (New York, 1989).

## References

---

- [361] J. G. Newman; B. A. Carlson, R. S. Michael, J. F. Moulder, T. A. Hohlt, Static SIMS Handbook of Polymer Analysis; Ed. T.A. Hohlt, Perkin-Elmer Corporation, (Minnesota, 1991).

*The second part of the thesis is a compilation of articles published or submitted during my PhD.  
Some of these articles are available online at :*

*<http://www.pcpm.ucl.ac.be/~delcorte/publications.html>*

Thin organic layers including cast and spin-coated films, Langmuir-Blodgett bilayers and alternate polyelectrolyte multilayers have been studied using Time-of-Flight Secondary Ion Mass Spectrometry (ToF-SIMS).

First, owing to these model organic and polymeric layers, a fundamental investigation of the secondary ion emission processes has been carried out, based on the interpretation of the kinetic energy distribution of the ejected species. Several mechanisms have been identified and explained, including the emission of low-energy, precursor-like species (i), of faster and strongly dehydrogenated ions (ii) and of unexpectedly energetic metal-cationised oligomers and molecules (iii). Our phenomenological model based on the concept of internal energy-dependent fragmentation of excited ejecta accounts for the periodic variation of the hydrocarbon ion kinetic energy in the case of triacontane and tricosenoic acid layers. Moreover, the measurements performed with poly(isobutylene) and poly(styrene) layers indicate that the same processes occur with polymers. On the other hand, the rather high kinetic energies of aromatic parent-like ions sputtered from dibenzanthracene, tetraphenylnaphtalene and poly(styrene) oligomers cast on silver are best explained by a multiple collision process. By the interpretation of the kinetic energy deficits, unimolecular dissociation reactions in the vacuum, e.g. H and H<sub>2</sub> losses, have been evidenced, too (iv). These findings have been tentatively taken into account in a comprehensive picture of the sputtering event. In a different approach, the information depth of atomic and molecular secondary ions has been determined by means of a combined analysis of model polyelectrolyte multilayers by ToF-SIMS, X-ray Photoelectron Spectroscopy and X-Ray Reflectometry. The results show that the mean emission depth is larger for atomic ions than for molecular ions.

Second, new results concerning multilayers built-up by alternate polyelectrolyte physisorption have been obtained by the combined use of ToF-SIMS and XPS. For poly(styrene sulfonate)/poly(choline methacrylate) (PSS/PCM) multilayers adsorbed on silicon, the multilayer growth is regular, with a 15 Å bilayer thickness, the complexation of the polyelectrolytes in the multilayer is nearly quantitative and the fraction of counterions remaining in the top polyelectrolyte layer of the assemblies is surprisingly weak. In the context of the (deposition + activation) method, leading to non-centrosymmetric assemblies, the successful polycation functionalisation and multilayer build-up have been assessed, too. Based on these preliminary results obtained for model substrates, the adsorption of polyelectrolyte multilayers on uncharged, standard polymer supports has been initiated. In this study, the use of ToF-SIMS and XPS was even more advantageous, since these systems are difficult to analyse by means of other characterisation techniques like XRR and AFM, which require either an optical or a mechanical contrast between the organic coating and the substrate. Remarkably, the multilayer build-up occurs on uncharged polymer substrates, too. Except for aliphatic hydrocarbons like poly(propylene), the secondary ion intensities related to the polymer supports are drastically reduced with only three PSS/PCM deposition cycles, which is comparable to the case of silicon. For poly(ethylene terephthalate), the results indicate the increase of the layer thickness at each step, up to 30 Å per bilayer. For poly(propylene) supports, better quality layers can be fabricated using more hydrophobic polyelectrolytes, as demonstrated by UV/vis, XPS and ToF-SIMS measurements. In practice, the limited adsorption on aliphatic polyolefins can be advantageously used to design patterned multilayers, too.